Charakterisierung neuer Materialien in der Chromatographie und Brennstoffzellen-Forschung mit Hilfe moderner NMR-Techniken

Characterization of new materials in chromatography and fuel cell development by modern NMR techniques

DISSERTATION

der Fakultät für Chemie und Pharmazie
der Eberhard-Karls-Universität Tübingen
zur Erlangung des Grades eines Doktors
der Naturwissenschaften

2007

vorgelegt von
Siri Schauff

Tag der mündlichen Prüfung:	22.03.2007
Dekan:	Prof. Dr. L. Wesemann
1. Berichterstatter:	Prof. Dr. K. Albert
2. Berichterstatter:	Prof. Dr. H.W. Spiess

Die vorliegende Arbeit wurde am Institut für Organische Chemie der Universität Tübingen unter der Anleitung von Herrn Professor Dr. Klaus Albert und am Max-Planck-Institut für Polymerforschung in Mainz unter der Anleitung von Herrn Professor Dr. Hans Wolfgang Spiess im Zeitraum von Januar 2004 bis März 2007 durchgeführt.

Herrn Professor Dr. Klaus Albert und Herrn Professor Dr. Hans Wolfgang Spiess danke ich sehr herzlich für die interessanten Themenstellungen, das stetige Interesse, das sie meiner Arbeit entgegenbrachten, für die Bereitstellung hervorragender Arbeitsbedingungen und für die Möglichkeit, an nationalen und internationalen Tagungen teilnehmen zu können.

Mein Dank gilt allen, die zum Gelingen dieser Arbeit beigetragen haben, insbesondere den gegenwärtigen und früheren Mitgliedern der Arbeitskreise von Prof. Dr. Albert und von Prof. Dr. Spiess, den Kollegen aus dem Graduiertenkolleg „Chemie in Interphasen“ und des BMBF-Projektes „DryD“.

Besonders bedanken möchte ich mich bei:

Benjamin Dietrich, Dr. Gerd Fischer, Volker Friebolin, Dr. Petra Hentschel, Dr. Manfred Krucker, Dr. Christoph Meyer, Dr. Karsten Putzbach, Jens Rehbein, Dr. Urban Skogsberg, Wolfgang Wilmes und Dr. Lothar Brombacher, Dr. Robert Graf, Dr. Anke Hoffmann, Dr. Young Joo Lee, Mihail Mondeshki, Chulsoon Moon, Dr. Daniel Sebastiani, Yefeng Yao und Dr. Anke Kaltbeitzel, Dr. Dilyana Markova, Dr. Hanna Steininger für das gute und angenehme Arbeitsklima und die Unterstützung bei Fragen und Schwierigkeiten.

Berthold Maier, Phong Thu Nguyen, Brigitte Schindler, Paul Schuler und Walter Schaal für die Unterstützung bei Messungen und technischen Fragen mit den Geräten.

Manfred Hehn und Hans-Peter Raich für die schnelle und kompetente Reparatur vieler Probenköpfe.

Michelle Drechsler und Verona Maus für ihre Hilfe zum Auffinden von Chemikalien, Geräten und Informationen.

Christoph Sieber für die Durchführung der Leitfähigkeitsmessungen.

Dr. Marc David Grynbaum für die HPLC-Messungen der Tocopherole und für die vielen hilfreichen Tipps.

Christoph Deller für viele angeregte Diskussionen über Deuteronen-NMR.

Dr. Katja Klimke und Dr. Matt Parkinson für die wertvollen Gespräche über NMR und die netten gemeinsamen Abende.

Dr. Gunther Brunklaus und seiner Frau Sabine für das schnelle Korrekturlesen und die Betreuung und Unterstützung während meiner Doktorarbeit.

Der Deutschen Forschungsgemeinschaft für die Förderung als Stipendiat im Rahmen des Graduiertenkollegs „Chemie in Interphasen“ und dem Bundesministerium für Bildung und Forschung für die finanzielle Unterstützung im Rahmen des „DryD“-Projektes.

Der Firma Bischoff Chromatography für die Bereitstellung der C_{18}-Phase für die HR-MAS-Experimente.

Der Firma PEMEAS für die Bereitstellung der Polyvinylphosphonsäure.

Mein ganz herzlicher Dank gilt:

Meinen Eltern für ihre uneingeschränkte Unterstützung, die diese Arbeit möglich gemacht hat.
Stefan, der immer für mich da war und mir mit Rat und Tat zu Seite stand.

Meinen Eltern und Stefan

Table of Contents

1 Introduction 1

2 Background 3

2.1 Fuel cells 3

2.1.1 Proton Conducting Materials 4

2.1.2 Proton Transport Mechanisms 4

2.1.3 Proton Conductivity Measurements 6

2.2 Liquid Chromatography 9

2.2.1 Separation Processes 10

2.2.2 Stationary Phase Materials 13

2.2.2.1 Characterization of Stationary Phases 15

2.2.2.2 Molecularly Imprinted Polymers (MIP) 17

2.3 Solid-state NMR Spectroscopy 19

2.3.1 Magic Angle Spinning (MAS) 19

2.3.1.1 Rotor Synchronization and Spinning Sidebands 20

2.3.2 Basic NMR Experiments 21

2.3.2.1 One-pulse Experiment 21

2.3.2.2 Cross Polarization Experiment 21

2.3.2.3 Solid-echo Experiment 22

2.3.3 ^{2}H NMR Spectroscopy 23

2.4 Suspended-state HR-MAS NMR Spectroscopy and its Application in Chromatography 26

2.4.1 Saturation Transfer Difference (STD) Experiment 27

3 Structure and Dynamics of Phosphonic acids 29

3.1 Characterization of Phosphonic acids 29

3.1.1 Methylphosphonic acid 29

3.1.2 Polyvinylphosphonic acid Ionomer 30

3.1.3 Polyvinylbenzylphosphonic acid 32

3.1.4 Polyphosphazenephosphonic acid 33

3.1.5 Polyvinylbenzylphosphonic acid / Polyetheretherketon Blockcopolymer 36

3.1.6 Siloxanephosphonic acid 37

3.2 Water Uptake Studies 39
3.2.1 Polyvinylphosphonic acid 39
3.2.2 Methylphosphonic acid 42
3.3 Dynamic Processes 43
3.3.1 ^{1}H NMR Spectroscopy 43
3.3.2 ^{2}H NMR Spectroscopy 45
3.3.2.1 ^{2}H MAS NMR Spectroscopy 45
3.3.2.2 ^{2}H Static NMR Spectroscopy 49
3.4 Proton Conductivity Measurements 52
3.5 Conclusion 56

4 Investigation of Chromatographic Stationary Phases 58
4.1 Characterization of Stationary Reversed Phases 58
4.1.1 C_{18} Phase 58
4.1.2 C_{30} Phase 60
4.1.3 Polyethylene-co-acrylic acid 62
4.1.4 Molecularly Imprinted Polymer (MIP) Particles 62
4.1.5 Molecularly Imprinted Polymer (MIP) Monolith 63
4.2 Study of Dynamics in Methylphenyl succinimide/ C_{18} Phase System 64
4.3 Dynamic Studies using STD NMR Spectroscopy 69
4.3.1 Interaction of Tocopherol Homologues with Reversed Phases 69
4.3.2 Interaction of Particulate MIP with 2,4-Dichlorophenoxyacetic acid 74
4.3.3 Interaction of MIP Monolith with Bupivacaine 75
4.4 Conclusion 78

5 Summary 79

6 Experimental Details 81

7 Literature 84

List of Abbreviations

α	selectivity
γ	magnetogyric ratio
σ	specific conductivity
ω	resonance frequency
ω_Q	quadrupolar frequency
AC	alternating current
ACN	acetonitrile
CE	capillary electrophoresis
CEC	capillary electrochromatography
CP	cross polarization
1D	one-dimensional
2,4-D	2,4-dichlorophenoxyacetic acid
DC	direct current
D_2O	deuterium oxide
DQ	double quantum
DQF	double quantum filtered
E_A	activation energy
EDMA	ethylene dimethacrylate
EFG	electric field gradient
FC	fuel cell
FID	free induction decay
GC	gas chromatography
HPLC	high performance liquid chromatography
HR	high resolution
IR	infrared
J	Joule
K	Kelvin
kHz	Kilohertz
LC	liquid chromatography
MAA	methylacrylic acid
MAS	magic angle spinning
MePA	methylphosphonic acid

MePhSucc	methylphenyl succinimide
MeOH	methanol
MHz	Megahertz
min	minute
MIP	molecularly imprinted polymer
NIP	non-imprinted polymer
NMR	nuclear magnetic resonance
NP	normal phase
PEM	proton exchange/ polymer electrolyte membrane
SEM	scanning electron microscopy
SPE	solid phase extraction
PBI	polybenzimidazole
PC4	polycarbonate
PDA	personal digital assistant
PEAA	polyethylene-*co*-acrylic acid
PEEK	polyetheretherketon
ppm	parts per million
PPPA	polyphosphazenephosphonic acid
PVBzPA	polyvinylbenzylphosphonic acid
PVPA	polyvinylphosphonic acid
rf	radio frequency
RP	reversed phase
SPA	siloxanephosphonic acid
SSB	spinning sideband
STD	saturation transfer difference
TMS	trimethylsilane
TRIM	trimethylolpropane trimethylacrylate
TSPSA	3-(trimethylsilyl) propane sulfonic acid Na salt
UV	ultra-violet
VPA	vinylphosphonic acid

1 Introduction

Due to a steady increase in the need for innovative products in daily life, new materials, suitable to meet these requirements, have to be developed. The demand for new materials is given in all different kinds of industry. Nowadays, above all, it is of importance to find regenerative energies to decrease pollution, to improve the understanding of human deseases and traditional natural drugs, and thus provide a larger offer on human health products and safe and clean transport possibilities in order to improve the quality of life.

Innovative materials for the application in new batteries and in liquid chromatography have to be characterized and evaluated in their suitability to cope with these requirements.

Over the last years, the field of chromatography has undergone a tremendous progress, with respect to speed, proof of amounts in the nanogram range and width of application to test analytes. It became more important to evaluate plants and drugs and study their metabolites in order to lengthen human life and preserve its health. History of medicine showed the need to separate active substances with similar structures to rule out unwanted effects on the human body. However, especially in liquid chromatography, the separating interactions are not yet well understood, thus a larger insight in the processes taking place in the interphase of a chromatographic system would lead to better results in the separation, obtained from carefully adjusted parameters. These include the synthesis of tailor-made stationary phase materials.

New materials are also required for further progress in fuel cell development. Nowadays, the need of regenerative batteries, especially in the field of automotive industry, has become to a well discussed issue, in order to preserve the environment and the ozone layer. Many car suppliers tend to develop new promising motive systems to offer a clean transport vehicle in the future, one of which is the hydrogen-powered car, which was already introduced a couple of years ago and is still the topic of further progress. However, most fuel cells are working under rough conditions, leading to the materials deterioration with running time. Above all, this is the case for the proton conducting material which is the key piece of each fuel cell. Therefore, new materials have to provide reliable and cheap motive abilities, driven by regenerative fuels, which have to cope with fuel cell conditions.

Dynamic processes are the driving force for both, the analyte separations in liquid chromatography and the proton conductivity of fuel cell materials. Since they are also responsible for the materials quality and properties, they have to be considered in order to obtain information about self-diffusion and/or diffusion of molecules, parts of molecules, and protons, driven by external influences.

This work deals with the examination of both kinds of materials using solid-state and suspended-state NMR spectroscopy, both found to be suitable to characterize a material and study dynamic processes therein.

Phosphonic acids, a new class of high-temperature proton conducting materials for fuel cell applications, will be evaluated with regard to their properties and local proton mobilities. The materials will be screened, and solid-state NMR spectroscopic experiments have to be tested to reveal suitable methods. Information about the proton transfer mechanism in “dry” high-temperature materials should be gained.

The dynamic interactions of various analytes with different *chromatographic sorbents* will be tested under the influence of the mobile phase via suspended-state NMR spectroscopy in order to gain information about the separation processes in reversed phase HPLC. Molecularly imprinted polymers will be investigated using the same method connected with the saturation transfer difference technique, yielding information about molecular recognition mechanisms.

2 Background

2.1 Fuel Cells

Fuel cells are referred to as “green batteries” which unlike normal batteries do not discharge with time. They provide electricity and heat as long as they are supplied with appropriate fuel. Due to the chemical electrolyte processes upon operation of fuel cells, they ideally emit only water. Thus, a complicated water management becomes crucial.

Independent of the type of fuel cell, they are working after the same mechanism: Two electrodes sandwich an electrolyte which can be liquid or solid. Oxygen is flushed at the cathode, hydrogen at the anode producing electricity, water, and heat. At the anode the hydrogen or a hydrocarbon fuel (e.g. methanol) is split into electrons and protons taking different pathways to the cathode. The electrons create an usable electric current, and the protons pass through the electrolyte to be recombined with the electrons at the cathode and provided oxygen to form water. For a schematic picture of a fuel cell and its electrode processes see figure 1.

In membrane fuel cells namely proton exchange/polymer electrolyte membrane fuel cells (PEMFCs) a proton conducting polymer membrane functions as electrolyte. PEM fuel cells provide long lifetimes and are highly efficient which causes their suitability for the application in automotive industry. Their compactness makes them also good candidates for replacing rechargeable batteries for transportable electronic devices (e.g. laptops, PDAs). However, they are sensitive to fuel impurities such as carbon monoxide which causes poisoning of the electrode catalyst. This is mainly observed at low operation temperatures (up to about 80 °C).

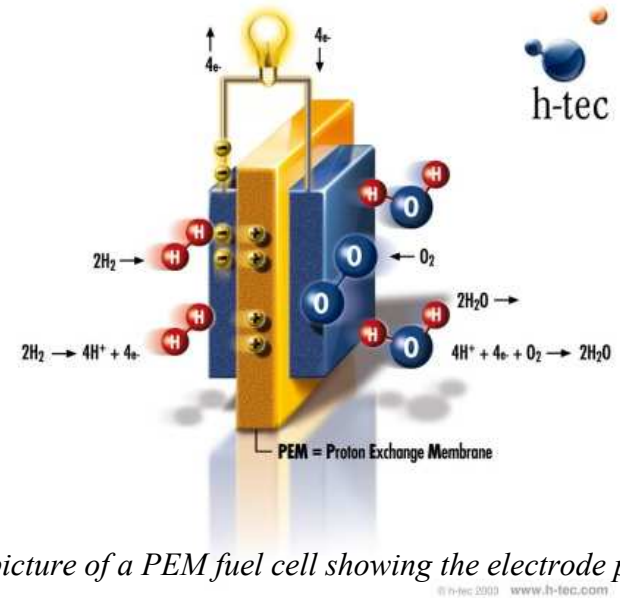

Figure 1: Schematic picture of a PEM fuel cell showing the electrode processes [h-tec 03].

2.1.1 Proton Conducting Materials

Proton conducting materials suitable for the application in fuel cells are mostly polymers with different functional groups to accomplish the proton transport through the membrane. Besides, also polymer membranes containing more liquid-like proton conductors (e.g. phosphoric acid) are used. Since water is a by-product in all working PEM-based fuel cells, phosphoric acid easily is washed from the material, thereby deteriorating the materials conductivity.

In the past, various polymers have been used as possible materials for PEMs. In particular, sulfonic acid functionalized polymers are nowadays commonly used as PEM materials, where Nafion, a sulfonated tetrafluoroethylene copolymer (Teflon derivative), is the most frequent representative. Nafion was discovered in the late 1960s by Grot et al [Grot 01] for DuPont company and has a proton conductivity of 10^0 $S \cdot cm^{-1}$. The major disadvantage of Nafion is the low operation temperature of only up to 80 °C (see also 2.1.2).

Imidazoles that constitute another class of polymers, revealed much lower proton conductivities than Nafion. Schuster et al. [Schuster 05] and Goward et al. [Goward 02] described a substantially different proton mobility mechanism than compared to Nafion. Due to their low conductivities, the interest in imidazoles was reduced.

At operation temperatures below 100 °C, catalysts poisoning can only be circumvented by the use of very clean fuel. Especially, the use of carbohydrates (e.g. methanol) as fuel is problematic since even traces of carbon monoxide adsorb on platinum-based electrodes, thus occupying the active sites. Platinum electrodes are generally used in methanol fuel cells to obtain a high degree of oxidation and therefore increase the fuel cells efficiency. To prolong the lifetime of the electrodes, it is necessary to test membrane materials with operation temperatures well above 150 °C. In this respect, phosphonic acid functionalized polymers proved to be a promising class of materials [Miyatake 01, Meng 03, Schuster 05].

2.1.2 Proton Transport Mechanisms

The proton transport mechanism of Nafion was previously investigated by Kreuer et al. [Kreuer 04]: A channel-like structured polymer allows the protons to travel through the membrane. This is accomplished by the attachment of the protons to water molecules, using those as vehicles, resulting in travelling hydronium ions. This so called “vehicle mechanism”

requires the “wet” state of the membrane material so that sufficient water is present to function as vehicle. Since a higher operation temperature above 100 °C would cause an evaporation of water, such materials cannot be used for high temperature applications.
A totally different proton transport mechanism is claimed for phosphonic acids [Kreuer 04, Kreuer 96]. Here, the protons could travel via the hydrogen bonds of neighboured phosphonic acid groups. This is referred to as the “Grotthus mechanism” working in “dry” materials. See figure 2 for schematic pictures of the two mechanisms.

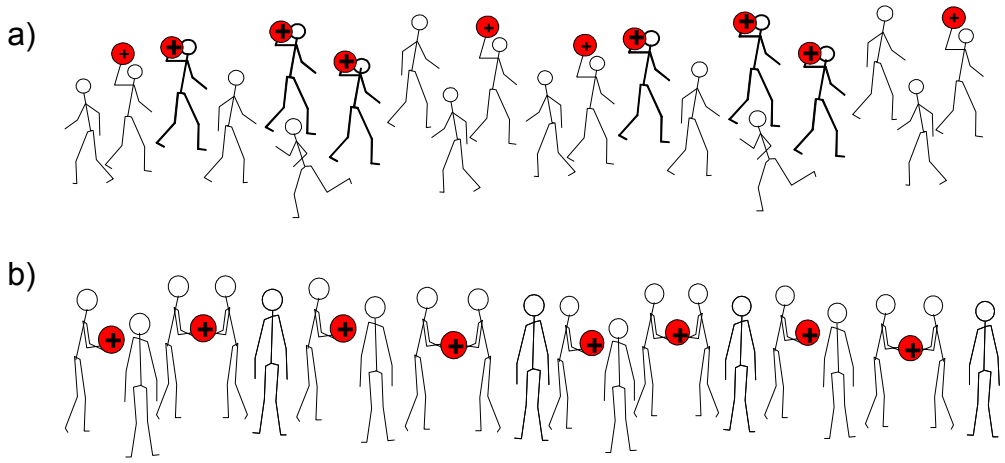

Figure 2: Schematic picture of the a) vehicle mechanism and b) Grotthus mechanism.

The “Grotthus mechanism” leads to a bond-breaking and bond-forming between the phosphonic acid groups while the proton is “hopping” to the next molecule (also termed “structure diffusion” [Kreuer 04]). This is considered possible when employing immobilized “proton-solvents” which are very mobile e.g. due to spacers. Spacers of medium length were found to be suitable in imidazoles and phosphonic acids in order to increase the mobility of the functional groups and thus enhance their aggregation leading to possible “structural diffusion” [Kreuer 04]. Such proton transport was found to be possible also for strong hydrogen bonds, whereas weaker hydrogen bonds facilitate the bond-breaking and bond-forming reactions [Kreuer 00]. The relation between hydrogen bond strength and proton mobility is complex, but in general, dynamic hydrogen bonds are desired in order to enhance the local mobility. However, a membrane material still has to be thermally and mechanically stable to cope with the stress of high pressure and temperatures in a working fuel cell.

2.1.3 Proton Conductivity Measurements

Proton conductivities can be determined by impedance spectroscopy, which uses an alternating current (AC) to measure the dielectric properties of a sample in a plate capacitor. Therefore, the sample is sandwiched by two inert electrodes (see figure 3 a and b). The application of an external current leads to a flow of protons through the material towards the other electrode.

To determine the dielectric properties of a sample, the amplitude I_0 and the phase shift θ of the resulting current $I(t)$ are measured:

$$I(t) = I_0 \sin(\omega t + \theta) .$$

The impedance $Z(\omega)$ is the complex AC resistance, which in case of linearity can be described as

$$Z(\omega) = \frac{U_0}{I_0} \exp(-i\theta) ,$$

thus its real and imaginary part are functions of frequency. To reveal the samples conductivity, it is of importance to calculate the complex conductivity $Y(\omega)$, which is reciprocal to $Z(\omega)$ and can be expressed as

$$Y(\omega) = \frac{1}{Z(\omega)} .$$

It is necessary to bring in information about the shape and size of the cell to determine the cell constant K from the surface area A and the sample thickness d

$$K = \frac{A}{d},$$

in order to directly obtain the specific conductivity $\sigma(\omega)$

$$\sigma(\omega) = \frac{1}{K} \cdot Y(\omega)$$

with its real part $\sigma'(\omega)$

$$\sigma'(\omega) = \frac{1}{K} Y'(\omega) .$$

The specific conductivity $\sigma(\omega)$ is a measure of the carried charge per time, whereas the relative dielectric constant $\varepsilon_r(\omega)$ determines the charge flow per frequency cycle.

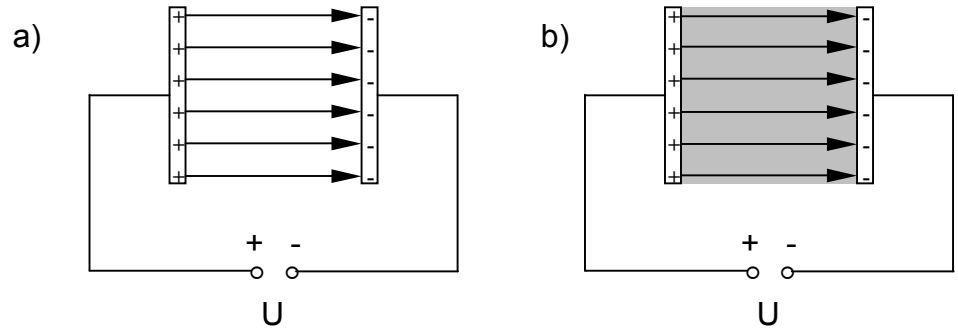

Figure 3: Schematic pictures of plate capacitors a) without sample and b) with dielectric sample in close contact [Göpel 94]. The dielectric is shown in grey.

When the electrodes are not smoothly in contact to the samples surface or block the ion/proton flow during the measurement, a polarization of the electrodes is obtained, leading to a decrease in conductivity. An AC conductivity plot versus frequency generally leads to the observation of three typical isotherm areas (see figure 4): The low frequency regime is determined by the electrode polarization, the frequency-independent plateau reflects the wanted transport phenomena, and the high frequency regime is due to relaxation effects. In the direct current (DC) plateau region, which shifts to higher frequencies with increased temperature, due to an overall increase of energy in the system, the dynamic processes are determined by random mobility. At higher frequencies, correlated jumps back and forth to distinct sites are dominating the spectra [Barsoukov 05].

In order to determine the DC conductivity σ_{DC} from the isotherms of $\sigma'(\omega)$, the conductivity values have to be derived from the part, where the conductivity is constant. If σ_{DC} is Arrhenius-activated, a plot of ln [$\sigma_{DC} \cdot T$ (Ω·cm/ K)] versus $1/T$ results in a straight line, where the activation energy E_A can be obtained from the slope.

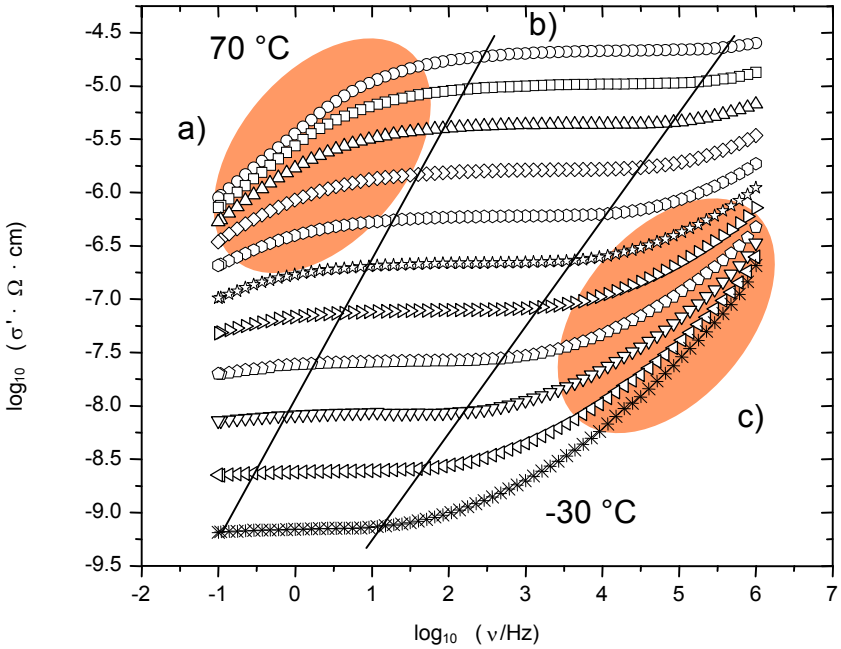

Figure 4: Typical conductivity plot showing three areas, a) the regime determined by electrode polarization, b) the DC plateau, and c) the dispersive regime.

The samples conductivity can be measured in two different ways: as membrane or as pellet. To obtain a membrane, the sample has to be dissolved in a suitable solvent and is directly coated on brass electrodes which later are used for the conductivity measurement itself. Some materials do not form membranes and are therefore pressed to pellets. To ensure efficient contact to the brass electrodes, the rough surface of the pellet has to be sputtered with gold. However, in some cases the recycling of the material is desired. In these cases flexible carbon cloth electrodes loaded with platinum particles can be used to ensure the contact (see figure 5 for a pellet with carbon cloth electrodes).

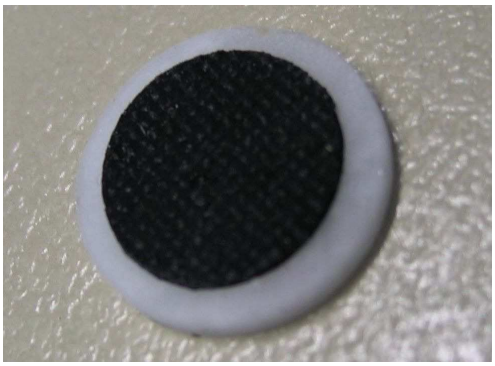

Figure 5: Picture of a MePA pellet including black carbon cloth electrodes.

2.2 Liquid Chromatography

Different types of chromatographic separation techniques are known, the electro-driven and the pressure-driven separation processes, with capillary electrophoresis (CE) and capillary electrochromatography (CEC) among the electro-driven separation techniques [Rapp 04].
In pressure-driven chromatography, analyte mixtures are separated due to their distribution between two phases, the mobile and the stationary phase. Two mainly known types of chromatography exist: gas chromatography (GC) for volatile samples and liquid chromatography (LC) for soluble samples.
In gas chromatography, the mobile phase is a gas, that transports the analyte molecules through the chromatographic column. The columns inner surface is modified with an immobilized liquid phase. The analytes separation is due to distribution between the gaseous mobile phase and the liquid phase, though the mobile phase does not directly interact with the analyte molecules [Skoog 92].
In liquid chromatography, the stationary phase is packed into a column (see figure 6) and consists of an adsorptive material, the mobile phase is a solvent which is flowing through the stationary phase eluting the separated compounds. Depending on the stationary phase material, desired separations can be performed, leading to a differentiation of several kinds of liquid chromatography: adsorption, affinity, ion exchange, ion, and size exclusion chromatography [Meyer 99]. The separation of distinct compounds is due to various interactions taking place between the analyte molecules and the stationary phase leading to different retention times on the column. (See section 2.2.1 for further discussion of separation processes.)

Figure 6: Picture of an HPLC column.

In high performance liquid chromatography (HPLC) the mobile phase is pumped with high pressures through the separation column while the analyte is dissolved in small amounts of the same solvent and injected directly. The dynamic distributional equilibrium and thus the

separation behaviour of the analyte on the stationary phase can be varied by switching the polarity of the solvent, even by mixing solvents. The application of polar solvents with non-polar stationary phases is referred to as reversed-phase HPLC (RP-HPLC) in which silica-based materials are widely used among other materials. (See section 2.2.2 for further discussion of reversed phases.) On the contrary, normal-phase HPLC (NP-HPLC) uses polar stationary phases (e.g. pure silica) and non-polar solvents.

The HPLC setup is given in figure 7. The major parts are solvent storage, high pressure pump, injector, column, and detector.

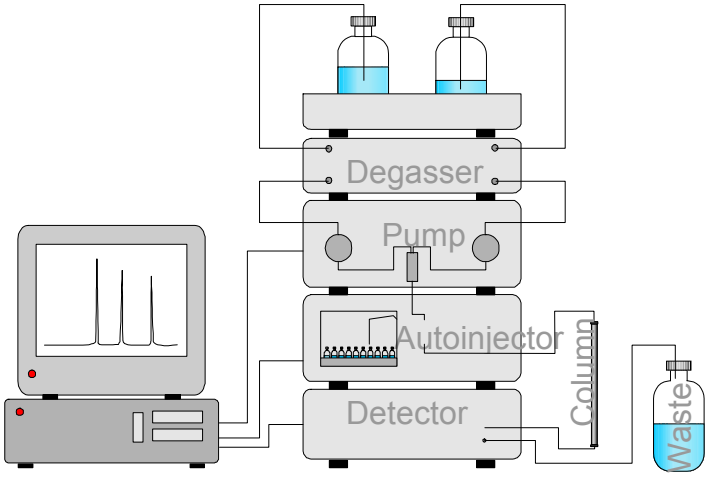

Figure 7: Schematic picture of the HPLC setup.

2.2.1 Separation Processes

In RP-HPLC, the separation generally is due to the distribution of analyte molecules between mobile and stationary phases due to their polarity (partition LC). The interactions taking place are often referred to as “hydrophobic interactions” of non-polar analyte with the non-polar chromatographic sorbent. However, numerous interactions and their effects on the separation cannot be ruled out since a chromatographic system is very sensitive to the change of various parameters.

The separation of compounds is due to interactions taking place with the stationary phase yielding different retention times t_R of the analyte molecules. A measure for the residence time in both phases is determined by the distribution coefficient K

$$K = \frac{c_{stat}}{c_{mob}}$$

with the concentration of analyte in the stationary phase c_{stat} and the mobile phase c_{stat}, and the retention factor k

$$k = \frac{n_{stat}}{n_{mob}}$$

with n_{stat} as the number of analyte molecules in the stationary and n_{mob} in the mobile phase in an equilibrated system. The dynamic partition equilibrium and thus the retention behaviour of the analytes can be changed by varying the chromatographic parameters, like the solvent composition, temperature, and flow rate.

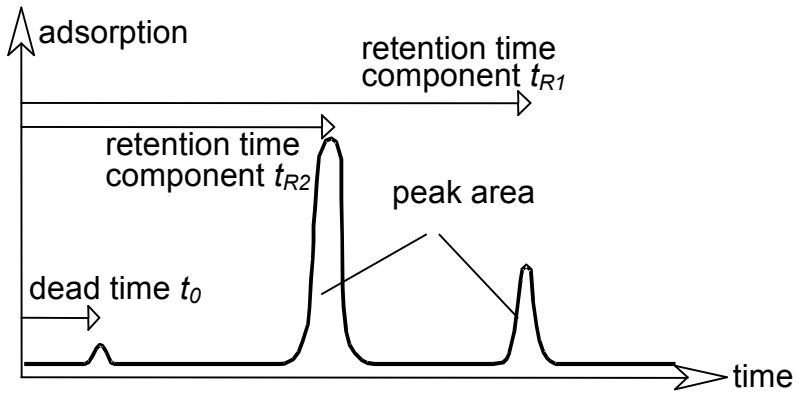

Figure 8: Schematic picture of a chromatogram.

A schematic picture of a chromatogram is given in figure 8. The dead time t_0 is an intrinsic property of a chromatographic setup, which is given by the time that is needed by the analyte to enter the column after injection. The retention time t_R of a compound is given as the time between injection and detection, also depending on the column length, temperature, and flow rate of the mobile phase. In order to compare different columns despite their length and flow rates, t_R can be corrected by the dead time t_0 yielding the dimensionless capacity factor k'

$$k' = \frac{t_R - t_0}{t_0}.$$

In order to separate two analytes, t_R and thus k' have to be different. The ratio of k' can be used to yield information about the separation behaviour, giving the selectivity α

$$\alpha = \frac{k_2'}{k_1'}, k_2' \geq k_1'.$$

The quality and efficiency of a chromatographic column can be expressed by the number of theoretical plates N existing in a column where a high number stands for a better separation. It can be altered by the packing material and procedure. The height equivalent to a theoretical

plate H is given as the distance in which the partitional equilibrium adjusts once. It can be determined by the column length L and N:

$$H = \frac{L}{N}.$$

H depends on the flow rate u of the mobile phase and some transport mechanisms and can be expressed by the so-called van Deemter equation:

$$H = A + \frac{B}{u} + C \cdot u.$$

The resulting van Deemter plot (see figure 9) consists of three graphs, each of which standing for one transport phenomenon (A: scattering diffusion, B: diffusion along the column, and C: matter exchange). The van Deemter curve shows a minimum indicating the optimal flow rate u_{opt} at which the separation should be performed.

The analyte molecules, transported through the column by the mobile phase, can take different pathways on the packing material which leads to a certain time gradient until all analyte molecules are eluted from the column. This effect is called scattering diffusion (see figure 10) and is enhanced by differences in particle size. In a porous stationary phase material, the matter transport in the pores is just determined by diffusion since the mobile phase cannot move in the pores. Here, the analyte molecule can interact with the stationary phase or diffuse back into the mobile phase.

These transport phenomena generally lead to band broadenings (e.g. “tailing”) in the chromatogram yielding worse separations [Meyer 99]. This can be circumvented by the application of smaller flow rates and/or non-porous particles [Schauff 03].

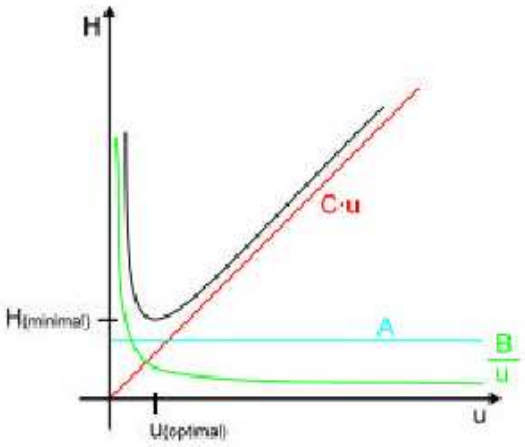

Figure 9: Van Deemter plot showing the “height equivalent to a theoretical plate” H curve from different transport phenomena (A scattering diffusion, B diffusion along the column, C matter exchange). U_{opt} indicates the optimal flow rate.

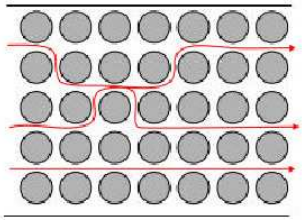

Figure 10: Schematic picture of the scattering diffusion. The red arrows indicate possible flow pathways between the phase particles (grey).

2.2.2 Stationary Phase Materials

Stationary phases for RP-HPLC mainly consist of pure polymer phases or silica-based materials, which can be surface-modified with organic molecules in order to change their polarity.

Pure polymer materials contain a major disadvantage, namely their lower pressure-stability and thus shorten the lifetime of the phase due to first deformation and second destruction of the particles. Therefore, they are limited to applications in low-pressure systems.

However, in RP-HPLC generally high pressure throughput is needed to obtain fast separations. Silica-based chromatographic sorbents are pressure-stable and known as particle and monolith materials. Both are widely used in chromatography.

Silica particles can be porous or non-porous (see figure 11 a) [Schauff 03]. Porous particles provide larger surfaces, thus such phases are highly loadable with analyte molecules. Disadvantages are the long retention times and band broadenings due to diffusion in the pores, whereas non-porous particles contain the advantage for fast separations. However, stationary phases, consisting of non-porous particles, have quite low loadabilities, resulting in effective materials for mainly analytical applications. Particles can be densly packed into columns leading to efficient analyte transport through the column. The particle size determines the pressure in the column which is higher for smaller particles, restricting the flow rate. To avoid scattering diffusion in a separation, all particles in a column should exhibit the same size. However, this is not always easy to accomplish by synthesis [Fischer 04, Schauff 03].

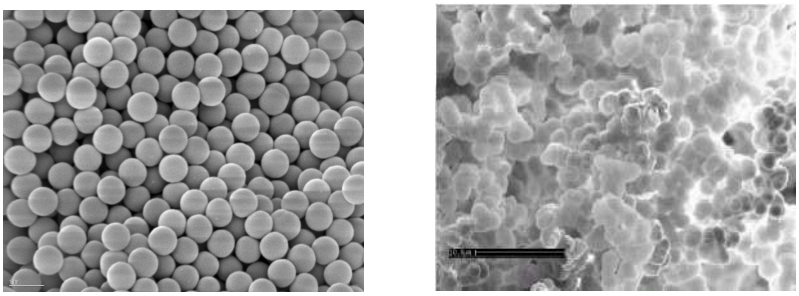

Figure 11: SEM picture of a) non-porous silica particles and b) an organic monolith.

Monoliths (see figure 11 b) are porous materials consisting of a single bead, the monolith, which is directly synthesized in a chromatography column to fit its size and therefore cannot be easily exchanged. The analyte is flushed through the pore network of the monolith. However, to rule out diffusion, a large pore network is advantegeous for an efficient matter transport [Courtois 06]. The decisive advantage of monolith phases is the low backpressure which is provided by the single bead [Miyabe 04, Roper 95].

Silica based materials are sensitive to acids and bases which is due to the reversibility of the sol-gel synthesis. The sol-gel synthesis produces silica [Stöber 68] and can be carried out in the acidic or basic medium. Thus the materials can “dissolve” in acids or bases leading to holes in the beads what can be partially circumvented by efficient organic modification.

Two different types of inorganic particle modification procedures are known, the covalent attachment of organic molecules via spacers to the surface and the surface coating with polymers. Both yield chromatographic sorbents which are highly applicable in RP-HPLC. Covalent modifications are generally more complicated and sometimes difficult to perform [Meyer 04] whereas coatings are easliy done in a solution polymerization step [Fischer 03, Schauff 03]. Coatings were first introduced by Partch et al [Partch 98, Bachmann 00] in order to prevent the destruction of silica when performing LC in the basic medium and to rule out interactions of analytes with residual silanol groups.

Since covalent modification of solid supports is performed using organosilanes, monomeric or polymeric stationary phases can be obtained by this procedure where the first is yielded from the reaction with a monofunctional silane, the latter from a trifunctional silane. The advantage of polymeric phases is due to their higher surface loading, and thus a more efficient coverage of the silica surface can be achieved.

The solid support of a chromatographic RP material (e.g. silica, titania) does not participate in the separation process. The organic modification is basically the interacting phase and can be

described as a immobilized solution, namely an interphase (see figure 12). But residual silanol groups also play an important role in the separation process.

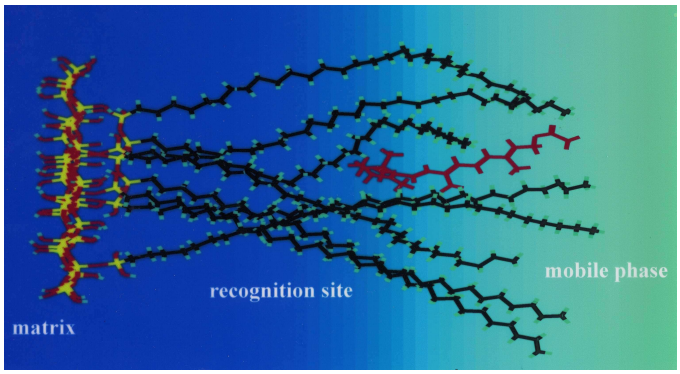

Figure 12: Schematic picture of an interphase, where the silica support is indicated as matrix. The analyte molecule (red) interacts with the stationary phase (black).

2.2.2.1 Characterization of Stationary Phases

Chromatographic RP materials can be characterized by infrared (IR) spectroscopy [Srinivasan 04] and solid-state NMR spectroscopy (see chapter 2.3 for solid-state NMR theory) yielding information about the solid support and the organic modification. The composition of silica can be monitored using ^{29}Si NMR spectroscopy since distinct silyl species can be resolved [Maciel 80]. A nomenclature for the silyl species was first given by Engelhardt et al [Engelhardt 87] (see figure 13). ^{13}C NMR spectroscopy can be used to characterize the organic modification of solid inorganic supports [Bayer 83]. Especially covalent modifications and thus a proof for the successful attachment of spacers can easily be monitored via NMR spectroscopy.

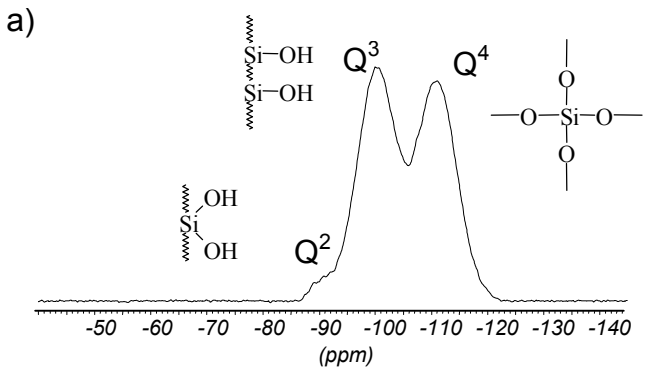

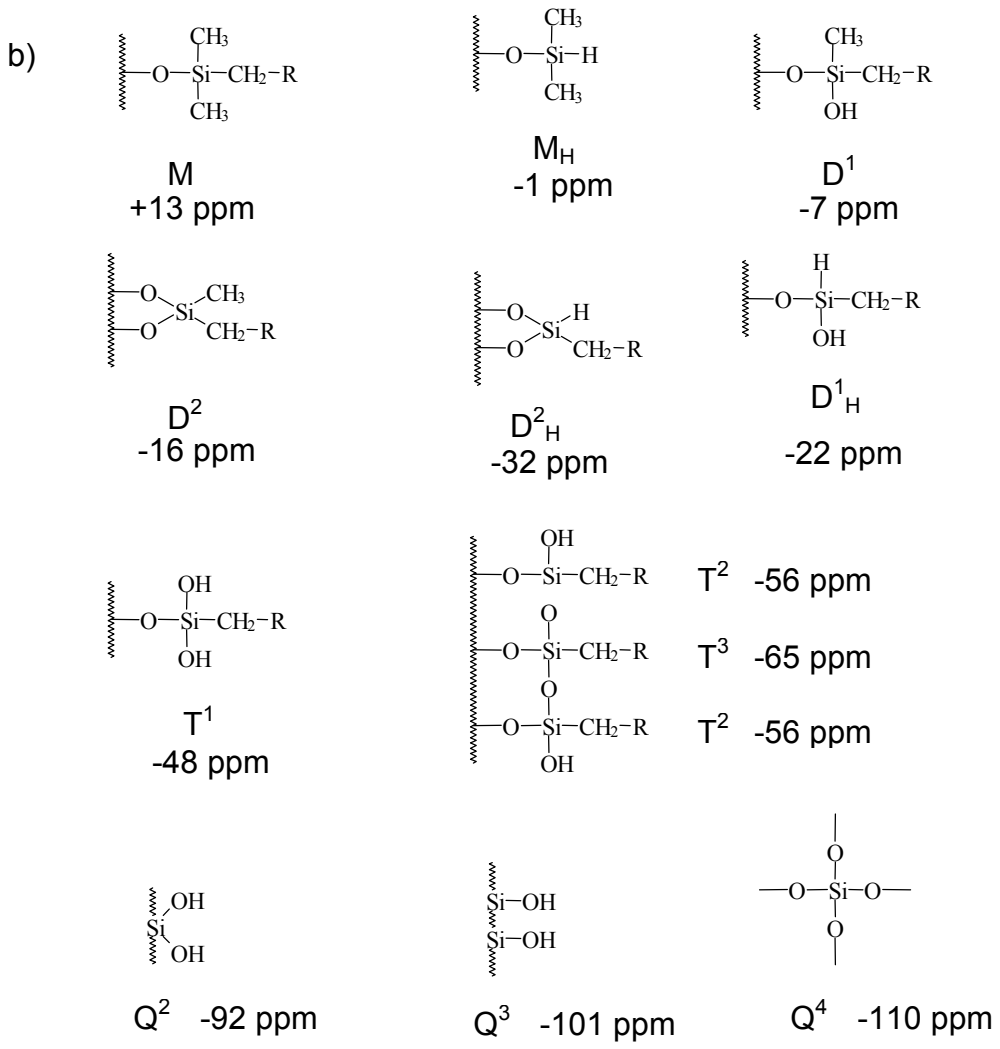

Figure 13: a) {^{1}H}-^{29}Si CP MAS NMR spectrum of non-porous silica particles and b) nomenclature of silyl species.

However, information also has to be gained about the particle size and the quality of the coating since both are important factors to obtain good separations. This can be achieved by scanning electron microscopy (SEM) (see figure 14 a for an example).

However, even though SEM is a powerful technique, light microscopy provides a much cheaper and faster method to screen large amounts of samples. For this, the particles are brought onto a microscope slide, and the background is coloured with ink (see figure 15) [Schetter 03]. An immersion oil light microscope can be used to observe the particles. The particle size can be extracted by comparison with a reference material (see figure 14 b for an example) [Fischer 04, Schauff 03].

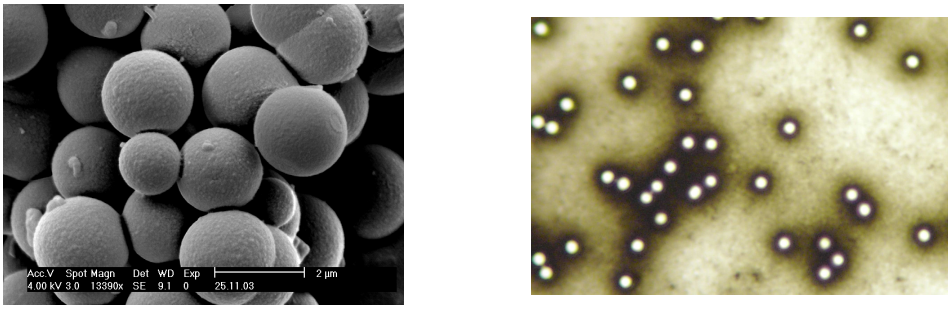

Figure 14: a) SEM picture of coated silica particles and b) light microscope picture of silica particles (coloured with ink).

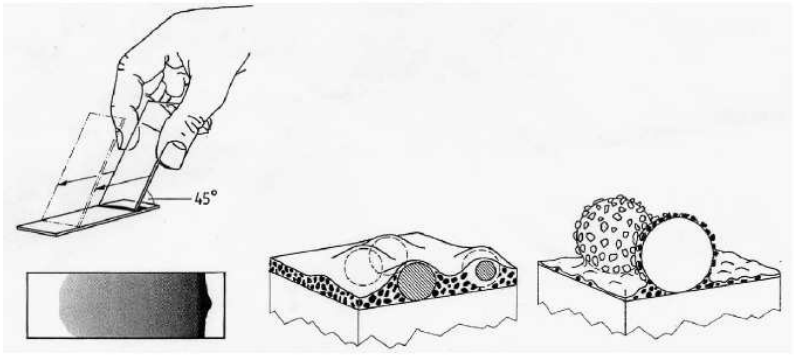

Figure 15: Schematic picture of the method to colour silica particles on a microscope slide.

2.2.2.2 Molecularly Imprinted Polymers

Materials which are able to separate analyte molecules due to a specific binding interaction are highly desirable in biological and environmental applications. Molecular recognition of so-called guest molecules is achieved by molecular imprinting of polymers [Dirion 03]. Molecularly imprinted polymers (MIPs) are widely used in separation techniques, above all in solid phase extraction (SPE) where target molecules are specifically “filtered” from a mixture. In contrast to pure chromatographic sorbents, ideal MIPs firmly bind their target molecules which will be exclusively washed by suitable solvents from the material after the binding step.

A highly specific binding is desired which leads to a special preparation technique in order to obtain suitable MIPs. MIP materials consist of pure polymers or coated silica-based materials, as particles or monoliths. However, the polymer will be imprinted by its polymerization in the presence of template molecules which are later the desired targets. Then the polymer is

crushed and rinsed with a suitable solvent in order to remove the template. The leftover is a material with a special imprint of the target molecule where it is supposed to rebind specifically from a mixture of various analyte molecules (see figure 16) [Welsch 05].

Since a high permeability is desired, the optimization of efficient materials porosity is necessary for each polymer and template which leads to time-consuming synthesis. This can be circumvented by the use of a substrate on which another polymer, containing the active sites, is grafted [Viklund 00]. The imprinted polymer then will form a shell around a preformed substrate which comprises already well-defined pore networks.

However, in aqueous solutions the hydrophobic surface of the organic polymer generally leads to non-specific binding due to hydrophobic interactions. Further, also unrelated non-polar compounds can bind to the MIP which has to be ruled out since the material will be blocked by undesired molecules and thus deteriorate. The MIP can generally be restored by washing procedures but sometimes has to be exchanged completely [Dirion 03].

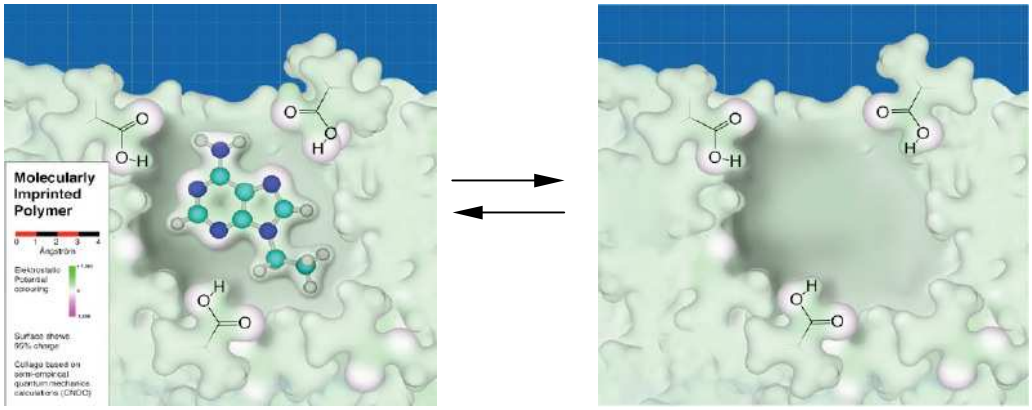

Figure 16: Schematic picture of a target molecule that rebinds at the imprint of a MIP. The principle is shown on the example of a polymer from EDMA and MAA with 9-ethyleneadenine as target.

2.3 Solid-state NMR Spectroscopy

While the signals in liquid-state NMR spectroscopy are mostly well resolved, solid-state NMR lineshapes often experience severe broadenings due to internal interactions present.
The most famous is the dipolar coupling which is caused by the spatial proximity of nuclear spins of the same kind (homonuclear) or different kinds (heteronuclear). Both lead to broadened peaks in the spectrum and can be circumvented by the application of additional techniques. Broadenings due to heteronuclear dipolar couplings can mostly be averaged out by Magic Angle Spinning (MAS) which will be presented in chapter 2.3.1 [Grant 96].
Nuclei with spin $I \geq 1$ possess an electric quadrupole moment Q that interacts with an electric field gradient (EFG) caused by the electrons of the molecule. This literally means that a quadrupolar nucleus "feels" a change in the molecular surroundings by the change of the EFG [Schmidt-Rohr 94]. Quadrupolar nuclei and the arising advantages and disadvantages will be discussed further on the example of ^2H ($I = 1$) in chapter 2.3.3.

2.3.1 Magic Angle Spinning

Anisotropic interactions among nuclear spins are generally averaged by the rapid tumbling motion of the molecules in solution-state NMR spectroscopy (Brownian motion). In solid-state NMR, anisotropic interactions (e.g. dipolar and quadrupolar) have a great influence on the resulting signal line shape. Various molecular orientations lead to many different resonance frequencies so that the resulting line shape is severely broadened.
This broadening can be overcome by a special technique called Magic Angle Spinning (MAS) [Lowe 59] in which the rotor is tilted at an angle of $\theta = 54.74°$, the magic angle, with respect to the external magnetic field and spun around its axis (see figure 17).

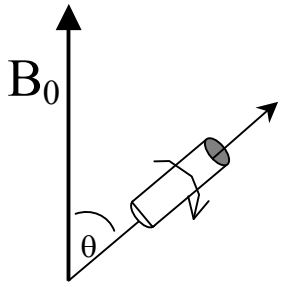

Figure 17: Rotor tilted in the magic angle.

Since the dipolar coupling is given by the equation

$$B_{lok} = \mu_i \frac{\left\langle 3\cos^2\theta - 1 \right\rangle}{R^3},$$

the overall expression will result in 0, if $\left\langle 3\cos^2\theta - 1 \right\rangle = 0$.

Desirable, the spinning frequency has to exceed the magnitude of the interaction frequency in order to average the interaction completely resulting in narrow lines. In most cases this is not possible since the maximum spinning frequency of commercial probeheads is nowadays in the range of 30-50 kHz. However, a moderate signal narrowing can still be achieved by applying lower spinning speeds.

2.3.1.1 Rotor Synchronization and Spinning Sidebands

With each rotation of the rotor, namely the rotor period τ_R, the resulting signal is refocussed which leads to the fact that the free induction decay (FID) consists of a series of rotational echoes (see figure 18).

When the data acquisition only takes place at the echo maxima (rotor synchronized), a single peak will result after the fourier transformation, and the anisotropic interactions will be averaged out. Acquisition of non-synchronized data points will lead to a set of spinning sidebands spaced by the MAS spinning frequency, arising from not fully averaged anisotropic interactions by MAS. The sidebands at low MAS spinning frequencies will show an envelope which resembles the static powder pattern so that information about the anisotropy of interactions can be extracted. However, fast MAS would combine the intensity of the sidebands under an intense center band and would consequently lead to small spinning sidebands.

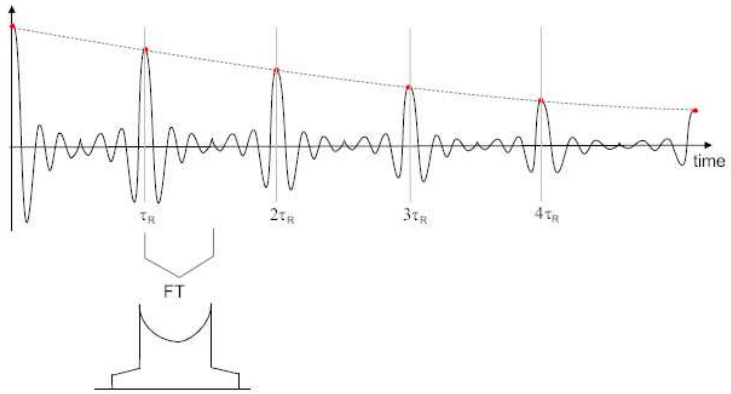

Figure 18: Free induction decay under MAS showing rotor echoes.

2.3.2 Basic NMR Experiments

2.3.2.1 One-pulse Experiment

The simplest NMR experiment is the so called one-pulse experiment (see figure 19) in which a single 90° pulse is applied on one kind of nuclei (e.g. ^{1}H).

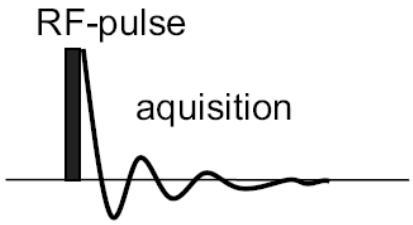

Figure 19: Sequence of the one-pulse experiment.

When a sample is brought into the external magnetic field (B_0), the nuclear spins will align along z (B_0) due to the Zeemann interaction that causes the splitting of the spins energy states in large magnetic fields. Consequently, all spins precess around the z-axis with the Larmor frequency, while the total magnetization is a vector which aligns along z in the undisturbed system.
Applying a 90°(x) pulse on an equilibrated system flips the magnetization from the z-axis into the xy-plane where the spins precess depending on their resonance frequencies. After the pulse is switched off, the magnetization returns to the z-axis with a rate given by the longitudinal relaxation time T_1. Meanwhile the spins precess in the xy-plane with the transverse relaxation time T_2 to destroy the coherent state [Grant 96].

2.3.2.2 Cross Polarization Experiment

Since NMR is a relatively insensitive method, the low natural abundance of some NMR nuclei (e.g. ^{13}C, n.a. = 1.1%) causes problems in the acquisition. Especially for ^{13}C, the magnetogyric ratio γ (^{13}C) is just a quarter of the γ (^{1}H) leading to prohibiting long acquisition times.
The time spent on the acquisition of well resolved spectra with reasonable signal-to-noise ratios can be significantly reduced by applying the cross polarization (CP) technique [Pines 72, Pines 73], which is normally combined with moderate MAS rates. It increases the

intensity in the spectrum by transferring the NMR properties of a high γ and abundant nucleus (e.g. ^{1}H) to the low γ nucleus in a double resonance experiment (see figure 20) [Stejskal 94].

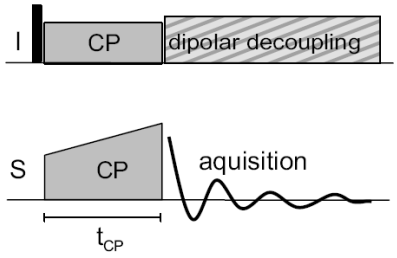

Figure 20: Pulse sequence of the CP technique, a double resonance experiment. The abundant spins I are decoupled during acquisition.

The ^{1}H magnetization is locked along the y-axis by applying a continuous weak 90°(y) rf pulse. The ^{1}H spins precess around the y-axis with their resonance frequency:

$\omega(^1H) = \gamma(^1H)B_1$

Another 90°(x) pulse is applied on ^{13}C which causes both nuclei to precess around y. During the contact time the polarization is transferred from the protons to the carbons by heteronuclear dipolar interactions. The magnetization transfer during the contact time can only be accomplished if the Hartmann-Hahn match is valid:

$\gamma(^1H)B_1(^1H) = \gamma(^{13}C)B_1(^{13}C)$.

Since the transfer strongly depends on dipolar couplings, one is forced to apply lower MAS frequencies. However, moderate spinning speeds are still desired to receive narrow lines.

2.3.2.3 Solid-echo Experiment

Free induction decays (FID) in solid-state NMR can be tremendously short yielding very broad lines. Occasionally, most of the FID is already decayed prior to the start of the acquisition. Here, switching delays of the NMR console have to be taken into account, as well as the dead time of each probehead: The applied rf pulses are much stronger than the resulting weak signals leading to a dead time in which the coil "rings" from the strong pulse while the FID cannot be recorded.

This loss of FID can be circumvented by the application of echo pulse sequences (see figure 21) in which a suitable refocussing pulse is applied after the initial 90° pulse and a following

delay τ. During the delay τ the spins evolve in the xy-plane and are refocussed after 2τ by a second pulse to form an echo.

The Hahn echo experiment uses a 180° pulse to generate the echo which is suitable for interactions like the heteronuclear dipolar coupling and the chemical shift [Hahn 50]. However, interactions like the quadrupolar and homonuclear dipolar coupling are refocussed by a 90° pulse which is phase shifted by 90° to the initial pulse [Schmidt-Rohr 94]. This solid-echo experiment is particularly interesting for the acquisition of ^{2}H spectra since molecular reorientations during the echo delay lead to characteristic changes in the line shape and thus yield information about molecular correlation times [Macho 01]. For further discussion please see section 2.3.3.

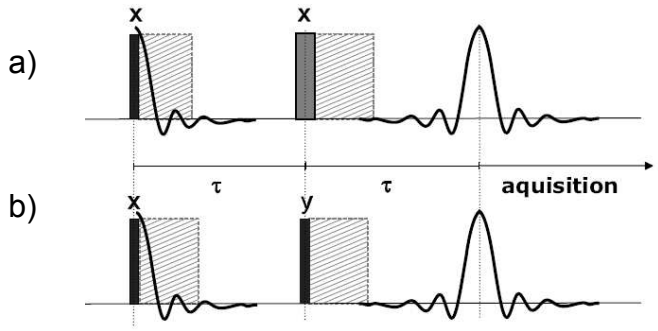

Figure 21: Experimental sequence of the a) Hahn echo experiment and the b) solid-echo experiment. The grey shaded areas indicate the dead time.

2.3.3 ^{2}H NMR Spectroscopy

Quadrupolar nuclei with spins I ≥ 1 possess an intrinsic electric quadrupole moment Q, which interacts with an electric field gradient (EFG) tensor of the molecule caused by surrounding electrons. The quadrupolar coupling constant c_Q then is given as

$$c_Q = \frac{e^2 qQ}{\hbar}.$$

^{2}H NMR is a well-known and established method to study molecular dynamics since the lineshape is influenced by the position of the EFG tensor yielding information about the molecular geometry [Macho 01, Schmidt-Rohr 94, Spiess 83]. For deuterons the quadrupolar coupling constant Q is rather small, and c_Q is normally in the range of 125-130 kHz.

Rotation of the molecule causes a change of an EFG tensor which influences the resulting quadrupolar coupling, leading to characteristic lineshapes in static ^{2}H spectra (see figure 22

for an example). In intermediate motional regimes, a loss in signal intensity is evidenced if the frequency of molecular motion is interfering with the quadrupolar frequency ω_Q due to their similar time scales. The degree of interference is characterized by the reduction factor *R*. In these regimes, even superpositions of distinct deuteron patterns can be observed, reflecting the two extreme limits [Villanueva 06, Rössler 90].

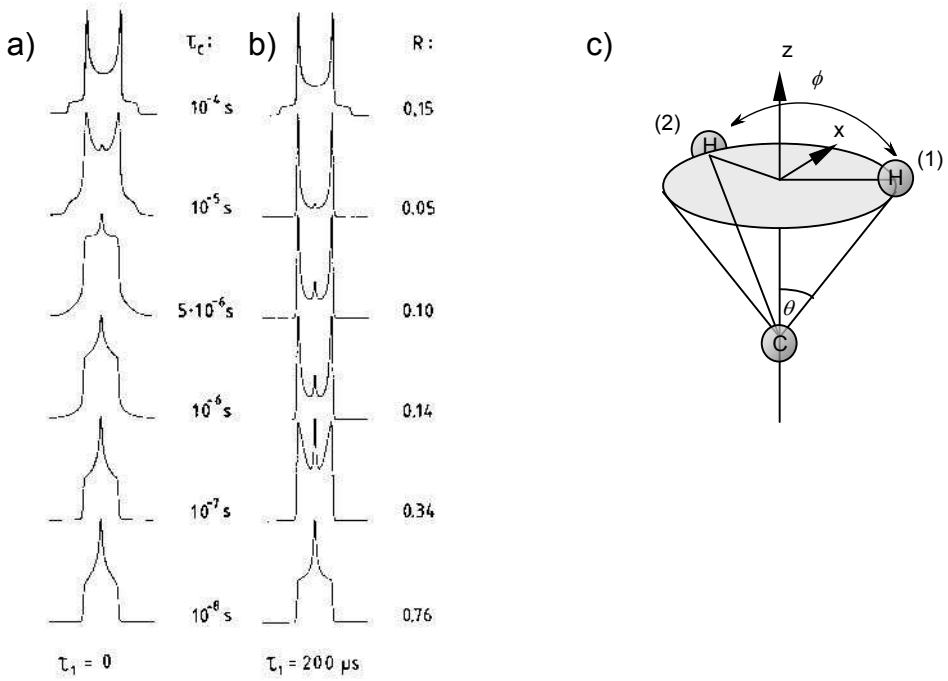

Figure 22: Simulated static ^2H spectra demonstrating the effect of a change in a) motional correlation time τ_c and b) reduction factor R on the lineshape [Spiess 85].
c) Schematic picture of the cone model.

The low natural abundance of deuterons (n.a. = 0.0155%) usually requires the enrichment of samples, e.g. by dissolving them in suitable deuterated solvents. The selective deuteration of acidic protons via simple exchange establishes a decisive advantage.

Under MAS conditions, the quadrupolar coupling information is completely lost in favour of chemical shift resolution. The experiments can easily be performed but the magic angle has to be set properly since even the slightest misadjustment will have a great influence on the resulting linewidth. However, information about the molecular dynamics can still be extracted, though to a smaller extent. In particular, both the linewidth and peak intensities are good indicators for dynamics showing severe linebroadenings and the decrease of intensity when shifting from the slow dynamic limit to an intermediate regime where the mobility is in the range of the quadrupolar coupling constant. This leads to an almost complete loss of signal at this point.

Activation energies for distinct dynamic processes can be obtained from an Arrhenius plot of the linewidth versus the inverse temperature.

The decrease and eventually complete loss of signal strongly depends on the motional correlation time τ_c of the species present in the system. If all molecules move with the same rate k ($\approx 1/\tau_c$), a minimal signal at $\tau_c \sim c_Q$ can be observed. Since in disordered systems (e.g. polymers), motional processes are less defined, the moving species will most likely experience a broad distribution of correlation times (see figure 23) [Wehrle 87]. In this case, no pronounced minimum is found.

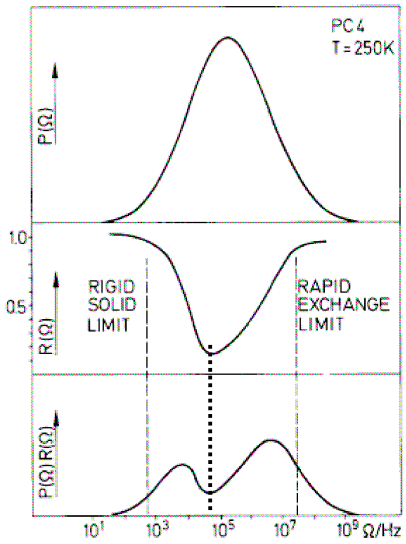

Figure 23: Simulation of a Gaussian motional correlation rate distribution P(Ω) on the example of PC4 [Wehrle 87]. The reduction factor R(Ω) is characterized by the loss in spectral intensity. The distribution in the total spectrum is governed by both factors P(Ω)R(Ω), yielding a signal intensity which differs from the true distribution P(Ω).

Due to selective deuteration of the acidic sites, it is possible to use ^{2}H NMR spectra for a more thorough assignment of proton spectra since these often do not show a sufficient resolution. The higher resolution in deuteron spectra is caused by spin dilution and smaller ^{2}H dipolar couplings. Another advantage is the similarity of chemical shift in ^{1}H and ^{2}H spectra even of hydrogen bonds so that they can be easily compared.

2.4 Suspended-state HR-MAS NMR Spectroscopy and its Application in Chromatography

Suspended-state high resolution magic angle spinning (HR-MAS) NMR spectroscopy is a hybrid technique between solid-state and liquid-state NMR spectroscopy [Moka 97, Tomlins 98]. It comprises the advantages of both techniques, yielding well resolved spectra even for samples that do not dissolve in any solvent [Händel 03].

Solid samples can be characterized by preparing a slurry in suitable solvents, transfer them to a rotor, and directly measure them under moderate MAS frequencies. By the increase in mobility of the solid via swelling, the ^{1}H homonuclear dipolar interactions and thus the linewidths decrease, yielding narrow lines. Eventually, even spectral resolution of emulsions can be increased comparing liquid-state NMR to suspended-state NMR (see figure 24 for an example) [Tseng 00].

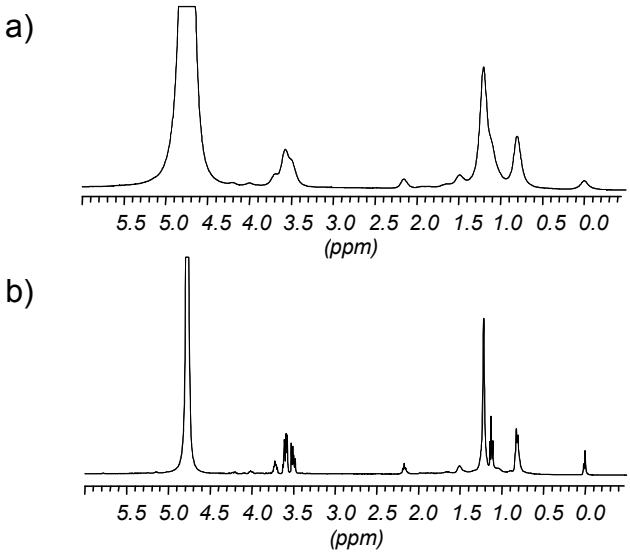

Figure 24: ^{1}H a) liquid-state and b) suspended-state HR-MAS NMR spectra of a skin lotion.

Many attempts have been made to study the numerous interactions taking place in a chromatographic separation process via NMR spectroscopy since chromatograms only show the sum of all interactions, and the retention mechanisms are still not fully understood. In solid-state NMR spectroscopy the chromatographic sorbent (eventually with rebound analyte) can be investigated. Liquid-state NMR spectroscopy gives an insight in the analyte, dissolved in the mobile phase. However, both techniques lack of picturing the complete process which is given as a sensitive system of the analyte, the mobile phase, and the stationary phase.

On the contrary, suspended-state HR-MAS NMR spectroscopy showed to be suitable to monitor the chromatographic processes since the chromatographic sorbent can be suspended, and the analyte can be dissolved in the mobile phase. The addition of solvent allows the alkyl chains of the stationary phase to increase their mobility transforming into the interphase. Thus, interactions between stationary phase and the analyte, in the interphase, can directly be mimicked [Hellriegel 04, Händel 03, Skogsberg 04, 06]. However, some differences towards chromatography have to be considered: The solid to liquid ratio is somewhat different in NMR spectroscopy since the rotor offers limited space, and the flow rate cannot be a part of the NMR model [Pages 06].

2.4.1 Saturation Transfer Difference Experiment

A special suspended-state ^{1}H HR-MAS NMR experiment, the saturation transfer difference technique (STD), was developed by Mayer et al. It is generally used to investigate receptor-ligand interactions taking place at the active sites of proteins [Mayer 99].
Macromolecules (e.g. polymers) can be selectively saturated by irradiation with a train of shaped pulses (see figure 25 for pulse sequence), and a complete saturation of the polymer is yielded due to efficient spin diffusion [Raitza 98]. The saturation then is transferred to ligands or analyte molecules, interacting/binding with the polymer. These saturated analyte molecules dissociate in a time scale, where the degree of saturation depends on the time the molecules were bound to the macromolecule (see figure 26). In solution the analyte can be studied by NMR spectroscopy yielding narrow lines. However, since it still memorizes the saturation for some time, ^{1}H peaks of molecules which were in contact with the polymer are reduced in intensity.

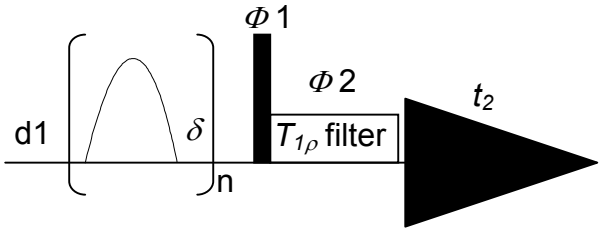

Figure 25: Pulse sequence of the STD NMR experiment.

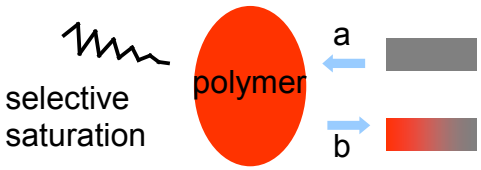

Figure 26: Schematic picture of the saturation transfer from the polymer (red) to the analyte (grey).

In order to obtain spectra only showing the saturation effects on analyte molecules, a difference experiment is performed. The spectrum of a non-saturated system is substracted from a saturated system by an appropriate phase cycle after each scan. This can be achieved by the acquisition of one spectrum with on-resonant and one spectrum with off-resonant irradiation. Both irradiation frequencies have to be set properly, the on-resonance frequency has to be set in some distance of the analyte signals or sidebands to prevent incident, direct saturation of the analyte. However, the pulse still saturates the polymer due to its broad background signal. On-resonance frequencies can be set in the range of ~ -1 ppm, off-resonance frequencies in the range of ~40 ppm [Meyer 03]. An additional spinlock filter (see figure 24) suppresses the background signal of the polymer in the difference spectrum.
In the difference spectrum, ^{1}H peaks can be observed, which are increased in intensity due to the analytes adsorption to the macromolecule. Thus, information about the affinity of analyte molecules to interact with a certain polymer can be obtained.

3 Structure and Dynamics of Phosphonic acids

Since phosphonic acids are promising materials for high temperature fuel cell applications they were investigated in this study. The main work focussed on the properties of the phosphonic acid groups, namely on their dynamics and anhydride formation.

3.1 Characterization of Phosphonic acids

3.1.1 Methylphosphonic acid

Methylphosphonic acid (MePA) is a crystalline, colourless, and strongly hygroscopic compound.

The ^{1}H MAS NMR spectrum shows two peaks, at 11.2 ppm for the acid protons and 1.5 ppm for the methyl group (see figure 27). The strong shift to high fields of the acid protons signal indicates the presence of considerable strong hydrogen bonds in the sample. With increasing water uptake, an additional signal at 9 ppm starts to rise reflecting adsorbed water. This will be further detailed in chapter 3.2.2.

Since a crystal structure could not be obtained by now, due to the strong hygroscopicity of MePA, the molecular structure was confirmed by a ^{1}H-^{1}H DQ NMR spectrum (see figure 28).

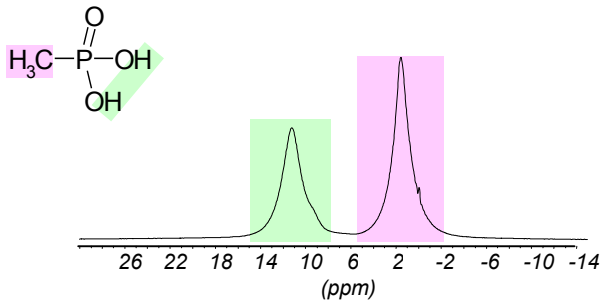

Figure 27: ^{1}H MAS NMR spectrum of MePA.

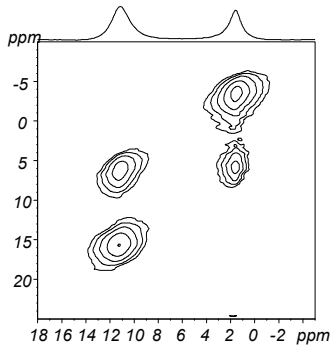

Figure 28: ^{1}H-^{1}H DQ MAS NMR spectrum of MePA.

The ^{31}P MAS NMR spectrum of MePA at room temperature shows one peak at 37.5 ppm resulting from the phosphonic acid group (see figure 29). It indicates that the acid groups in MePA do not form condensation at room temperature, but after annealing the sample at 120 °C for 4 days, an additional signal at 30.7 ppm reveals anhydride formation of the acid groups [Lee].

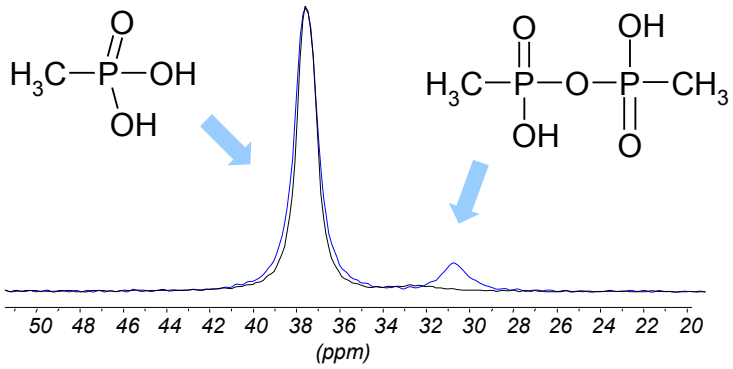

Figure 29: ^{31}P MAS NMR spectra of MePA (black) and annealed MePA (blue) indicating the "free" acid and the anhydride.

3.1.2 Polyvinylphosphonic acid Ionomer

A polybenzimidazole (PBI) membrane containing a polyvinylphosphonic acid (PVPA) ionomer is an industrial product for the application in fuel cells. The membrane containing the ionomer and the pure ionomer were characterized independently.

The membrane is a brown-coloured flexible material whereas the pure ionomer is yellowish and brittle. The ionomer is strongly hygroscopic and thus water-soluable. In contrast, the membrane does not dissolve but rather swells while being stirred in water.

In the ^{1}H MAS NMR spectrum three peaks at 10.7 ppm (acid protons), 6.2 ppm (adsorbed water), and 2.2 ppm (vinyl backbone) could be observed (see figure 30). The nature of the ionomer can be derived from the ^{31}P MAS NMR spectrum where a distribution between the two peaks at 33 ppm and 19 ppm is visible (see figure 31). The broad high frequency signal was assigned to PVPA, the narrow low frequency signal to vinylphosphonic acid (VPA). Since a distribution between both signals is conspicuous, it is concluded that oligomers are also present in the sample.

The ^{1}H and ^{31}P MAS NMR spectra of the membrane containing the ionomer show the same peaks including a broad background from the PBI protons in case of the ^{1}H spectrum. The $\{^{1}H\}$-^{13}C CP MAS NMR spectrum is shown in figure 32.

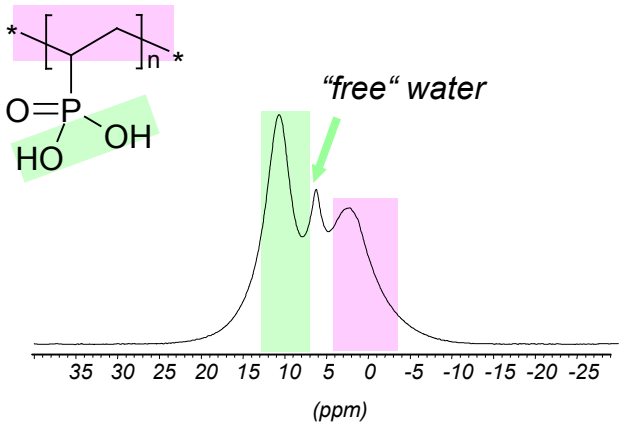

Figure 30: ^{1}H MAS NMR spectrum of PVPA ionomer.

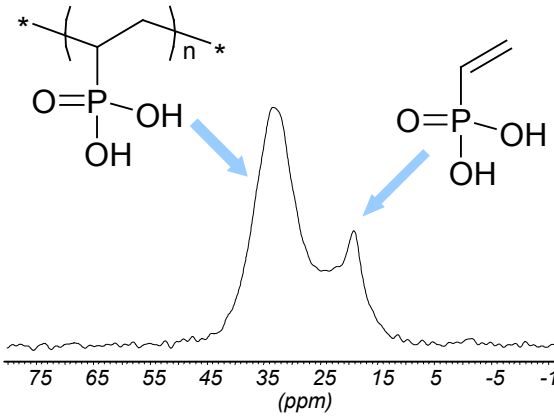

Figure 31: ^{31}P MAS NMR spectrum of PVPA ionomer.

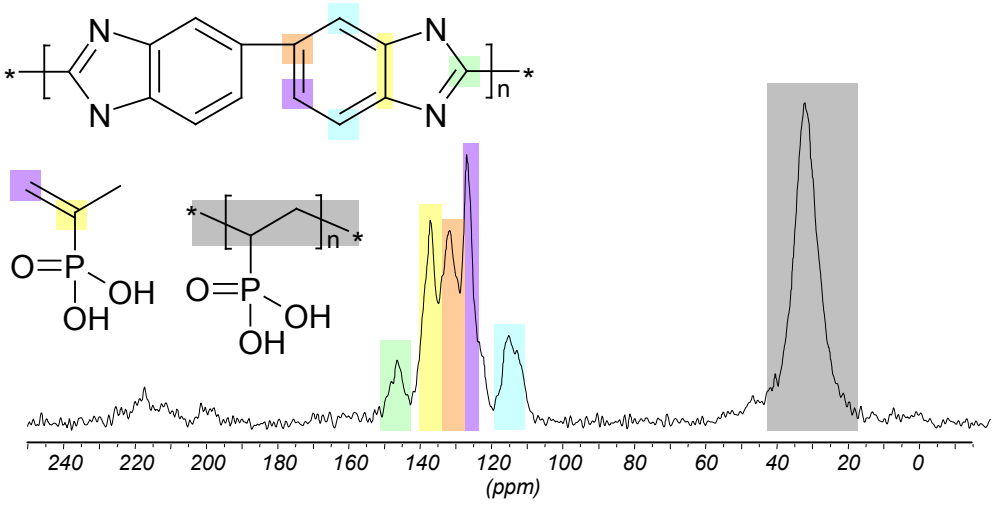

Figure 32: $\{^{1}H\}$-^{13}C CP MAS NMR spectrum of PVPA ionomer.

3.1.3 Polyvinylbenzylphosphonic acid

Polyvinylbenzylphosphonic acid (PVBzPA) consists of a meta- and para-isomer mixture (see figure 33 for the structure). It is a brownish non-hygroscopic sample which can be dissolved in methanol [Markova].

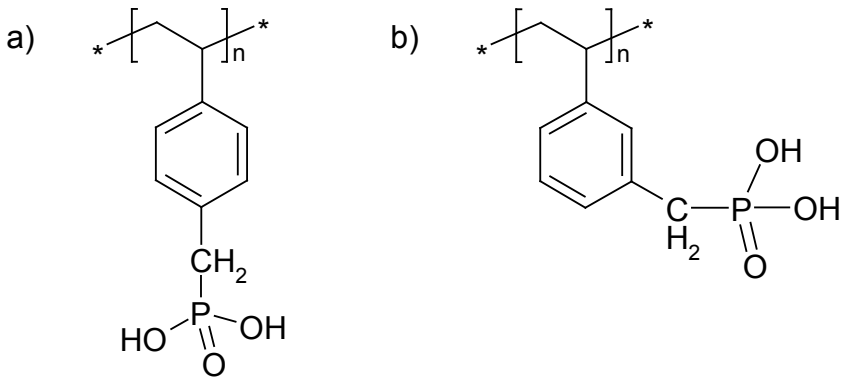

Figure 33: a) Para- and b) meta-isomers of PVBzPA.

The ^{1}H MAS NMR spectrum of PVBzPA shows peaks at 8.6 ppm, 7.2 ppm, and 3.2 ppm which were assigned to the acid protons, the aromatic ring protons and the polyvinyl backbone protons (see figure 34). In the ^{31}P MAS NMR spectrum a single signal at 27 ppm for the acid is visible which can be converted into two signals at 27 ppm and 20 ppm by annealing the sample at 200 °C for 18 hours (see figure 35). The peak at 20 ppm most probably reflects the condensation product.
The {^{1}H}-^{13}C CP MAS NMR spectrum is given in figure 36.

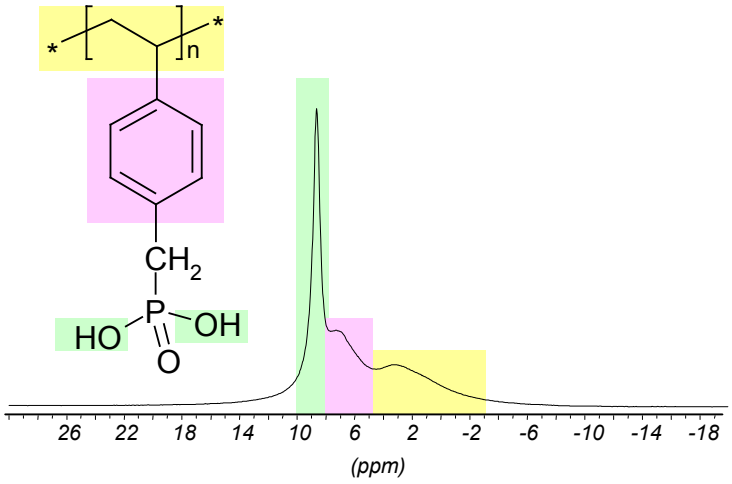

Figure 34: ^{1}H MAS NMR spectrum of PVBzPA.

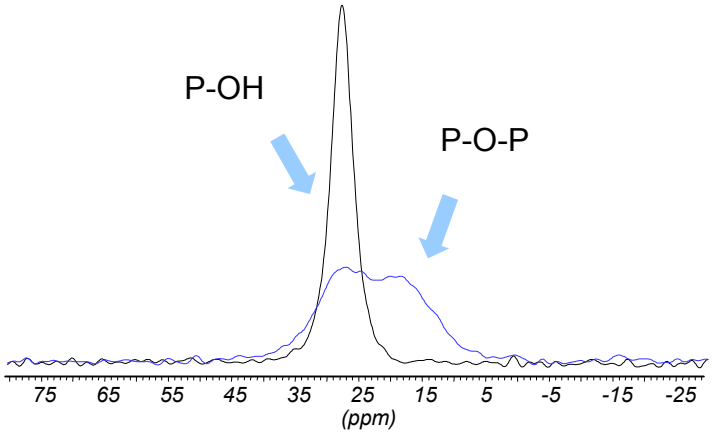

Figure 35: ^{31}P MAS NMR spectrum of PVBzPA.

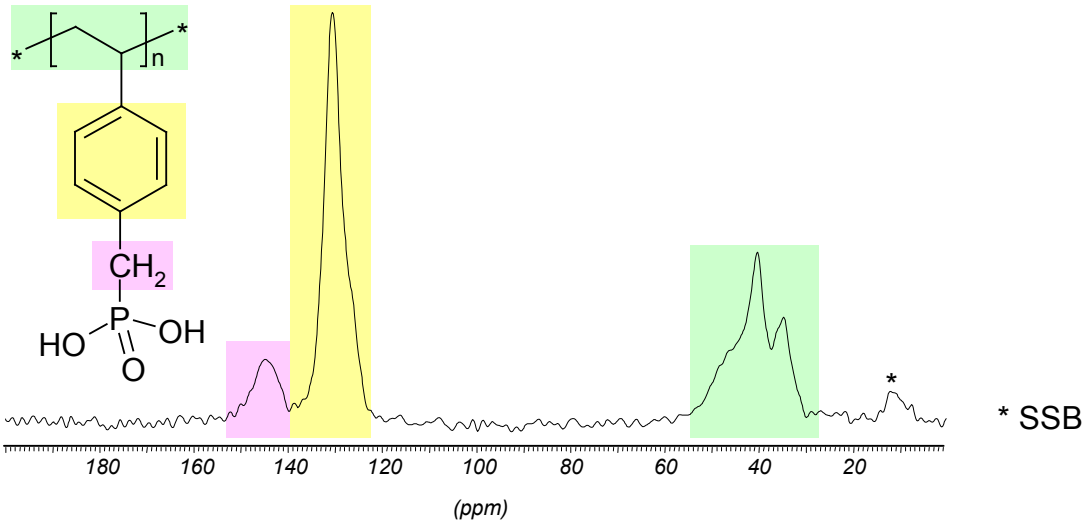

Figure 36: $\{^{1}H\}$-^{13}C CP MAS NMR spectrum of PVBzPA.

3.1.4 Polyphosphazenephosphonic acid

Polyphosphazenephosphonic acid (PPPA) is a strongly hygroscopic colourless sample [Allcock 02]. Two different batches were investigated: The first contained two phases, a rather viscous, and a crystalline fraction (see figure 37). The crystals were manually separated from the viscous, amorphous material revealing differences in the solid-state NMR spectra. However, a complete separation could not be accomplished.

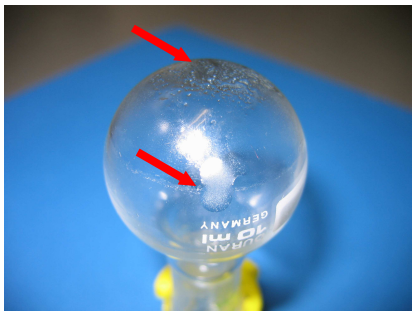

Figure 37: Picture of the crystalline and the amorphous phase in PPPA, both indicated by red arrows.

The ^{1}H MAS NMR spectra for the two phases and the structure are given in figure 38. Two sets of peaks are visible at ~8 ppm (acid) and ~3 ppm (spacer). The difference between the crystalline and the amorphous phase can be clearly seen since the peaks are much broader for the viscous sample. The observed chemical shifts of both spectra are in good agreement, the signals assigned to the spacer and the lower frequency peak of the acid resonating at about 7 ppm. A splitting of the low frequency set of peaks can be observed for the crystalline phase. However, the ^{1}H chemical shift of the samples higher frequency peak differ. The acid group of the crystalline phase resonates at 8.6 ppm and the one of the amorphous phase at 9.2 ppm. Due to the uncomplete separation of phases, it is assumed that the peak at about 7 ppm can be assigned to the viscous sample.

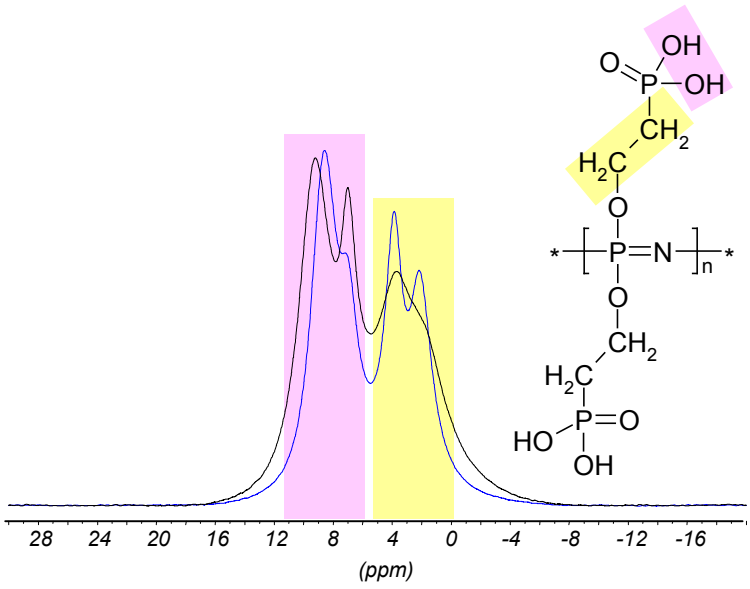

Figure 38: ^{1}H MAS NMR spectra of the crystalline (blue) and the amorphous (black) phase of PPPA.

The peak at 1 ppm in the ^{31}P MAS NMR spectrum (see figure 39) was assigned to the polyphosphazene backbone, the acid groups to either the signals at 27 ppm and 24.5 ppm (viscous phase) or 24 ppm (crystalline phase), respectively. The mere presence of the signal at 27 ppm for the viscous compound is anticipated for a pure amorphous phase. It is known from PVPA that phosphonic acid anhydride resonates at lower frequencies than the acid itself with a ^{31}P chemical shift difference of about 10 ppm [Lee]. A similar shift difference was also observed for MePA, PVBzPA, and siloxane phosphonic acid. Then, in PPPA the resonance at ~24 ppm most likely does not result from condensation. The second peak for the acid probably points out two phosphonic acid groups with different magnetic surroundings in the crystal. However, the presence of amorphous and crystalline phase in the sample indicate its poorly defined condition.

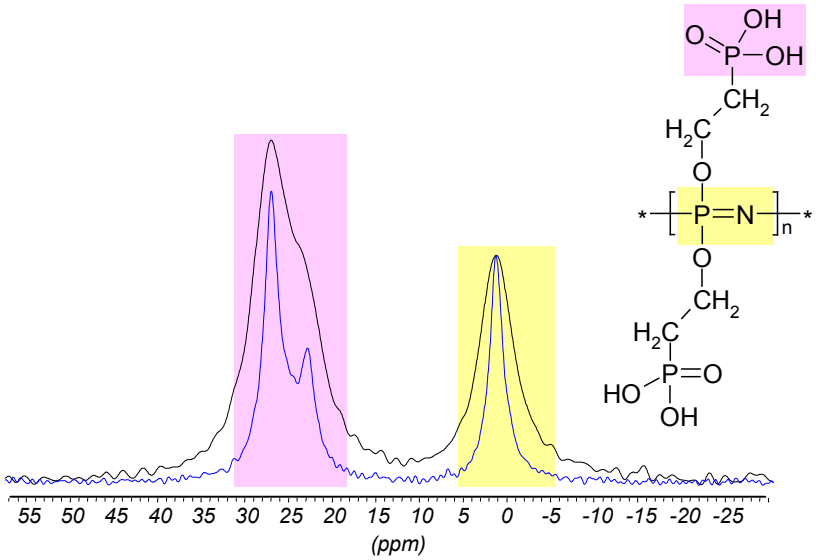

Figure 39: ^{31}P MAS NMR spectra of the crystalline (blue) and the amorphous (black) phase of PPPA.

The second batch of PPPA consists of a purely amorphous sample. It is a whitish, strongly hygroscopic, and firm compound. The ^{1}H and ^{31}P MAS NMR spectra were quite similar to those of the viscous sample in the first batch but showed broader peaks, in general indicating the amorphous nature of the sample.

3.1.5 Polyvinylbenzylphosphonic acid / Polyetheretherketon Blockcopolymer

Polyvinylbenzylphosphonic acid / polyetheretherketon ABA blockcopolymer is a greenish coloured powder that is only soluble in DMSO.

Its structure and ^{1}H MAS NMR spectrum are shown in figure 40. The four peaks at 8.9 ppm, 7.2 ppm, 3.8 ppm, and 1.3 ppm were assigned to the acid protons, the aromatic ring protons, the CH_2 protons, and the methyl protons respectively.

The single peak at 26 ppm observed in the ^{31}P MAS NMR spectrum (see figure 41) indicates no anhydride formation in the sample.

The $\{^{1}H\}$-^{13}C CP MAS NMR spectrum is given in figure 42.

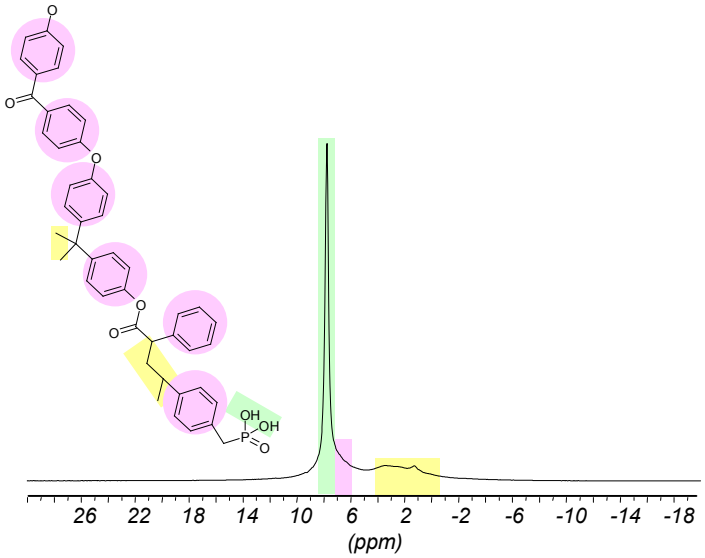

Figure 40: Structure and ^{1}H MAS NMR spectrum of PVBzPA/PEEK copolymer.

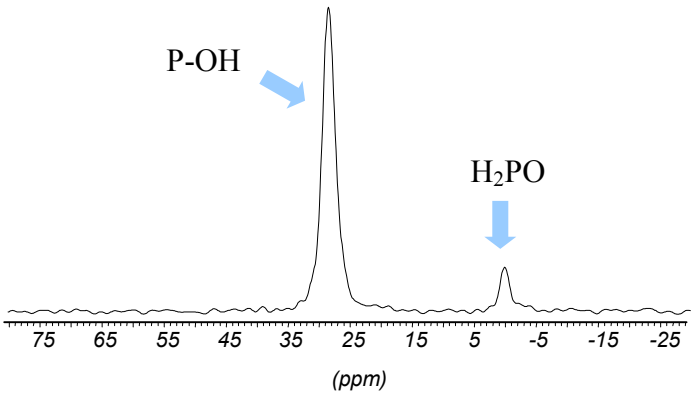

Figure 41: ^{31}P MAS NMR spectrum of PVBzPA/PEEK copolymer.

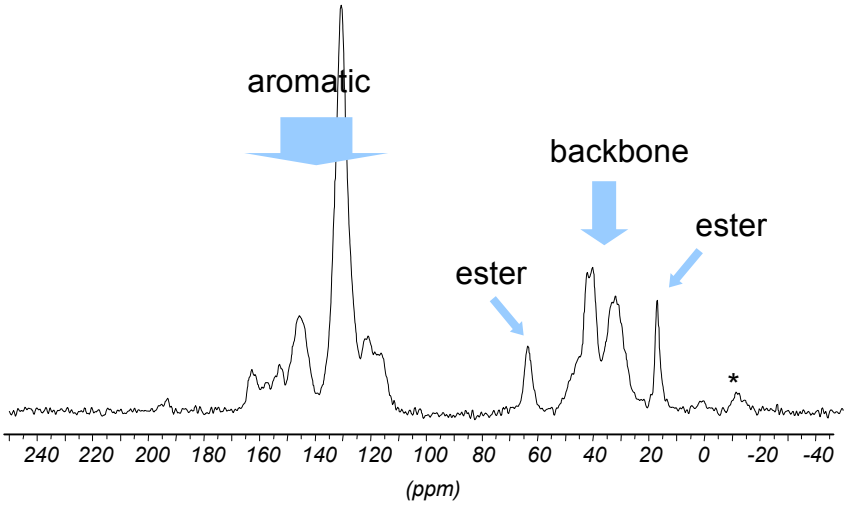

Figure 42: {^{1}H}-^{13}C CP MAS spectrum of PVBzPA/PEEK copolymer.

3.1.6 Siloxanephosphonic acid

Siloxanephosphonic acid (SPA) is a viscous, colourless, and highly hygroscopic compound [Steininger 06]. It consists of cyclic oligosiloxanes (n = 3-5) containing spacers with one phosphonic acid group at the end of each spacer (see figure 43).

The corresponding ^{1}H MAS NMR spectrum shows three peaks at 10 ppm, 1.3 ppm, and 0.2 ppm, respectively, which were assigned to the acid protons, the spacer protons and the methyl protons (see figure 43).

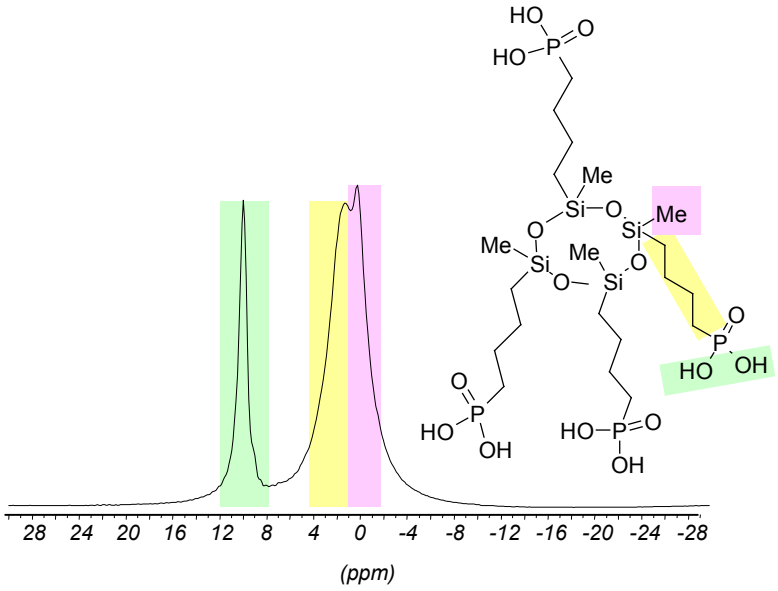

Figure 43: Structure and ^{1}H MAS NMR spectrum of SPA (n = 4).

The ^{31}P MAS NMR spectrum strongly suggests the presence of anhydride even at room temperature, indicated by the signals at 32 ppm and 22 ppm where the high frequency signal is the “free” acid group (see figure 44).

The {^{1}H}-^{13}C CP MAS NMR spectrum is given in figure 45.

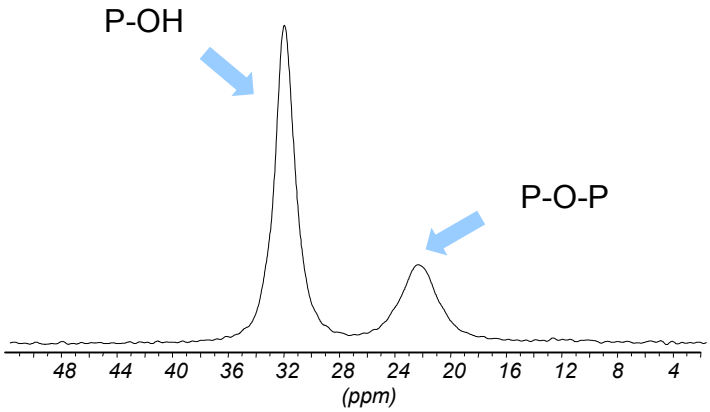

Figure 44: ^{31}P MAS NMR spectrum of SPA.

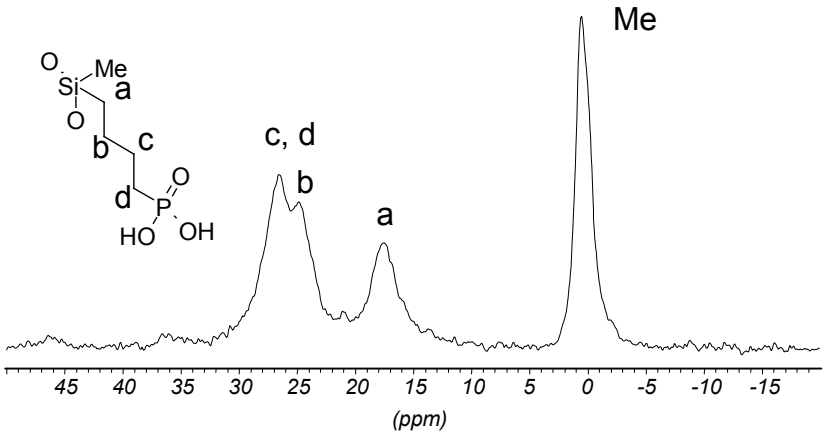

Figure 45: {^{1}H}-^{13}C CP MAS NMR spectrum of SPA.

3.2 Water Uptake Studies

Some phosphonic acids show a pronounced affinity to anhydride formation even at room temperature, while other samples can be forced to condensate upon annealing.
However, the occurring condensation reflects a significant obstacle on the way to high proton mobilities especially at higher temperatures. If we prefer dry structural diffusion to be responsible for the phosphonic acid proton conductivity above 100 °C, condensation most probably prevents the proton transport by both reducing the amount of charge carriers and hampering the formation of hydrogen bridges.
The effects of anhydride formation were examined in more detail by water uptake studies for PVPA. Small sample amounts were stored for several days in open aluminum containers over various saturated salt solutions in Erlenmayer flasks equipped with stoppers, thus equilibrating the samples in different well-defined water atmospheres [Greenspan 77]. The respective water uptake was measured by weight, Karl Fischer analysis [Fischer 35], and solid-state NMR spectroscopy.

3.2.1 Polyvinylphosphonic acid

The ^{31}P MAS NMR spectrum of pure PVPA [Bingöl 06] exhibits signals at 33 ppm and 24 ppm, respectively, that were assigned to “free” phosphonic acid groups and the condensated form. A dried sample of PVPA leads to three signals in the ^{1}H MAS NMR spectrum at ~10.6 ppm for the acid protons, 6 ppm for adsorbed water and 2.2 ppm for the polyvinyl backbone protons (see figure 46 and 47 for assigned ^{1}H and ^{31}P spectra).

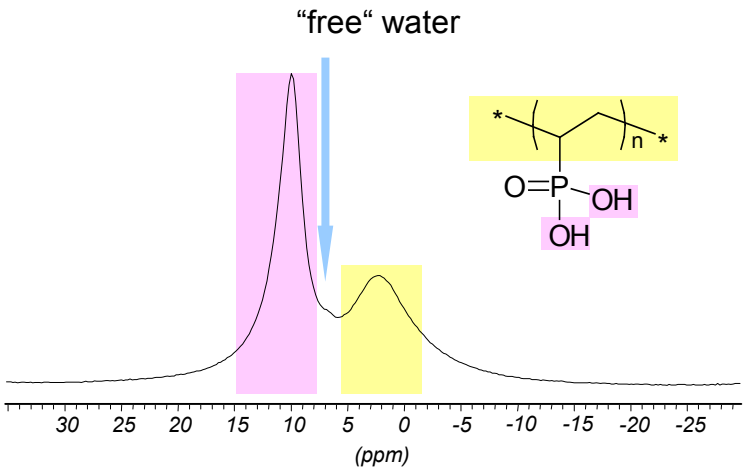

Figure 46: ^{1}H MAS NMR spectrum of PVPA.

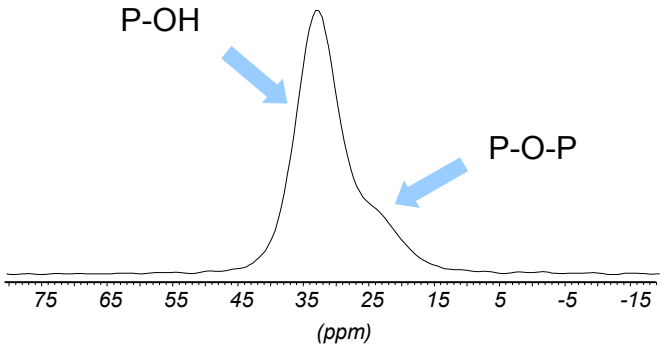

Figure 47: ^{31}P MAS NMR spectrum of PVPA.

When PVPA is stored in well-defined water vapor atmospheres, an uptake of water is monitored via NMR spectroscopy. The corresponding ^{31}P MAS NMR spectra (see figure 48) clearly indicate that the amount of condensation is reduced by water uptake, while it increases by drying PVPA.

The comparison of the ^{1}H MAS NMR spectra of the PVPA samples (see figure 49) reveals that only one peak in the spectra changes significantly upon water uptake. The high frequency signal narrows and shifts to lower frequencies with uptake of water until it finally reaches the chemical shift of adsorbed water. This is most likely due to the adsorption of water at the acidic phosphonic acid groups forming hydration shells [Pereira 01]. The ^{1}H chemical shift is much more sensitive to the water load in the sample than the ^{31}P shifts. Unexpectedly, the chemical shift and the observed integral of the adsorbed water peak at ~6 ppm remains unchanged for all samples. Since uptaken water is most likely adsorbing at the phosphonic acid groups, it can be assumed that “free” water is already trapped within the PVPA backbone during synthesis. This is supported by an annealed sample still showing the peak at 6 ppm.

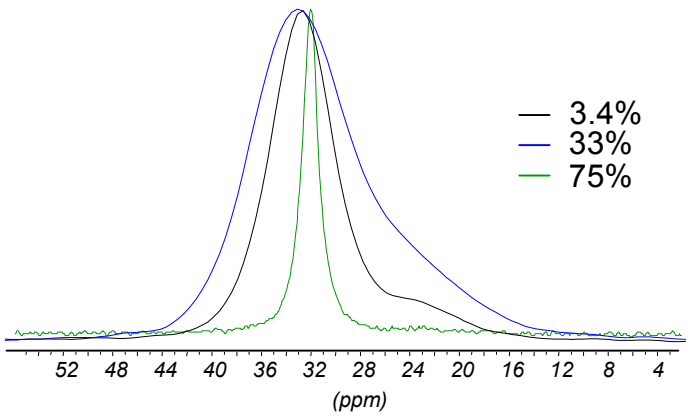

Figure 48: ^{31}P MAS NMR spectra of PVPA samples which were stored in different water atmospheres. Relative humidities are given in the right corner.

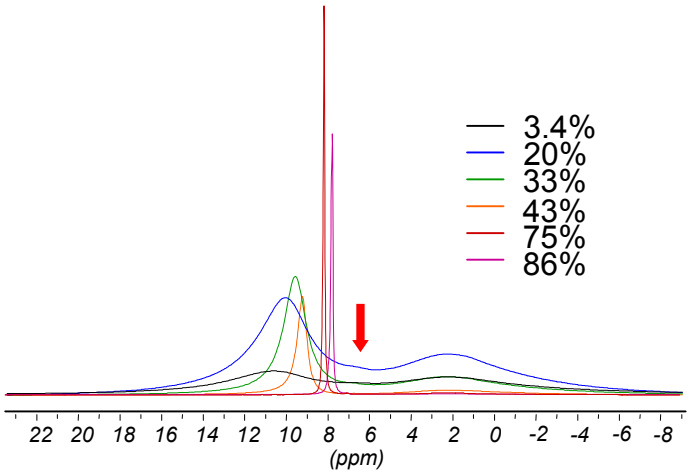

Figure 49: ^{1}H MAS NMR spectra of PVPA samples which were stored in different water atmospheres. Relative humidities are given in the right corner. The red arrow indicates the water peak at ~6 ppm.

A freeze-dried PVPA sample was directly measured yielding a ^{1}H chemical shift and a degree of condensation comparable to a sample stored in a water vapor atmosphere of 20% indicating the strong hygroscopicity of PVPA.

The ^{1}H and ^{31}P spectra were deconvoluted employing both DM-Fit [Massiot 02] and WinNMR [Bruker]. The integrated fraction of adsorbed water is consistent with the data obtained from weight analysis and Karl Fischer titration [Kaltbeitzel]. The amount of water in PVPA could be estimated from the assumed linear relation between the observed ^{1}H chemical shift δ^{H}_{obs} and the proton fraction of uptaken water $x^{H}_{H_2O}$:

$$\delta^{H}_{obs} = x^{H}_{PA} \cdot \delta^{H}_{PA} + x^{H}_{H_2O} \cdot \delta^{H}_{H_2O},$$

where δ^{H}_{PA} and $\delta^{H}_{H_2O}$ are the ^{1}H chemical shifts of the acid and water protons respectively, and x^{H}_{PA} is the proton fraction in the acid. A plot of the water uptake in PVPA derived from the chemical shifts and gravimetric studies is given in figure 50 [Kaltbeitzel].

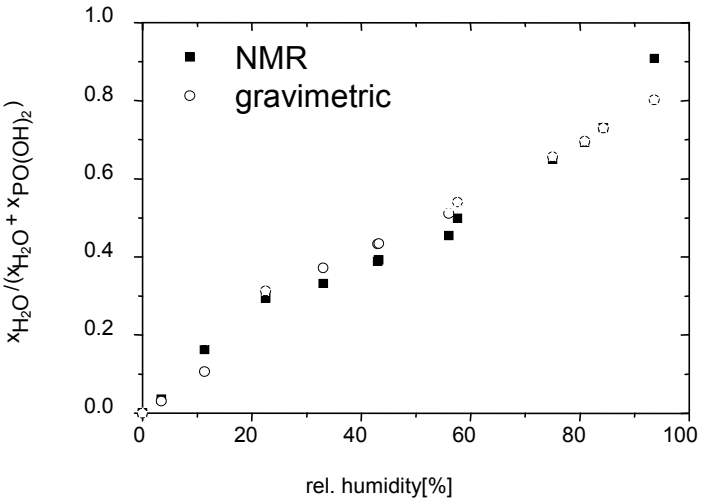

Figure 50: Plot of the water uptake in PVPA. The data were obtained from solid-state NMR spectroscopy and gravimetry.

3.2.2 Methylphosphonic acid

MePA samples were stored in well-defined water vapor atmospheres. The analysis of the corresponding ^{1}H MAS NMR spectra was performed, since MePA does not show condensation at room temperature, and only slight fraction of condensation after prolonged annealing.

It is clearly visible from the ^{1}H MAS NMR spectra (see figure 51) that an additional signal at about 9 ppm arises with a relative humidity of 43%. At even higher water uptakes it further narrows and shifts towards 6 ppm whereas the initial signal at 11.2 ppm vanishes. While MePA stored in 43% relative humidity still was a solid powder, MePA with 75% showed already the viscosity of a liquid.

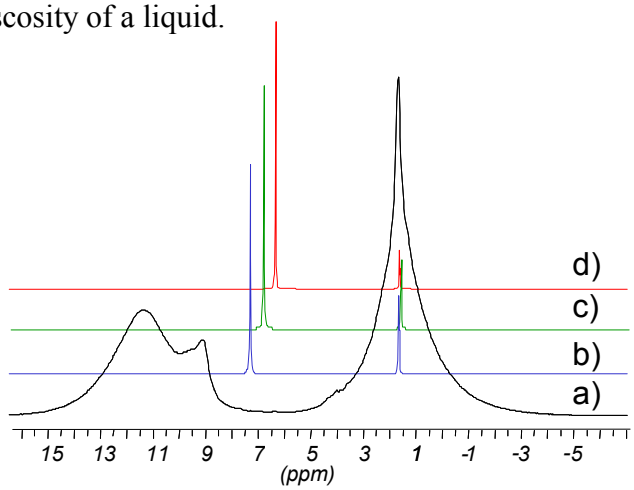

Figure 51: ^{1}H MAS NMR spectra of MePA stored in atmospheres with different humidities: a) 43%, b) 75%, c) 84%, d) 97%.

3.3 Dynamic processes

Since the aim of the study is the understanding of the proton mobility in PEMs operating at high temperatures, it is crucial to relate structural proton transport details with bulk mobility. In particular, it is desired to establish non-vehicular, "structural diffusion" mechanism as the source of proton mobility.

All prospective phosphonic acid based PEM materials were investigated by ^{1}H, ^{2}H, and ^{31}P solid-state NMR spectroscopy.

Unfortunately, we were not able to monitor particular dynamic behaviour in phosphonic acids by ^{31}P NMR. Rather ^{1}H and ^{2}H NMR spectra were acquired at different temperatures, thereby yielding information about the dynamics of protons involved in hydrogen bonding.

Here, we focus on three different materials, namely MePA, PVBzPA, and PVPA ionomer, representing distinct structures, which will be compared with respect to their properties and dynamics [Schauff 06].

3.3.1 ^{1}H NMR Spectroscopy

The ^{1}H MAS NMR spectra of MePA, PVBzPA, and PVPA ionomer at different temperatures are shown in figure 52. In all samples the acidic ^{1}H signal was sufficiently resolved and therefore could be assigned to the high frequency region of the spectrum.

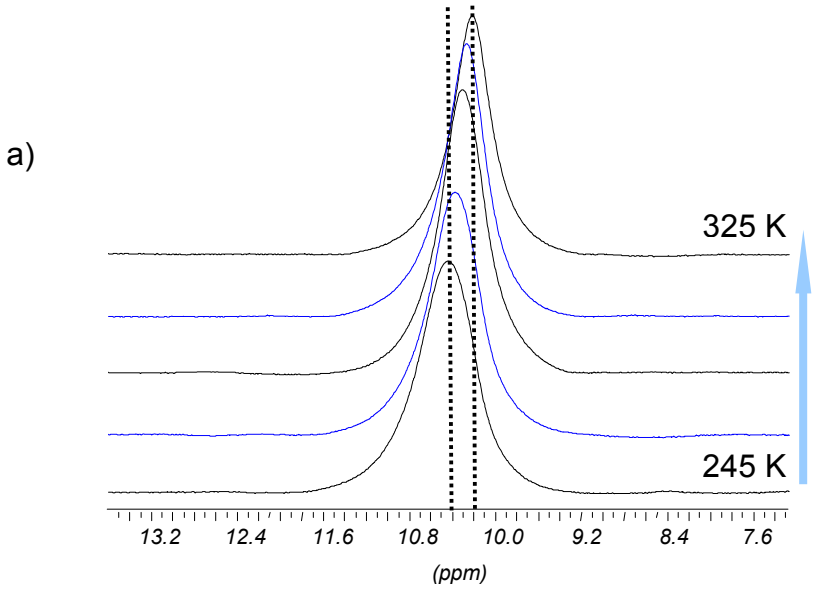

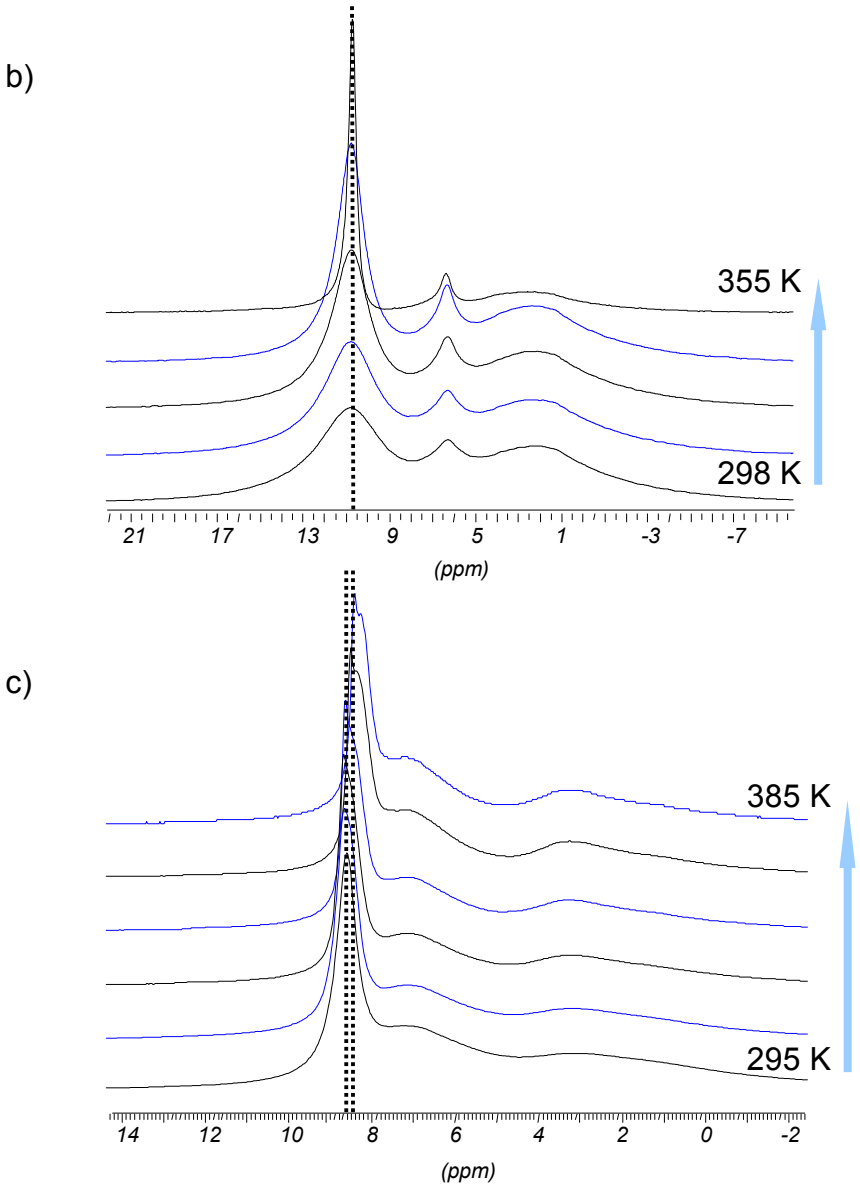

Figure 52: ^{1}H MAS NMR spectra of the samples a) MePA, b) PVPA ionomer, and c) PVBzPA at different temperatures.

All samples do not show significant changes in the ^{1}H chemical shift of the acid group with increasing temperature. Small changes occur because the strength of hydrogen bridges in most systems decrease with higher temperatures. The finding is consistent with protons that populate equivalent sites.

At room temperature, the acidic protons of MePA have a ^{1}H chemical shift of 10.4 ppm, the ones of PVPA ionomer 10.8 ppm, whereas the acidic protons of PVBzPA resonate at 8.6 ppm. Consequently, in MePA and PVPA ionomer the exchangeable protons are in similar

chemical environments and reveal rather strong hydrogen bonds while the acid protons in PVBzPA form weaker hydrogen bonds.
In the ^{1}H NMR spectra of PVBzPA at higher temperatures a splitting of the acidic proton signal can be observed that is probably caused by the meta- and para-isomer mixture present in the material.
The motion of protons in MePA was deduced from the ^{1}H linewidths depending on temperature since this sample showed the best chemical shift resolution. However, the value of about 3 kJ/mol, obtained from the slope of an Arrhenius-type plot, just resembles an apparent activation energy, since it appears to be rather small. It is reported in literature [Ye 06, Lee] that the activation energies of hydrogen bonds in O-H functional groups are in the range of about 20-40 kJ/mol. In contrast, our result indicates that the acidic protons in MePA do not show any mobility which is also supported by ^{2}H NMR data (see section 3.3.2).

3.3.2 ^{2}H NMR Spectroscopy

Since ^{1}H NMR spectroscopy often does not yield well resolved peaks, ^{2}H NMR spectroscopy can be performed instead.
In the next sections ^{2}H NMR spectra of the samples MePA, PVBzPA, and PVPA ionomer under fast and slow MAS and in static condition will be shown.

3.3.2.1 ^{2}H MAS NMR Spectroscopy

^{2}H MAS NMR spectra of MePA, PVBzPA, PVPA ionomer, and PPPA were acquired in a rotor synchronized fashion at high MAS frequencies. All spectra exhibit only one ^{2}H signal that is assigned to the acidic protons. The temperature dependent rotor synchronized ^{2}H MAS NMR spectra are given in figure 53.
Since PPPA is a highly viscous sample, only rotor synchronized MAS spectra were obtained due to the high mobility of the material preventing spinning sidebands. For all other samples (MePA, PVBzPA, and PVPA ionomer) the spinning sideband spectra, which were recorded in a non rotor synchronized way at low MAS frequencies, are presented in figure 54.

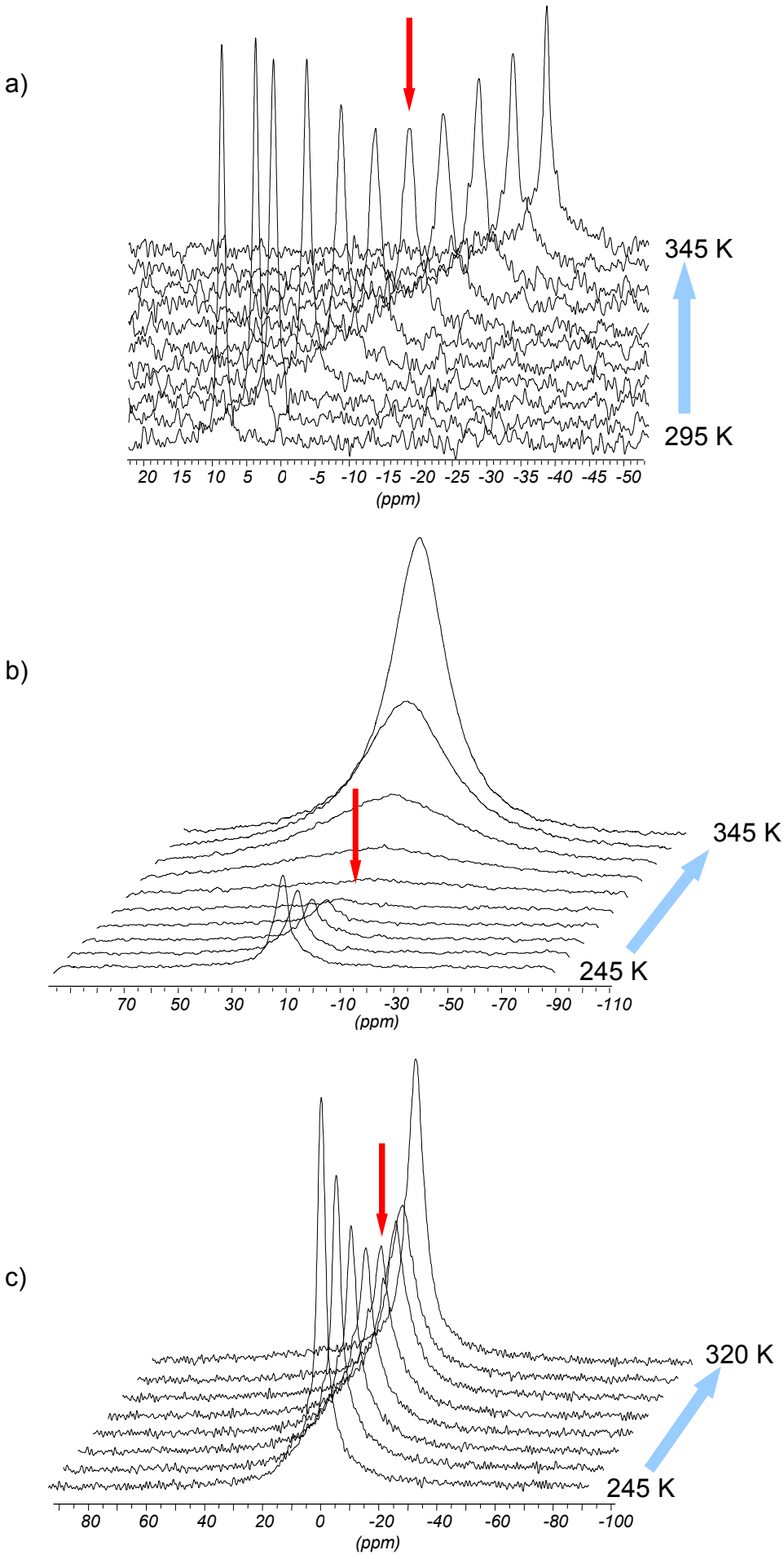
a)
345 K
295 K
20 15 10 5 0 -5 -10 -15 -20 -25 -30 -35 -40 -45 -50
(ppm)
b)
345 K
245 K
70 50 30 10 -10 -30 -50 -70 -90 -110
(ppm)
c)
320 K
245 K
80 60 40 20 0 -20 -40 -60 -80 -100
(ppm)

Figure 53: Rotor synchronized ^2H MAS NMR spectra of the samples a) MePA, b) PVPA ionomer, and c) PVBzPA at different temperatures. Red arrows indicate the point where $\tau_c \sim c_Q$.

In contrast to PVPA ionomer, MePA and PVBzPA do not show a complete intensity reduction in the temperature dependent rotor synchronized nor in the spinning sideband MAS NMR spectra. This strongly suggests a broad distribution of correlation times especially for MePA and to a lower degree for PVBzPA. Therefore, we have to consider the activation energies extracted from the ^2H linewidth versus temperature as apparent energies. Nevertheless, these values can still be used for comparison of the samples.

An apparent activation energy of 27 kJ/mol was obtained for MePA, 38 kJ/mol for PVPA ionomer, and 19 kJ/mol for PVBzPA. Since activation energies of temperature-activated processes in hydrogen bonds are generally in a range up to 120 kJ/mol [Goward 02], the obtained values for MePA and PVBzPA most probably indicate that the deuteron mobilities cannot be described by a single thermally activated process. This emphasizes that the ^1H linewidth does not reflect proton mobility.

With respect to the correlation time distribution, one can assume that the high value for PVPA ionomer ensues from a well-defined motional process of the deuterons and its strong hydrogen bonds, whereas a somewhat smaller apparent activation energy is noticed for MePA. The smallest value is observed for PVBzPA, which is most probably due to its much weaker hydrogen bridges and a preaveraging effect, evidenced in the spinning sideband spectra of PVBzPA.

The spinning sideband ^2H NMR spectra of MePA and PVBzPA show very stable sideband patterns that do not change their shape over temperature and only collapse when the overall mobility of the sample increases due to melting. This phenomenon is an indicator for rigid hydrogen bond systems in both samples.

Comparing the spinning sideband spectra of MePA and PVPA ionomer, a similar quadrupolar frequency can be observed, whereas PVBzPA shows a much more narrow set of sidebands.

Values and further discussion will be given in section 3.3.2.2 since exact frequencies can just be obtained by static ^2H NMR spectroscopy.

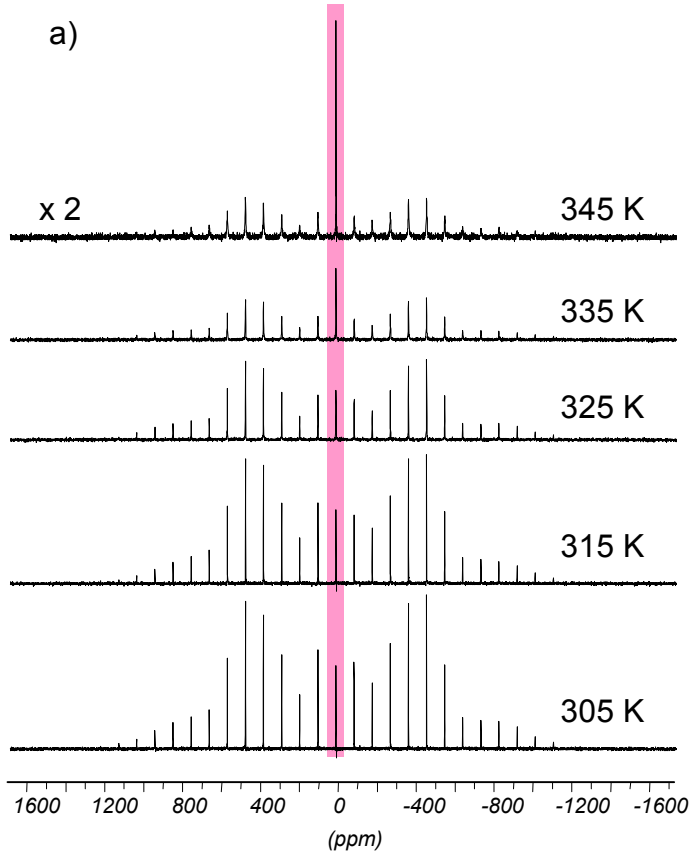
a)
x 2
345 K
335 K
325 K
315 K
305 K
1600 1200 800 400 0 -400 -800 -1200 -1600
(ppm)

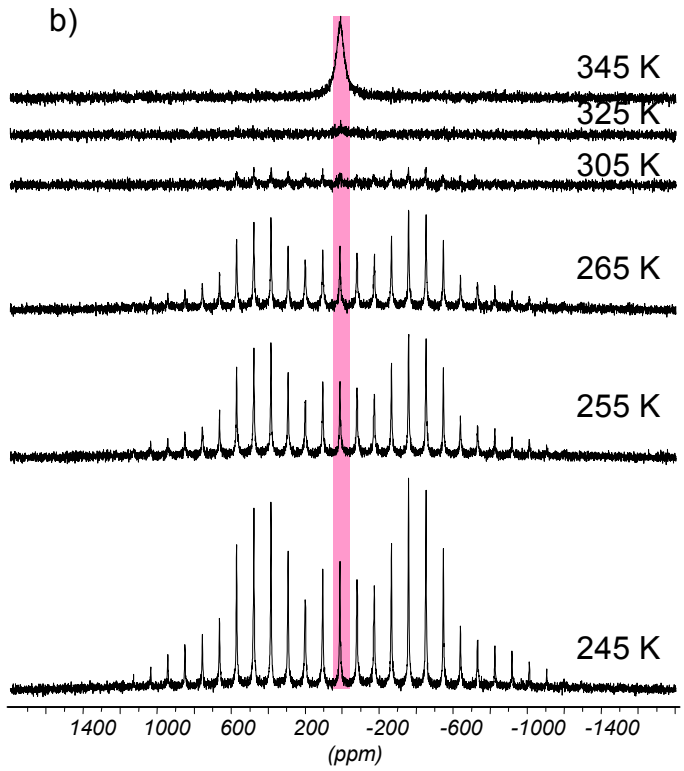
b)
345 K
325 K
305 K
265 K
255 K
245 K
1400 1000 600 200 -200 -600 -1000 -1400
(ppm)

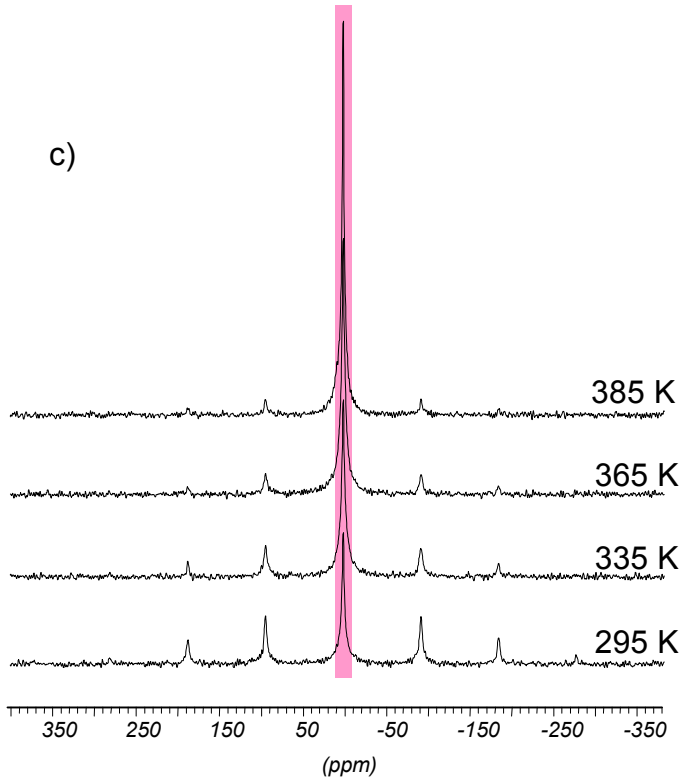

Figure 54: SSB ^2H MAS NMR spectra of the samples a) MePA, b) PVPA ionomer, and c) PVBzPA at different temperatures. The highlighted area indicates the point where $\tau_c \sim c_{Q.}$

3.3.2.2 ^{2}H Static NMR Spectroscopy

The ^{2}H NMR static lineshapes were monitored over a temperature range of 220 K to 300 K for PVPA ionomer (see figure 55) and from 230 K to 340 K for MePA (see figure 56). The static NMR spectra for PVBzPA are not given since we were not able to receive a reasonable signal-to-noise ratio, probably due to the very low degree of deuterons in the acid groups with respect to the polymer backbone.

At room temperature, a narrowing of the ^{2}H lineshape in the PVPA ionomer sample is obtained which at higher temperatures leads to a single sharp peak. Even at low temperatures a typical Pake pattern could not be observed, most probably due to a poorly defined sample condition. In fact, the ionomer is represented by a broad statistical distribution of poly-, oligo-, and monomers. However, similar spectra were found for well-defined PVPA [Lee], indicating a general structural property in PVPA. The low-temperature spectra of PVPA ionomer could in principle be simulated assuming a tetrahedral two-site jump of the deuterons

(see figure 57). Nevertheless, a respective simulation of the high-temperature spectra was not possible, yielding indication for at least two motional mechanisms, one of which reflects the two-site jump (broad pattern), the other a fast movement (averaged peak).

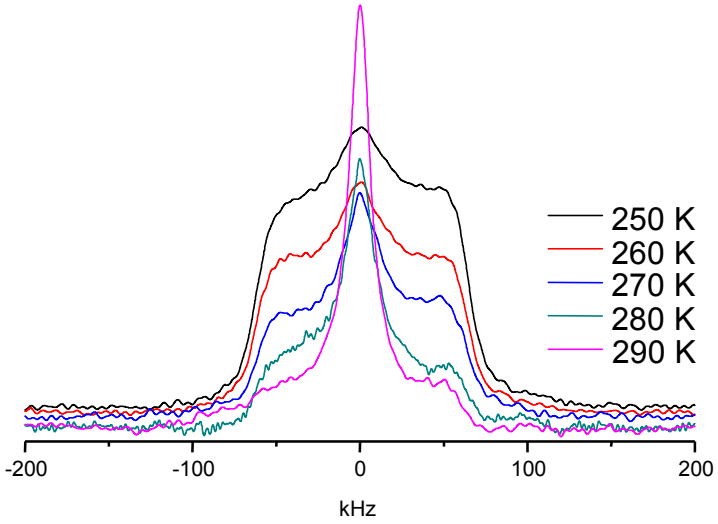

Figure 55: Static ^{2}H NMR spectra of PVPA ionomer at different temperatures.

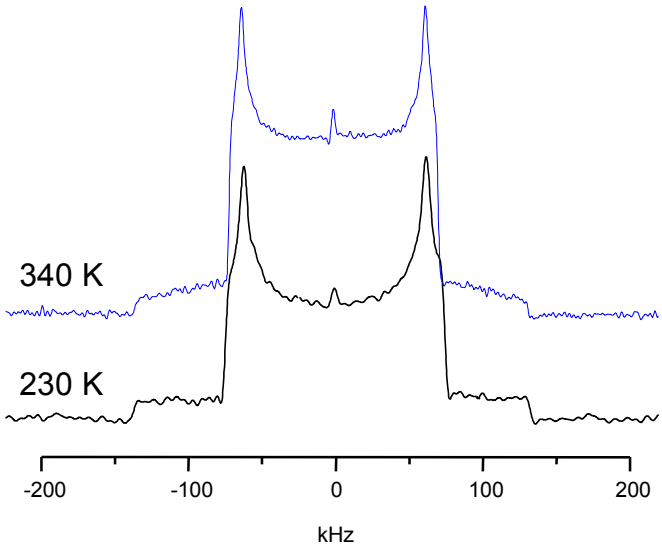

Figure 56: Static ^{2}H NMR spectra of MePA with simulated line (blue) at two different temperatures.

On the contrary, MePA shows a typical Pake pattern with a small asymmetry parameter ($\eta \approx 0.1$), which does not change significantly over a temperature range of 110 K. In good agreement with the ^{1}H NMR data (see section 3.3.1), this clearly implies the lack of deuteron mobility. When heating above 340 K, an additional sharp signal, rising from the centre of the Pake pattern, was observed, reflecting the melting of MePA. This is supported by the spectrum at 380 K where a single sharp line is left (data not shown).

The quadrupolar frequencies of MePA and PVPA ionomer are in the range of 120 kHz, whereas the obtained ω_Q of PVBzPA at the same temperature only amounts to 40 kHz, hence only 1/3. This pre-averaging is reminiscent to a rotation around a three-fold axis, most likely around the C-P bond.

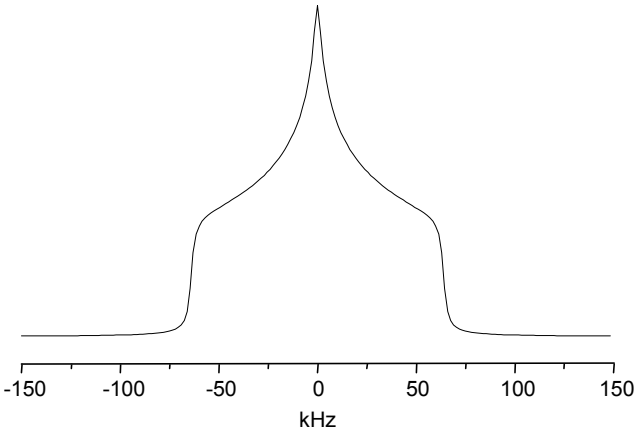

Figure 57: Simulation of a tetrahedral two-site jump using the NMR-WEBLAB [Macho 01].

3.4 Proton Conductivity Measurements

Plots of the frequency dependent AC proton conductivity σ_{AC} (T) for MePA, PVBzPA, and PVPA ionomer are given in figure 58. All measurements were performed at similar temperatures like the NMR experiments in order to receive comparable data. The samples were pressed to pellets since MePA and PVPA ionomer do not form membranes.

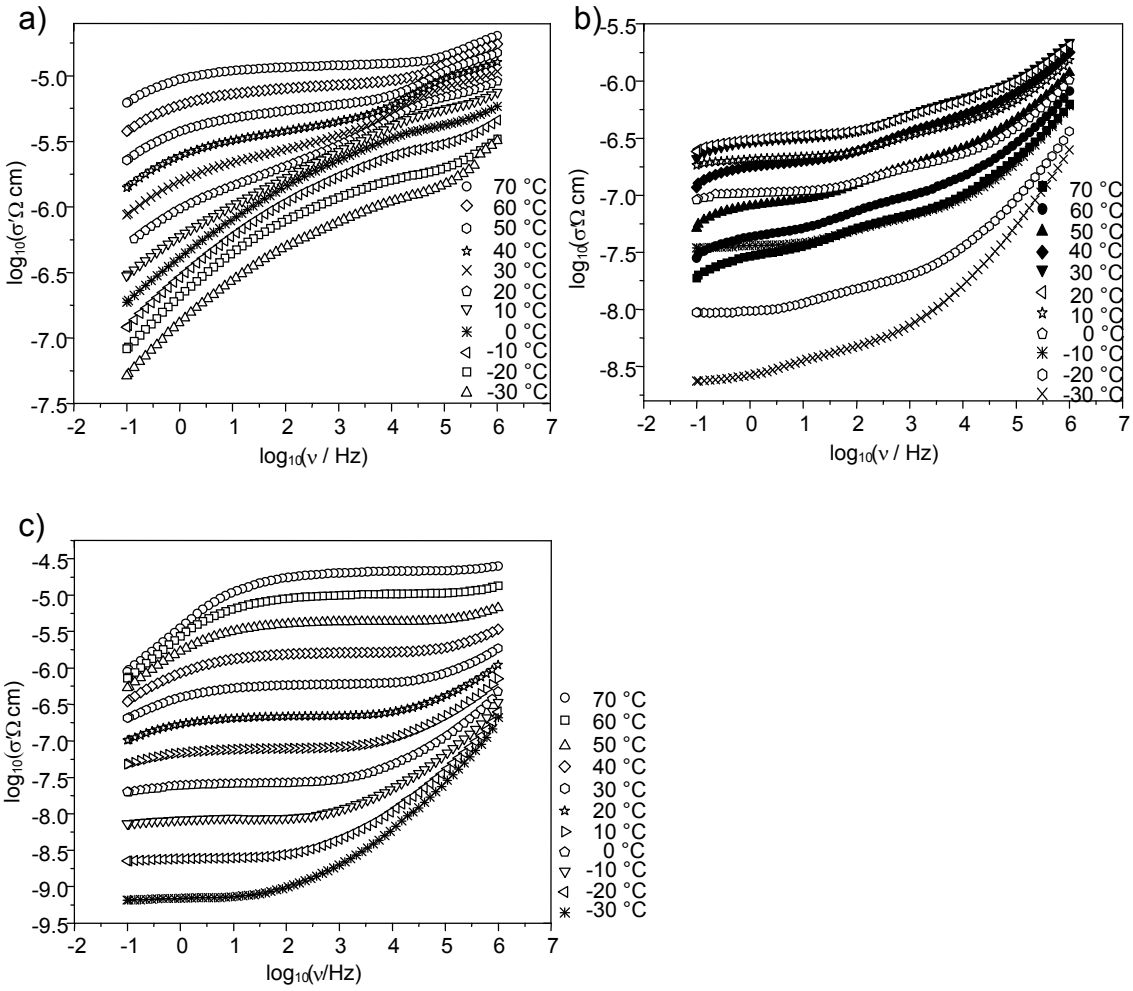

Figure 58: Frequency dependent AC conductivity plots of a) MePA, b) PVBzPA, and c) PVPA ionomer.

Unlike MePA and PVBzPA, the AC conductivity plot of PVPA ionomer shows typical isotherms (see figure 58 c), with bulk DC conductivities of up to 10^{-4} S·cm^{-1}. This fits the NMR observations of high proton mobilities. Moreover, the sample contains low molecular weight compounds with high boiling points which may allow vehicular transport. From an Arrhenius-type plot of DC conductivity versus inverse temperature, an activation energy of

about 75 kJ/mol was obtained, where the linear fit covers several orders of magnitude of conductivities and thus indicates a single motional process present in the sample.

On the other hand, the isotherms of MePA show an odd behaviour, that is at some temperatures distinct DC plateaus are not visible, but strong indications of electrode polarization are observable (see figure 58 a). Since we cannot rule out the presence of water in the sample pellet, this is most likely due to melting and evaporation of water, thereby deteriorating the electrode contacts. However, for some temperatures the DC proton conductivities of up to 10^{-5} S·cm^{-1} could be extracted (see figure 59 a). For molten MePA (110 °C to 180 °C, closed system) conductivities of up to 10^{-1} S·cm^{-1} were obtained (see figure 60) [Steininger], yielding an apparent activation energy of about 36 kJ/mol (low temperature regime). However, the low proton mobilities, as observed by NMR spectroscopy suggest that the proton conductivity does not reflect an intrinsic property of the sample but rather is due to traces of adsorbed water.

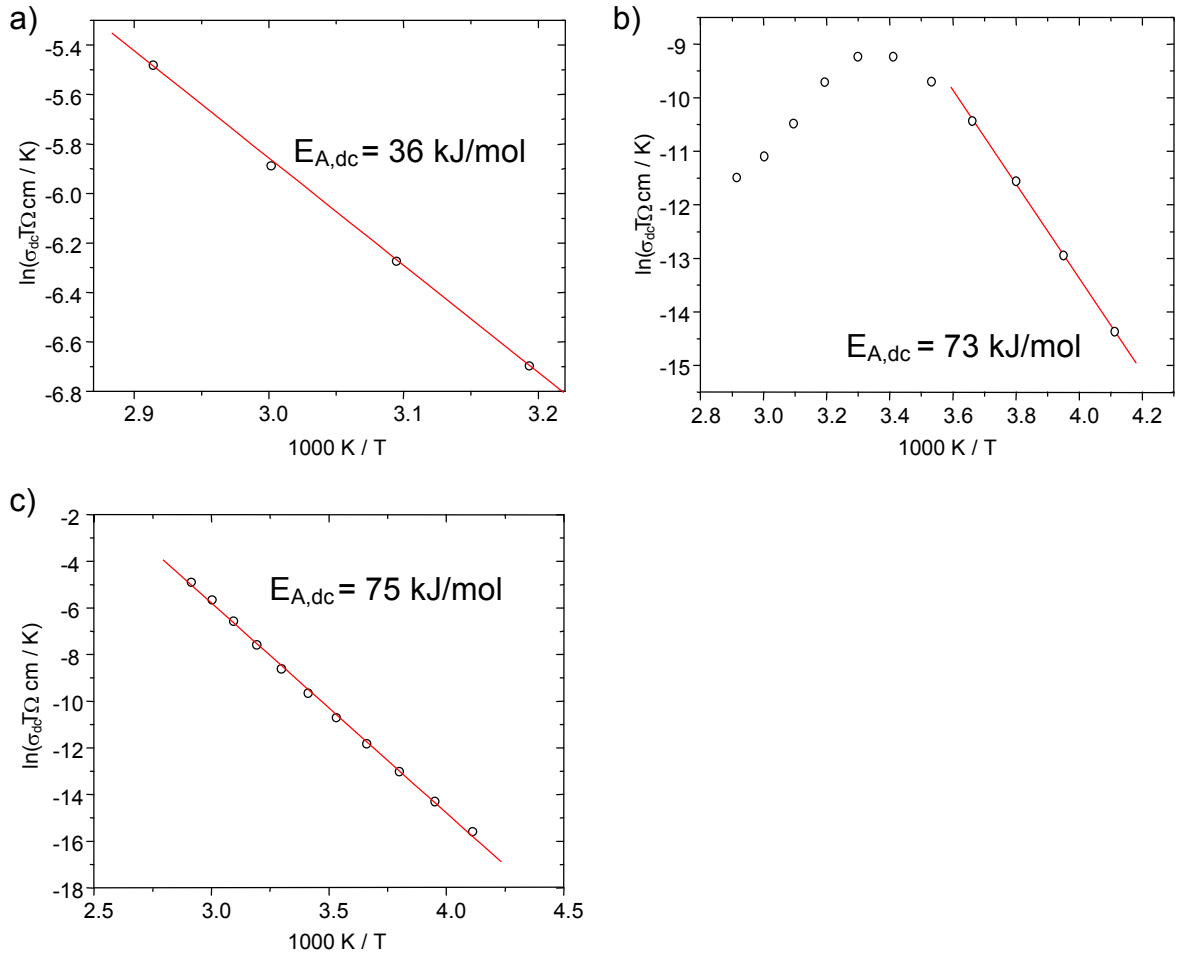

Figure 59: DC proton conductivity plots of a) MePA, b) PVBzPA, and c) PVPA ionomer.

The isotherms in the plot of σ_{AC} (T) for PVBzPA indicate bad electrode contacts during the measurement, similar to the observation made for MePA (see figure 58 b). This effect is also visible in the DC conductivity plot, where a turning point at around 20 °C indicates evaporation of small molecular compound(s) (see figure 59 b). In fact, when pressing the pellet, an acrid smell of the originally odourless PVBzPA was noticed, letting us assume that the material is not pressure stable. The overall AC conductivity is very low with values up to 10^{-9} S·cm^{-1}. Indeed, this is consistent with the ^{1}H and ^{2}H NMR data indicating low proton mobilities.

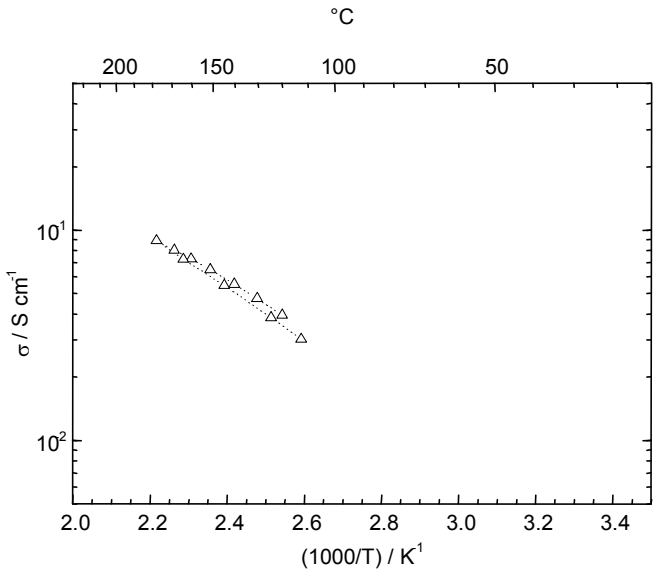

Figure 60: Plot of proton conductivity obtained from dried MePA in a closed system at different temperatures.

An overview of proton conductivities for various compounds containing phosphonic acid functional groups is given in figure 61. In contrast to the measurements of the three samples discussed before, these were conducted under a water pressure of 10^5 Pa leading to overall higher proton conductivities [Steininger]. The plot shows quite good properties, especially for PPPA, whereas SPA reveals much lower conductivities, probably due to its high degree of anhydride formation.

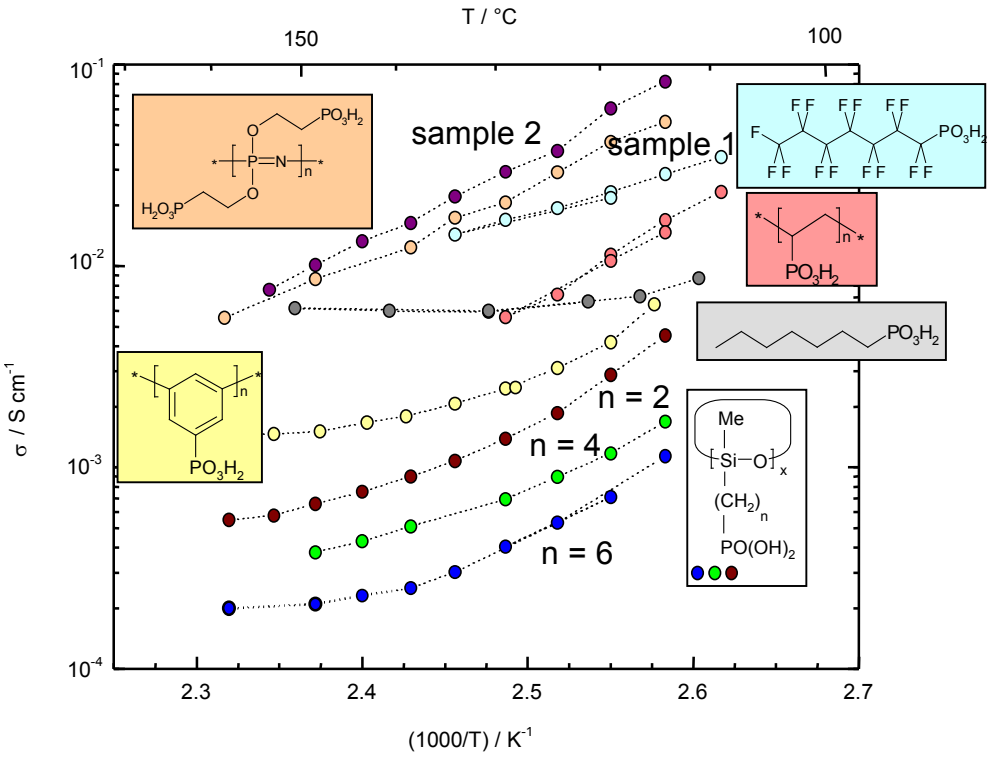

Figure 61: Proton conductivity plot of several phosphonic acids.

3.5 Conclusion

It was demonstrated that the water uptake in phosphonic acid samples could be monitored almost quantitatively via ^{1}H chemical shifts. Also, the reversibility of phosphonic acid anhydride formation was observed using ^{31}P MAS NMR spectroscopy, thereby proving the versatility of even simple NMR experiments.

^{1}H and ^{2}H NMR spectroscopy have been successfully utilized to gain information on both, the nature of hydrogen bonds and proton/deuteron mobilities in phosphonic acid groups.

Variable temperature ^{1}H MAS NMR spectra of MePA, PVPA ionomer, and PVBzPA showed no significant chemical shift changes, and thus suggest proton populating equivalent sites. Qualitative hydrogen bond strengths could be obtained, decreasing from PVPA ionomer to PVBzPA.

Rotor synchronized and spinning sideband ^{2}H MAS NMR spectra revealed a well defined motional process for PVPA ionomer, but correlation time distributions in MePA and PVBzPA.

MePA did not show proton/deuteron mobility due to a network of rigid hydrogen bonds present in the sample, as established from apparent activation energies, obtained from ^{1}H and ^{2}H MAS NMR spectra, and from the observation of temperature-independent spinning sideband patterns and static ^{2}H NMR spectroscopy.

The ^{1}H MAS NMR spectra of PVBzPA revealed rather weak hydrogen bonds, and the protons/deuterons proved to be rather immobile, even though the phosphonic acid groups are attached to the backbone via spacers. Thus, PVBzPA and MePA are structurally rather different, yet both immobile.

In contrast, PVPA ionomer revealed the strongest hydrogen bonds as well as highest proton mobility. The strong temperature-dependence of the ^{2}H NMR spectra indicates the presence of a single motional correlation time. At low temperatures the static spectra most likely exhibit the presence of a tetrahedral two-site jump, whereas at higher temperatures an additional fast motion sets in.

These findings can be expressed in figure 62. The scheme illustrates that PVBzPA contains the weakest hydrogen bonds, whereas MePA and PVPA ionomer possess stronger hydrogen bridges. Thus, highest proton mobilities would be expected for PVBzPA since weaker hydrogen bonds are easier to break and therefore facilitate the reorientation of structural units. The ^{1}H chemical shifts indicate a stronger hydrogen bond network in MePA and PVPA ionomer, which are assumed to be rather rigid.

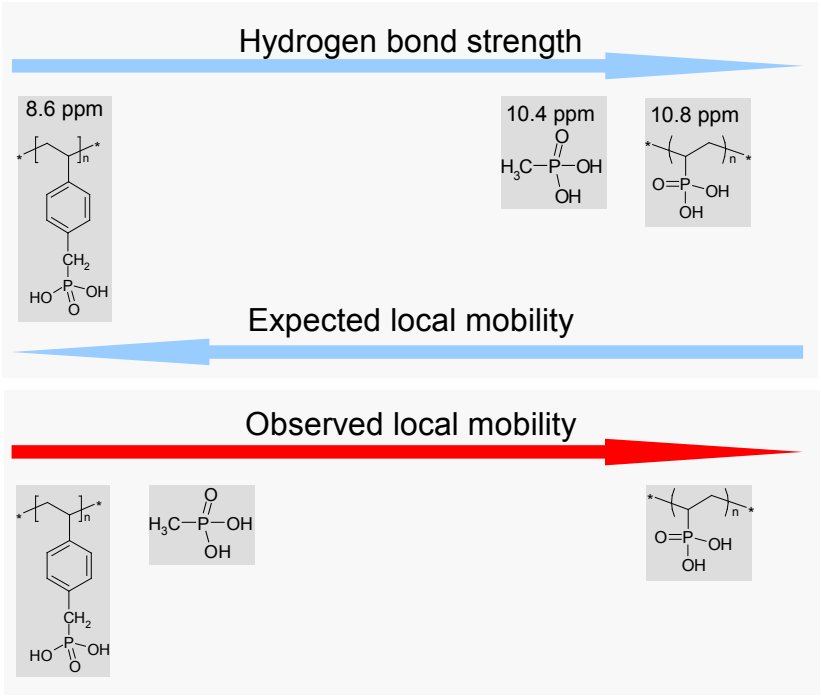

Figure 62: Scheme relating hydrogen bond strength and proton mobility of the samples MePA, PVBzPA, and PVPA ionomer. The ^{1}H chemical shifts are given as indicators for hydrogen bond strength.

However, unlike the mobile PVPA ionomer, low proton mobilities were observed for PVBzPA and MePA, demonstrating that there is no simple connection between hydrogen bond strength and proton mobilities. In addition, subtle packing differences must be present in MePA and PVPA ionomer, and the "spacer concept" is not necessarily valid in phosphonic acid funtionalized polymers.

This study shows that information about local dynamics present in a sample can be gained by application of simple of ^{1}H and ^{2}H NMR experiments.

4 Investigation of Chromatographic Stationary Phases

4.1 Characterization of Stationary Reversed Phases

4.1.1 C_{18} Phase

The structure of a monomeric C_{18} functionalized phase is given in figure 63. The $\{^1H\}$-^{13}C CP MAS NMR spectrum (see figure 63) shows several peaks for the organic ligand at 1.4 ppm (methyl groups), 18.3 ppm (C1 and C18), 23.7 ppm (C2 and C17), 30.2 ppm (C4 to C15), and 33.8 ppm (C3 and C16). The peak at 1.4 ppm which was assigned to the methyl groups is quite broad, thus comprises the CH_3 functionalities at the silane and an endcapping on the silica surface. Endcappings are generally present in commercial phases since they are desired to prevent unfavourable interactions with residual silanol groups (see figure 64).

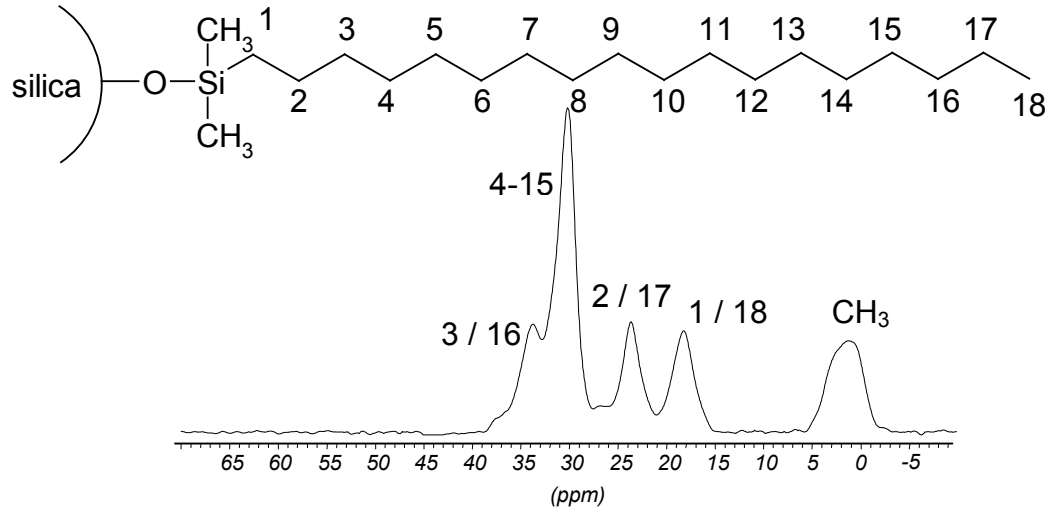

Figure 63: $\{^1H\}$-^{13}C CP MAS NMR spectrum of a monomeric C_{18} phase.

This is supported by the $\{^1H\}$-^{29}Si CP MAS NMR spectrum (see figure 65). Silyl species can be observed at –110.2 ppm for Q^4, at -101.3 ppm for Q^3, and at 13.3 ppm for M groups. The M species are due to both, the methyl groups at the silane and the endcapping procedure. Further, Q^2 species cannot be observed which suggests that a quite complete crosslinkage of silanoles was achieved.

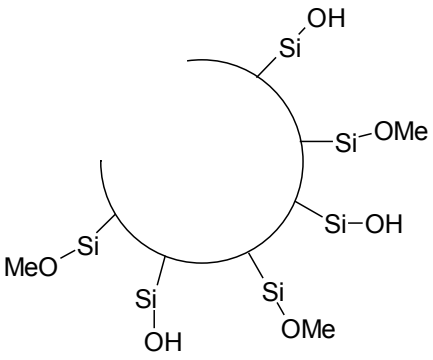

Figure 64: Schematic picture of endcappings (-Me) which "cover" residual silanol groups (Si-OH) on the silica surface.

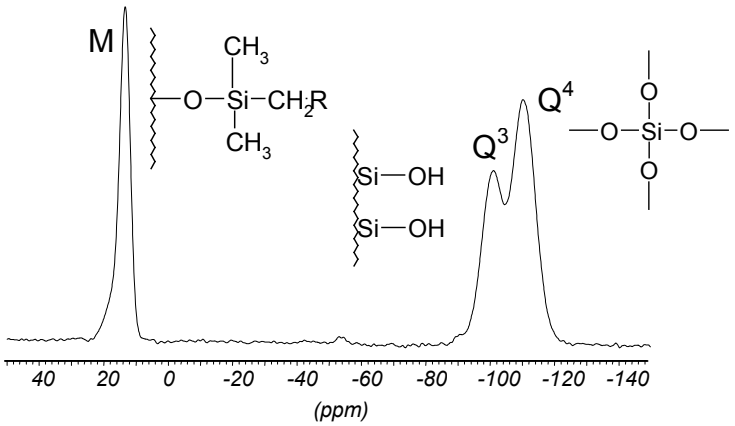

Figure 65: {^{1}H}-^{29}Si CP MAS NMR spectrum of a monomeric C_{18} phase.

Basically three peaks are visible in the ^{1}H HR-MAS NMR spectrum of the C_{18} phase in a mixture of 80% water and 20% acetonitrile (D_2O/ACN-d_3), at 0.04 ppm, 0.82 ppm, and at 1.27 ppm which were assigned to Si-CH_3 groups, C18, and C1-C17 respectively (see figure 66). The peak at 4.63 ppm is the residual water peak, the one at 2.06 ppm originates from residual protonated ACN.

A ^{1}H double quantum filtered (DQF) MAS NMR spectrum can yield information about the mobility in a C_{18} phase (see figure 67). The same peaks as in the ^{1}H HR-MAS NMR spectrum can be observed at a slightly different chemical shift for Si-CH_3 since no solvent influences are present. In particular, the peak for the carbon chain changes in intensity upon increase of recoupling time, which confirms the higher mobility of the chain whereas methyl groups are more rigid.

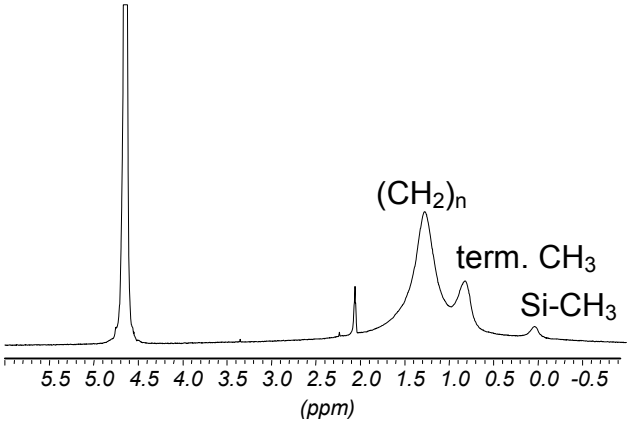

Figure 66: ^{1}H suspended-state HR-MAS NMR spectrum of a monomeric C_{18} phase in 80% D_2O and 20% ACN-d_3.

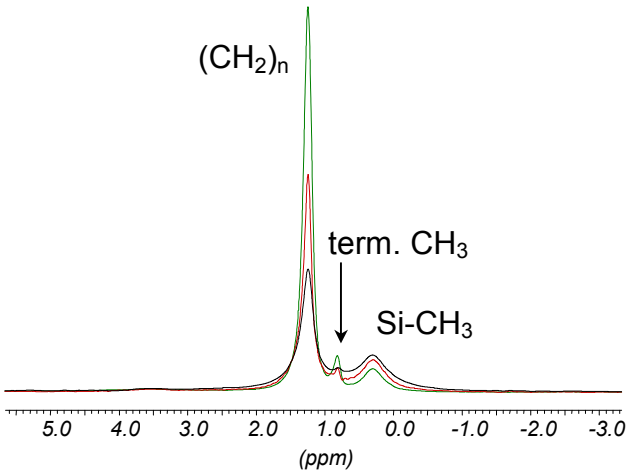

Figure 67: ^{1}H DQF MAS NMR spectrum of a monomeric C_{18} phase with recoupling times of one rotor period (black), two rotor periods (red), and three rotor periods (green).

4.1.2 C_{30} Phase

A polymeric C_{30} phase was investigated by Raitza et al [Raitza 98, 00]. The $\{^{1}H\}$-^{13}C CP MAS NMR spectrum (see figure 68) shows peaks at 12 ppm (C1), 14 ppm (C30), 23 ppm (C29), 24 ppm (C2), major peaks at 30 ppm and 32.5 ppm (C4-C27), and a shoulder at 35 ppm (C3 and C28) [Raitza 98]. The main chain (C4-C27) reveals a splitting in two peaks which has been found to originate from chain clusters at different mobilities where the peak at 30 ppm is assigned to mobile gauche conformations and the signal at 32.5 ppm to rigid trans

conformations (see figure 69) [Raitza 00]. This finally leads to a shape selectivity for the separation of trans/cis isomers in chromatography [Albert 96, Strohschein 98].

C_{30} phases were developed in order to perform demanding separations of carotenoid isomers [Sander 94] but also have proven suitable to separate tocopherols [Strohschein 98] (see section 4.3.1 for further investigations).

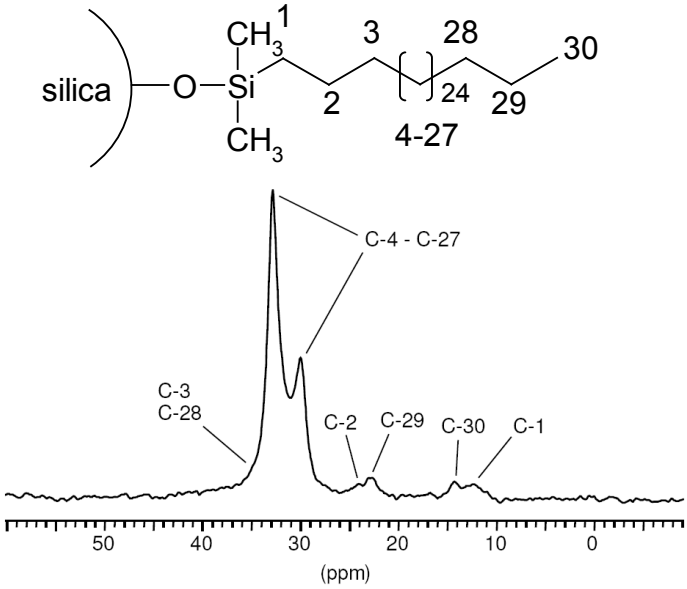

Figure 68: {^{1}H}-^{13}C CP MAS NMR spectrum of a polymeric C_{30} phase.

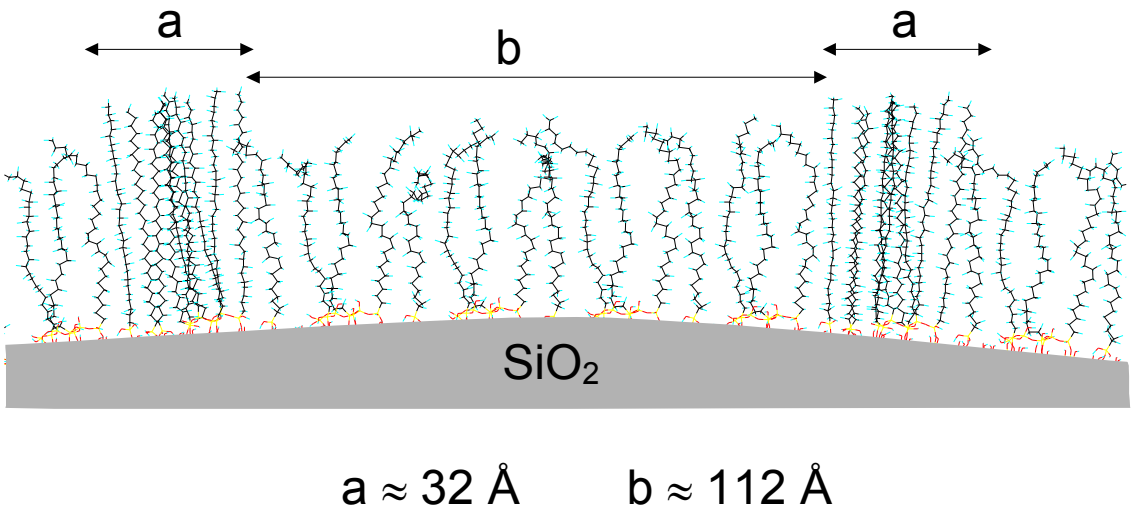

Figure 69: Schematic picture of the brush-type model showing a C_{30} functionalized silica surface with a) rigid (trans) and b) mobile (gauche) alkyl chains.

4.1.3 Polyethylene-*co*-acrylic acid

Polymeric polyethylene-*co*-acrylic acid (PEAA) phases were developed by Meyer et al [Meyer 04] in order to achieve similar separation properties as C_{30} phases though higher overall loadabilities. A $\{^1H\}$-^{13}C CP MAS NMR spectrum of a PEAA with an acid mass fraction of 5% reveals signals at ~8 ppm (C1), ~23 ppm (C2), ~30 ppm and ~33 ppm (C9), ~43 ppm (C8 and C10), ~73 ppm (C3-C6) (see figure 70) [Meyer 04, 06]. It seems obvious that a similar splitting in trans and gauche moieties is observed for C9 like for the centre chain in the C_{30} phase, thus the PEAA phase should also exhibit shape selective recognition capabilities.

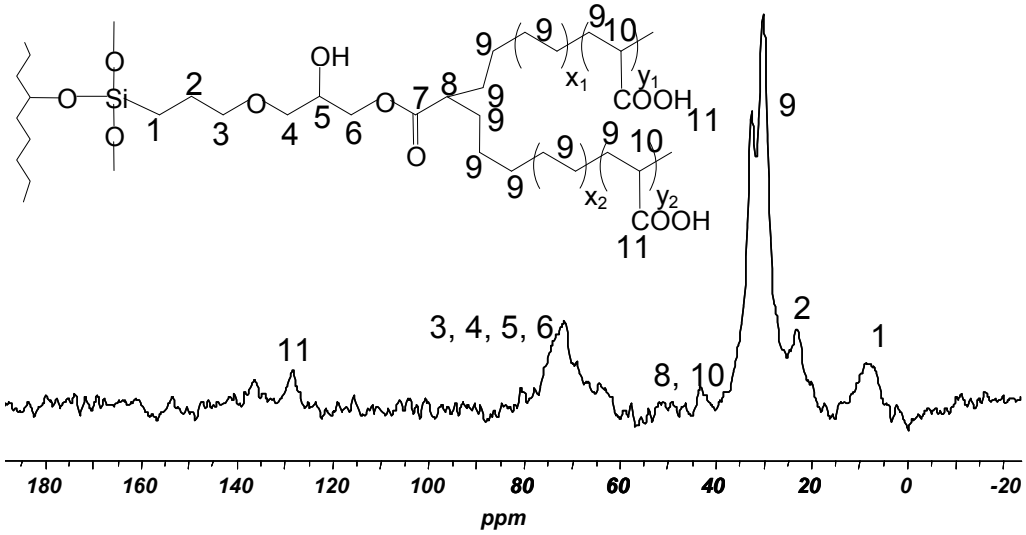

Figure 70: $\{^1H\}$-^{13}C CP MAS NMR spectrum of a polymeric PEAA phase.

4.1.4 Molecularly Imprinted Polymer Particles

A molecularly imprinted particulate, organic polymer, using 2,4-dichlorophenoxyacetic acid (2,4-D) as template in a solution of methanol and water, and an imprinted particulate polymer, using pure acetic acid in toluene as template, were provided by cooperation partners [Zurutuza]. Both were synthesized by radical polymerization from 4-vinylpyridine and ethyleneglycol dimethacrylate. The first will be referred to as MIP, the second as NIP (non-imprinted polymer) since the rebinding of 2,4-D was investigated.

4.1.5 Molecularly Imprinted Polymer Monolith

A monolithic molecularly imprinted polymer and a non-imprinted polymer of the same kind were provided by the cooperation partner [Courtois 06 b]. The MIP, polymerized from methylacrylic acid (MAA) and ethylene dimethacrylate (EDMA), was grafted on a trimethylolpropane trimethylacrylate (TRIM) based core. It was synthesized in the presence of bupivacaine yielding imprinted monoliths [Courtois 06 a, b]. The NIP was synthesized in the same manner but in the absence of the template.

Both samples were prepared to fit in a 4 mm rotor suitable for solid-state NMR spectroscopy. The $\{^1H\}$-^{13}C CP MAS NMR spectra reveal similar signals, thus confirming the chemical equivalence of both materials (see figure 71).

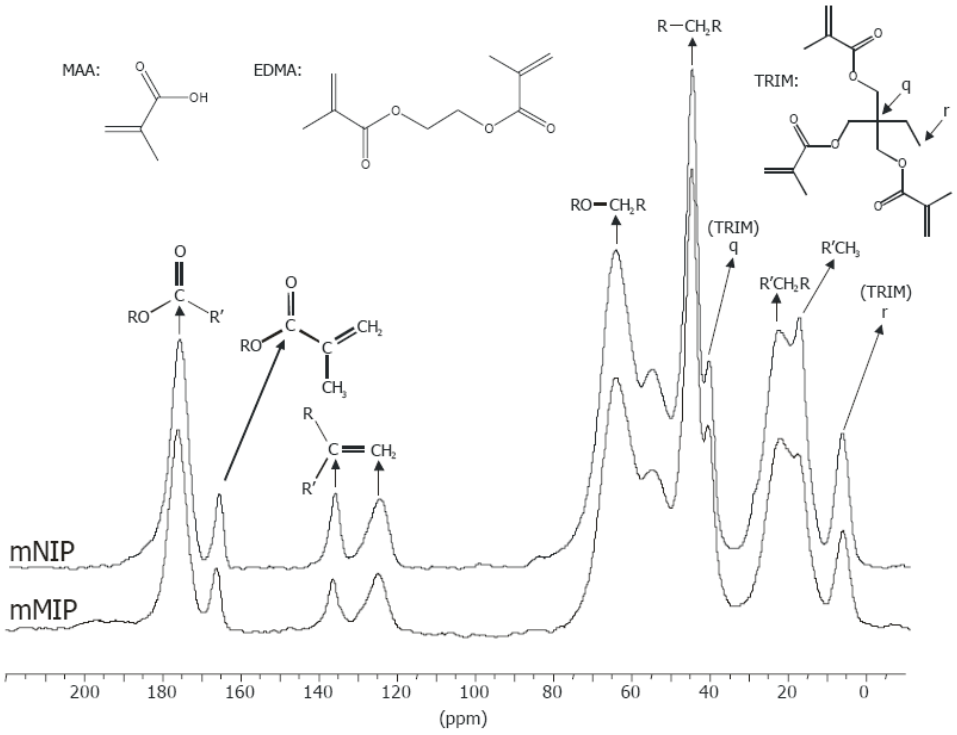

Figure 71: $\{^1H\}$-^{13}C CP MAS NMR spectrum of a TRIM based MIP.

4.2 Study of Dynamics in Methylphenyl succinimide/ C_{18} Phase System

In chromatography, the variation of different parameters is necessary to obtain optimized separations. Attempts have been made to model the chromatographic separation process in a suspended-state HR-MAS NMR experiment also by varying similar parameters and thus observing the influences in the spectra.

Methylphenyl succinimide (MePhSucc) is an organic compound containing a prochiralic CH_2 group. The ^1H HR-MAS NMR spectrum of a 0.1 molar solution of MePhSucc in 80% D_2O and 20% ACN-d_3 shows basically three sets of peaks which were assigned to the methyl group at 1.68 ppm, to the CH_2 group at 3.02 ppm, and the aromatic ring at ~7.3 ppm (see figure 72). However, the CH_2 signal reveals a splitting to a doublet of doublet due to its prochirality yielding narrow lines.

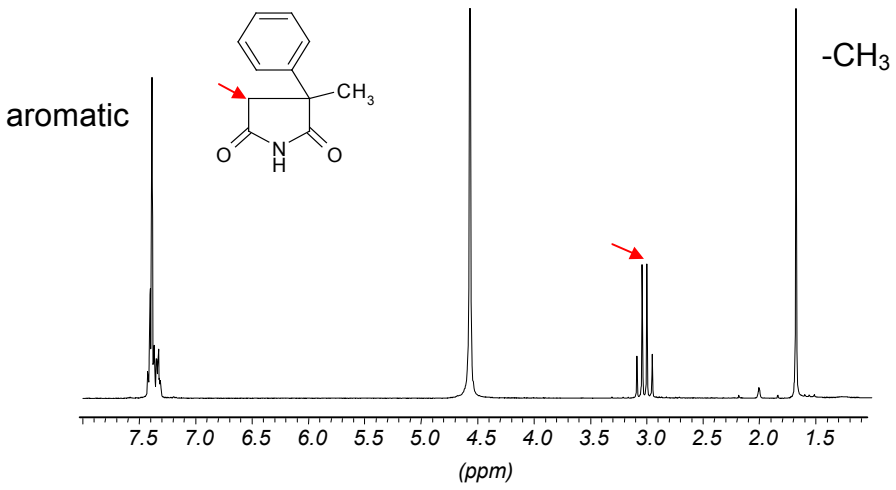

Figure 72: ^1H HR-MAS NMR spectrum of methylphenyl succinimide solution in 80% D_2O and 20% ACN-d_3. The red arrow indicates the CH_2 signal.

Addition of a chromatographic sorbent, namely an endcapped, monomeric C_{18} phase, to the analyte solution led to the observation of a CH_2 peak doubling (see figure 73). Surprisingly, the original signal kept its linewidth and stayed at the same chemical shift whereas the second peak showed a severe broadening and moved to lower frequencies. The chemical shift of the broad peak is at ~2.77 ppm, and the narrow peak stayed at ~3.02 ppm for a 0.1 molar analyte solution.

Since this could not be explained in a rather simple way, additional studies were performed via suspended-state NMR spectroscopy in a closeby chromatographic system. MePhSucc solutions in D_2O/ACN-d_3 mixtures were investigated under the influence of the C_{18} stationary

phase described before. H_2O/ACN is a common solvent composition for mobile phases in RP-HPLC, and therefore suspended-state investigations can yield valuable insight in the interactions taking place. In order to prevent suppression of the analyte by the solvent signals, generally deuterated solvents are chosen, the amount of which is limited due to the fact that the rotor only contains about 60 µl per measurement.

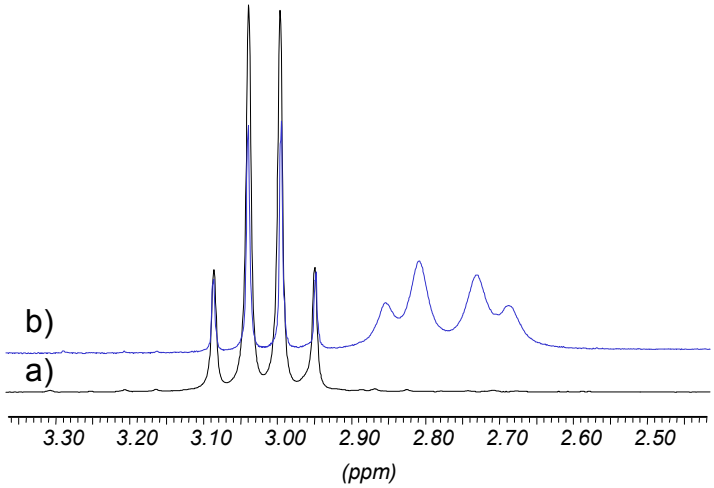

Figure 73: ^1H suspended-state HR-MAS NMR spectrum (CH_2 peak) of a 0.1 molar MePhSucc solution (80% D_2O and 20% ACN-d_3) in a) absence (black line) and b) presence (blue line) of C_{18} phase.

Indeed, the variation of parameters like the mobile phase composition and concentration showed rather large influences on the CH_2 signal. When decreasing the analyte concentration in a fixed mobile phase composition of 80% D_2O/ 20% ACN-d_3, the broad peak shifted towards the high frequency signal until it turned in one final peak for an analyte concentration of 0.01 mol/l (see figure 74). The final peak was quite narrow but did not yet reveal the same linewidth of the initial peak not influenced by stationary phase. It was not possible to decrease the concentration any further, due to the relatively low sensitivity of NMR. However, surprisingly, the narrow highfrequency peak also shifted, but in a rather strange manner. At an analyte concentration of 0.05 mol/l it shifted towards higher frequencies whereas at even lower concentrations it shifted back towards lower frequencies. It did not reach its initial chemical shift, but revealed a chemical shift of ~3.04 ppm [Schauff 04].

We assume that an excess of analyte (0.1 mol/l) in the system leads to a possible intrapment of the analyte molecules between the alkyl chains of the stationary phase leading to two separate peaks of two different species (entrapped analyte and “free” analyte) whereas at lower concentrations the molecules could perform a fast exchange.

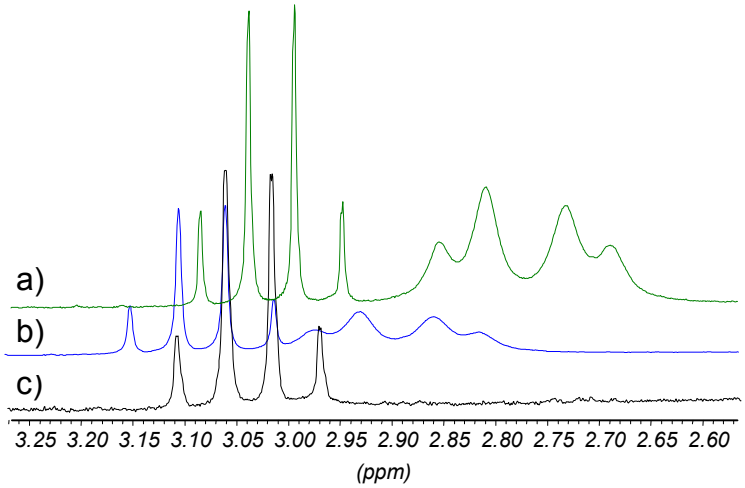

Figure 74: ^{1}H suspended-state HR-MAS NMR spectra of a a) 0.1, b) 0.05, and c) 0.01 molar solution of MePhSucc in 80% D_2O and 20% ACN-d_3 in presence of C_{18} phase.

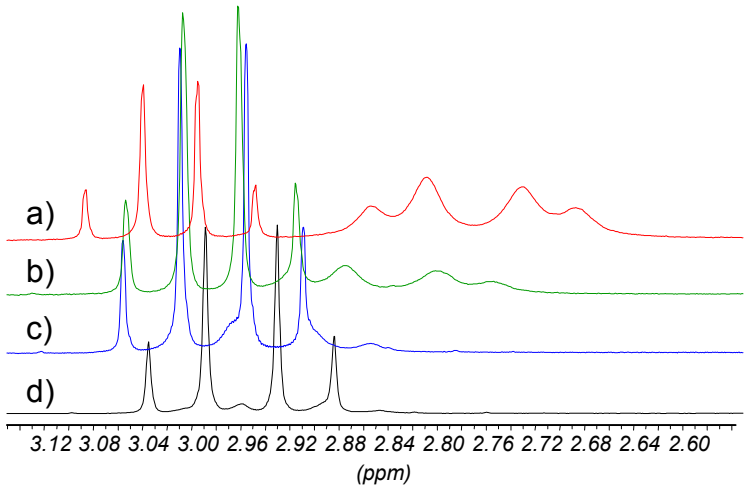

Figure 75: ^{1}H suspended-state HR-MAS NMR spectra of 0.1 molar MePhSucc solutions in D_2O/ACN-d_3 mixtures of a) 80%/20%, b) 70%/30%, c) 50%/50%, and d)40%/60% in presence of C_{18} phase.

The change of the mobile phase composition, thus the polarity of the solvent, at a fixed concentration of 0.1 mol/l led to a similar phenomenon (see figure 75). With higher organic fractions in the mobile phase, the broad peak shifted towards higher frequencies whereas the narrow highfrequency peak shifted towards lower chemical shifts until both merged to a single signal. The final peak, yielded from a solvent composition of 40% D_2O and 60% ACN-d_3, reveals a chemical shift at about 2.96 ppm which indicates the strong influence of mobile phase polarity on the analyte. Chemical shift influences on solvent peaks depending on the composition of the solvent are already known from liquid-state NMR spectroscopy and can be checked in special NMR tables for 50% mixtures [Bruker b]. However, the chemical shift

change depends on the analyte, and the stationary phase should also have an influence on the sensitive system revealing changes in the chemical shift.

The results obtained from different mobile phase compositions are most likely due to polarity effects on the analyte. Since MePhSucc is a non-polar molecule, it will be attracted by non-polar solvents and interact hydrophobically with the C_{18} chains of the stationary phase. At a mobile phase composition of 80% D_2O and 20% ACN-d_3, a part of the analyte molecules certainly is pushed among the C_{18} chains since the solvent is more polar. The analyte molecules will probably stay within the stationary phase and thus no exchange will happen yielding a broadened peak of "immobilized" molecules. However, since more analyte molecules than active sites at the sorbent are present in the experiment, some molecules are forced to stay in solution. These resonate in a narrow signal at higher frequencies. When the polarity of the mobile phase is changed to a more non-polar composition, an exchange between "free" and interacting analyte is more likely to take place. Thus the signals merge to a single which shifts to lower frequencies [Schauff 04]. The final shift of this peak will most probably be the centre between the initial two peaks. Nevertheless, at a certain point of solvent polarity, the single narrow peak can also be caused by analyte molecules which only stay in solution and do not interact with the chromatographic sorbent at all.

However, a completely different explanation can be given when considering the most recent results of Gritti et al [Gritti 05, 06]. They investigated C_{18} stationary phases of another company using RP-HPLC and found the existence of three adsorption sites present in the material at room temperature. The amount of adsorption sites reduced to only two with increase of temperature and thus with increase of chain mobility. They assumed this to be due to the disappereance or non-accessibility of the third site after the chain structure changes. It was concluded that the adsorption behaviour of low-molecular weight compounds on C_{18} phases is complex, thus several distribution constants must be present [Gritti 06].

Application of C_{18} phases (see figure 76) in pure water is known to tie up the chains, thus generally deteriorates the phase. We then must assume that a mere change in solvents polarity must also have a tremendous influence on the C_{18} chains. It might be possible that analyte molecules interacting with more than one adsorption site could be observed by the ^1H HR-MAS NMR experiment. At a mobile phase composition of 80% D_2O and 20% ACN-d_3, the chains should have clustered already to a certain degree, thus appear "frozen" and open all possible adsorption sites among which might be one of particular strength. Analyte molecules, which adsorb at this particular site, would then interact stronger with this site, leading to the additional broadened peak of "immobilized" molecules in the spectrum. Decrease of the

solvents polarity then most probably leads to a new arrangement of the C_{18} chains, thus blocking an adsorption site probably by sterical hindrance, leading to the loss of one peak in the spectrum. Since the broad peak vanishes, we must assume that it is the strongest adsorption site which is no longer accessible. However, a chromatographic separation is generally driven by somewhat weaker interactions since the elution of all compounds is desired. This leads to the assumption that a high quality separation is not possible on a C_{18} phase in pure water due to the strong adsorption phenomena which is also supported by the general application of water/non-polar solvent mixtures.

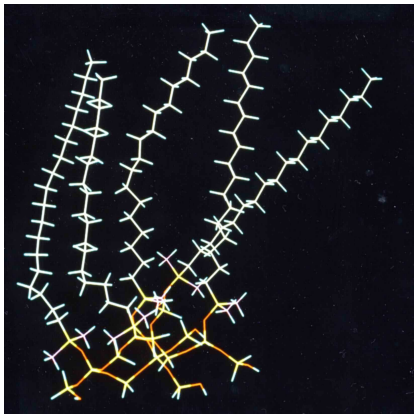

Figure 76: Schematic picture of a monomeric C_{18} phase. The stationary phase (white) is attached at the solid silica matrix (coloured).

To rule out eventual errors, in particular referencing mistakes, the measurements were performed several times. Exact referencing was performed externally by the application of 3-(trimethylsilyl) propane sulfonic acid Na salt (TSPSA) for each solvent composition (see experimental details section). The organic salt of trimethylsilane (TMS) had to be used since the organic fractions in the mobile phases were generally quite low.

4.3 Dynamic Studies using STD NMR Spectroscopy

In several cases, simple solutions to explain the separation behaviour of stationary phases interacting with analytes cannot be given.
STD NMR spectroscopy was performed to gain further insight in the chromatographic system of different reversed phase materials interacting with tocopherol homologues. Furthermore, two MIP/analyte systems were investigated using the same technique.

4.3.1 Interaction of Tocopherol Homologues with Reversed Phases

Vitamin E is an important antioxidant and radical scavenger which showed anticarcinogenic effects in several studies [Biesalski 97] and can be found in most vegetable oils and nuts. Tocopherol constitutes a major part in vitamin E and consists of four different homologues, namely α-, β-, γ-, and δ-tocopherol.
Preceding studies revealed the superiority of C_{30} phases to separate all four tocopherol homologues [Strohschein 98] which is surprising since they cannot be separated on all stationary phases due to their structural similarity (see figure 77).

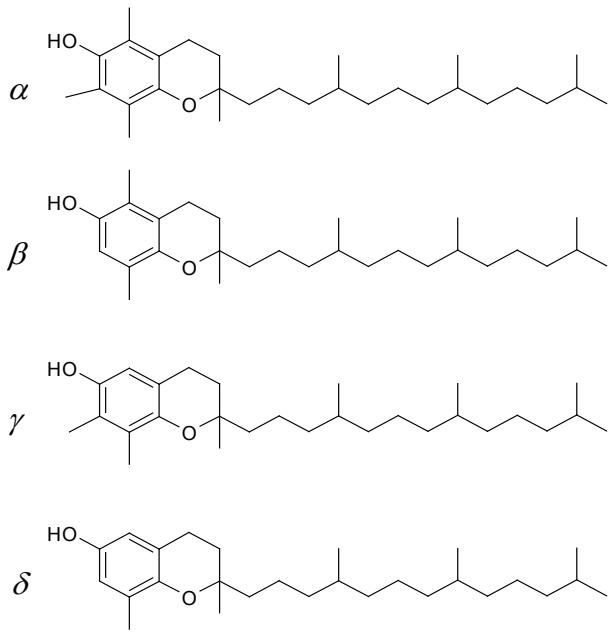

Figure 77: Structures of the tocopherol homologues.

To obtain a closer understanding of the separation process and estimate the influence of shape selectivity on the separation, the interaction behaviour of β- and γ-tocopherol on three different RP materials was investigated using ^{1}H STD HR-MAS NMR spectroscopy.

A monomeric C_{18} phase, a polymeric C_{30} phase, and a polymeric PEAA phase [Meyer 06] were compared with respect to their interaction strength to β- and γ-tocopherol. HPLC of each system was performed in methanol as mobile phase yielding the respective chromatograms which are given in figure 78. The chromatograms on C_{18} and C_{30} were obtained from analytical HPLC [Krucker 04], whereas the chromatogram on PEAA was obtained from capillary-HPLC [Grynbaum 06], though the retention order is still comparable.

For all phases, the same retention order, namely δ - γ, β - α, is observable. However, a full separation can be performed on the C_{30} phase (see figure 78 a), whereas only a slight separation of β- and γ-tocopherol is achieved on PEAA (see figure 78 b). The C_{18} phase was not capable to separate β- and γ-tocopherol (see figure 78 c).

a)

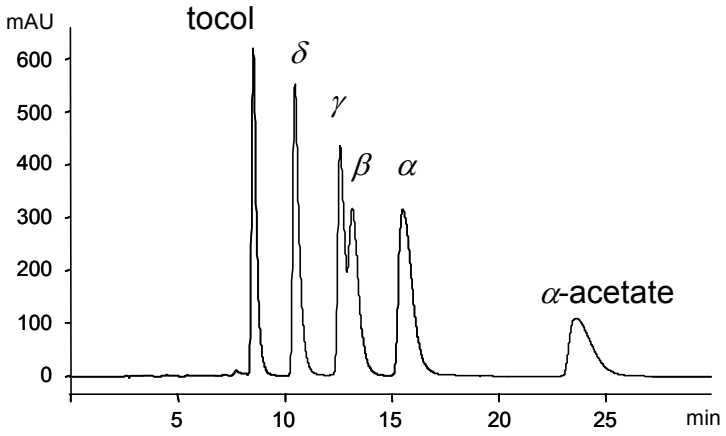

b)

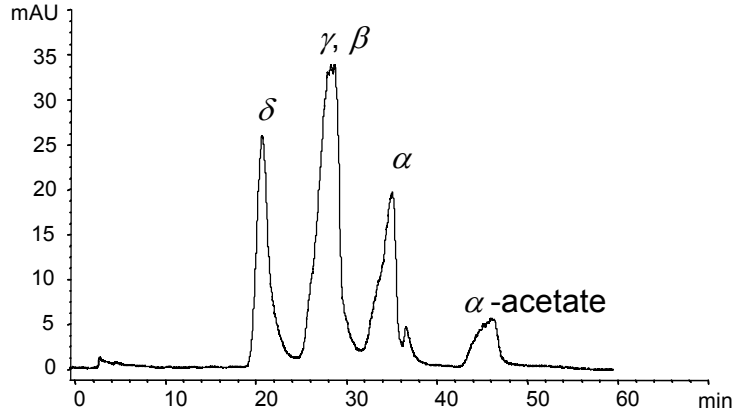

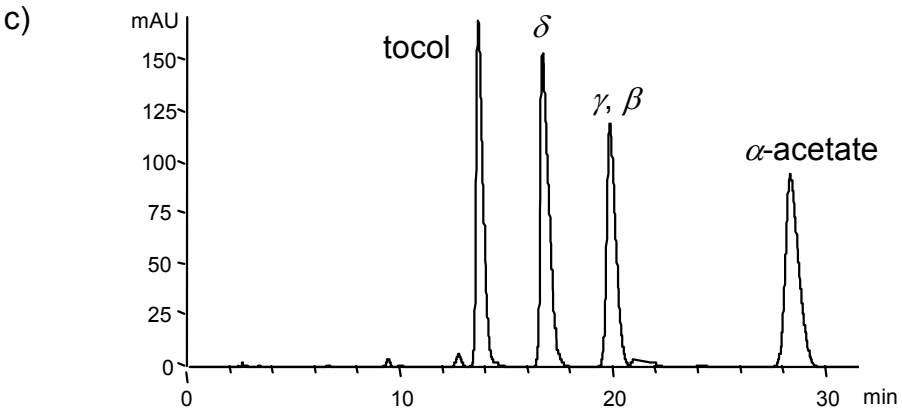

Figure 78: Chromatograms of the tocopherol separation in methanol on a a) C_{30} phase, b) PEAA phase, and c) C_{18} phase. Analytical HPLC was performed on a) and c) and capillary-HPLC on b).

The tocopherols only differ in the amount and sterical order of their methyl groups, located at the aromatic ring. Since the aromatic ring of α-tocopherol contains three methyl groups, and δ-tocopherol only contains one methyl group, we must assume a difference in hydrophobicity of these two homologues, thus revealing stronger interactions for α-tocopherol leading to its later elution from the chromatographic column. β- and γ-tocopherol both contain two methyl groups at the aromatic ring indicating their elution in the middle band. However, since the sterical order of their methyl groups is not alike, they might be separated due to shape selectivity.

^{1}H HR-MAS NMR spectra of β- and γ-tocopherol dissolved in methanol-d_4 reveal the structural difference of both homologues (see figure 79). The CH_2 group (b) of γ-tocopherol resonates at ~2.65 ppm, whereas the CH_2 signal for β-tocopherol experiences a lowfrequency shift due to the neighboured methyl group. The opposite shift behaviour is the case for the aromatic proton signals at ~6.32 ppm (γ-tocopherol) and ~6.44 ppm (β-tocopherol) respectively.

The ^{1}H STD HR-MAS NMR spectra of β- and γ-tocopherol in the presence of each phase respectively are given in figure 80. The peak intensities of the well-resolved signals were integrated and compared in table 1. Surprisingly, intensity differences could be seen from distinct tocopherol protons revealing the suitability of STD NMR spectroscopy to unveil closer information about the part of molecule adsorbing at the stationary phase. Since the substantial interaction sites are expected to be present in the aromatic region (structural difference of β- and γ-tocopherol) and the alkyl chain (hydrophobic interactions) of the

tocopherols, peak b at the heterocycle is referenced to an integral of one. However, only a qualitative assumption can be made from the obtained values.

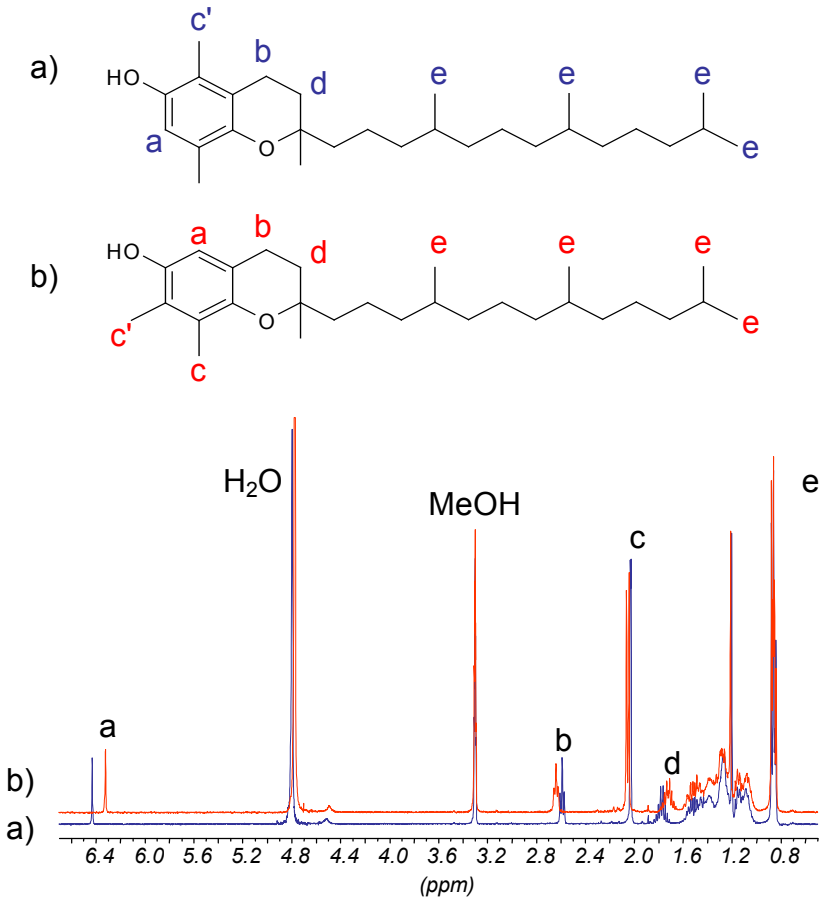

Figure 79: ^{1}H HR-MAS NMR spectra of a) β-tocopherol and b) γ-tocopherol in MeOD-d_3.

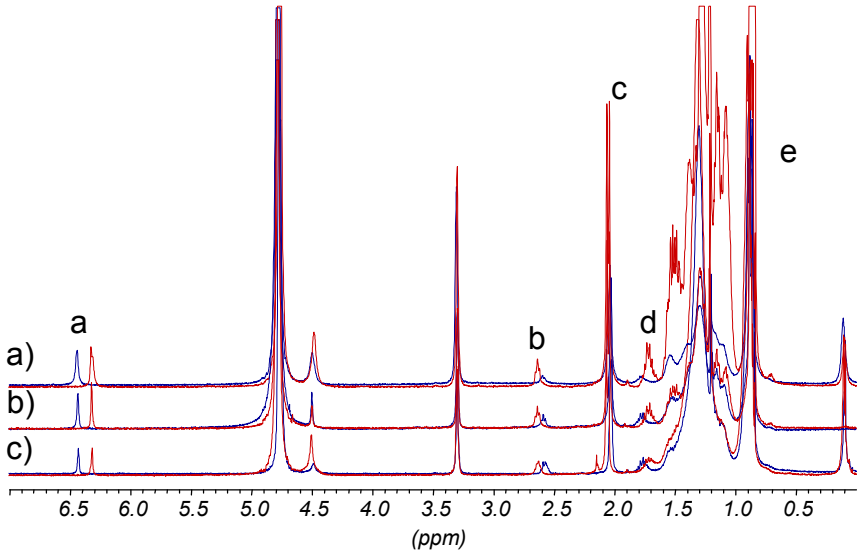

Figure 80: ^{1}H suspended-state STD HR-MAS NMR spectra of β- and γ-tocopherol solutions in MeOD-d_3 in presence of a) C_{30} phase, b) PEAA phase, and c) C_{18} phase.

	a	b	c	d	e
β-tocopherol*	0.5	1.0	3.1	1.1	6.5
γ-tocopherol*	0.5	1.0	3.2	1.1	6.5
β + C_{30}	2.2	1.0	9.6	1.4	37.6
γ + C_{30}	1.1	1.0	7.6	2.4	51.1
β + PEAA	1.4	1.0	8.1	1.8	32.1
γ + PEAA	0.8	1.0	6.1	1.7	22.0
β + C_{18}	0.7	1.0	6.2	2.0	41.7
γ + C_{18}	0.7	1.0	5.5	2.6	42.1

Table 1: Relative integrals of proton peaks derived from the ^{1}H STD HR-MAS NMR spectra of β- and γ-tocopherol in MeOD-d_3 in pure solution (*) and in presence of the three phases respectively.

For comparison and as a proof of principle, the first two lines in the table show integrals of pure tocopherol solutions without stationary phase. It is clearly visible, that the integrals of β- and γ-tocopherol peaks are identical, leading to an identical behaviour in the pure solution. However, addition of the C_{30} phase causes a difference in peak intensity of both homologues. An increase of intensity was observed for the aromatic ring protons in β-tocopherol compared to γ-tocopherol whereas the alkyl chain showed the opposite. A similar effect could be observed in the case of PEAA, though to a smaller extent. Besides, addition of this phase reveals a different behaviour of the tocopherols alkyl chain. Predictably, the tocopherols show similar peak integrals in the presence of the C_{18} phase.

Since the STD experiment yields difference spectra (see section 2.4.1), the obtained ^{1}H STD HR-MAS NMR spectra reveal the most intense peaks for parts of analyte molecules which show the strongest interaction with the stationary phase.

Due to these observations, assumptions can be derived from the obtained NMR data described before. The aromatic region of the tocopherol homologues seems to interact with the C_{30} and PEAA phases, where the strongest interaction is observed for the C_{30} phase, which also reveals the largest difference on the homologues. A somewhat weaker interaction is observed for the tocopherols in the presence of PEAA, and no interaction in presence of the C_{18} phase. Since the spectra of β-tocopherol in comparison to γ-tocopherol show the strongest interactions for the aromatic methyl protons, we can assume that β-tocopherol will most probably elute later from a C_{30} phase than γ-tocopherol. These results match the information obtained from chromatography.

In order to explain the retention behaviour of both tocopherol homologues on a C_{30} phase, we suggest that β-tocopherol (methyl groups are arranged on opposite sides of the aromatic ring) is able to penetrate deeply between the C_{30} chains whereas γ-tocopherol (methyl groups are located on one side of the aromatic ring) might penetrate in a more askew way, thus interacting weaker and eluting earlier.

4.3.2 Interaction of Particulate MIP with 2,4-Dichlorophenoxyacetic acid

An imprinted particulate polymer (MIP) was investigated with respect to its selective affinity to its template 2,4-dichlorophenoxyacetic acid (2,4-D). It was compared to the same polymer which was imprinted with acetic acid (NIP).

A ^{1}H HR-MAS NMR spectrum was aquired on a buffered solution of 2,4-D in 50% MeOD-d_3 and 50% D_2O yielding four sample peaks at 7.37 ppm, 7.18 ppm, and 6.8 ppm, and at 4.49 ppm, which were assigned to the aromatic protons and the CH_2 group respectively (see figure 81). For clarity, an enlarged section of the aromatic signals is provided.

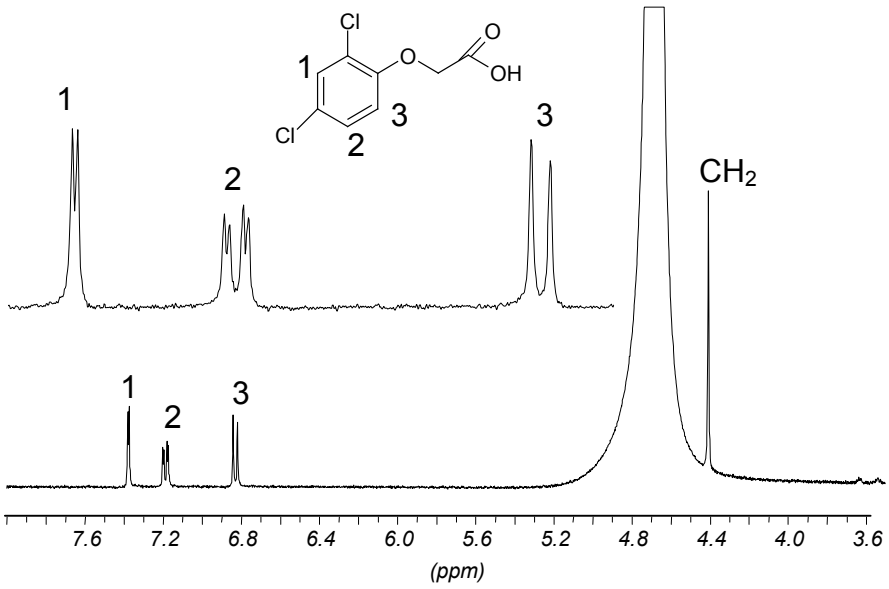

Figure 81: ^{1}H HR-MAS NMR spectrum of a buffered 2,4-D solution in 50% MeOD-d_3 and 50% D_2O.

The ^{1}H STD HR-MAS NMR experiment was performed in order to obtain information about the rebinding selectivity of the chemically alike MIP and NIP. When adding an appropriate amount of NIP to the analyte solution, the ^{1}H STD NMR spectrum revealed three analyte

peaks at 7.47 ppm and 7.27 ppm (aromatic protons), and at 4.49 ppm (CH_2), indicating the interaction of the side chain and part of the aromat with the NIP (see figure 82 a). However, upon addition of MIP to the analyte solution, four peaks are observable in the spectrum (see figure 82 b), namely at 7.43 ppm, 7.23 ppm, and 6.87 ppm (aromatic protons), and at 4.46 ppm (CH_2). Even though the intensity of all analyte signals in the STD spectra is quite weak, which is most probably due to the large water peak present, we assume that this additional peak present in the STD spectrum belongs to an aromatic proton which reveals selective binding to the MIP. Besides, we can conclude, that also non-specific binding is present due to the observed peaks of the 2,4-D in presence of the NIP.

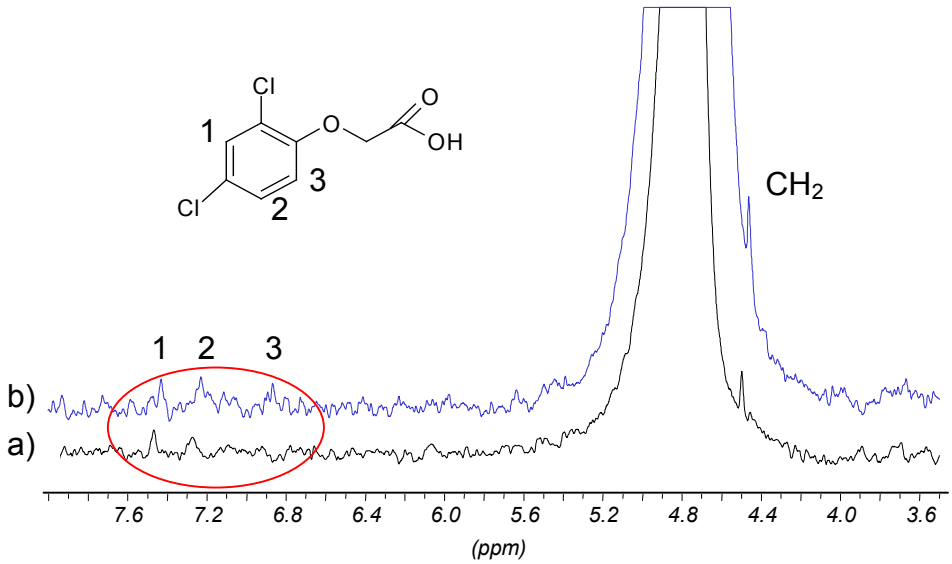

Figure 82: ^1H suspended-state STD HR-MAS NMR spectra of a buffered 2,4-D solution in 50% MeOD-d_3 and 50% D_2O in presence of a) NIP and b) MIP.

4.3.3 Interaction of MIP Monolith with Bupivacaine

Bupivacaine is a local anaesthetic, which was applied as template for the imprinting process on the monolith since it is soluble in water and organic solvents [Courtois 06 a, b]. The hydrochloric salt of bupivacaine was used as analyte in the recognition study for simplicity.

The molecular recognition of bupivacaine on grafted MIP and NIP monoliths was investigated using the STD HR-MAS NMR technique in order to reveal the imprinting quality and the selectivity of the respective binding sites.

The ^1H HR-MAS NMR spectrum of a 0.1 molar solution of bupivacaine in ACN-d_3 is given in figure 83, revealing peaks at 0.91 ppm (methyl groups), 1.31 ppm, 1.50 ppm, and 1.73 ppm

(alkyl chain), 2.77 ppm and 3.18 ppm (heterocycle), 7.07 ppm (aromatic ring), and 8.24 ppm (NH group).

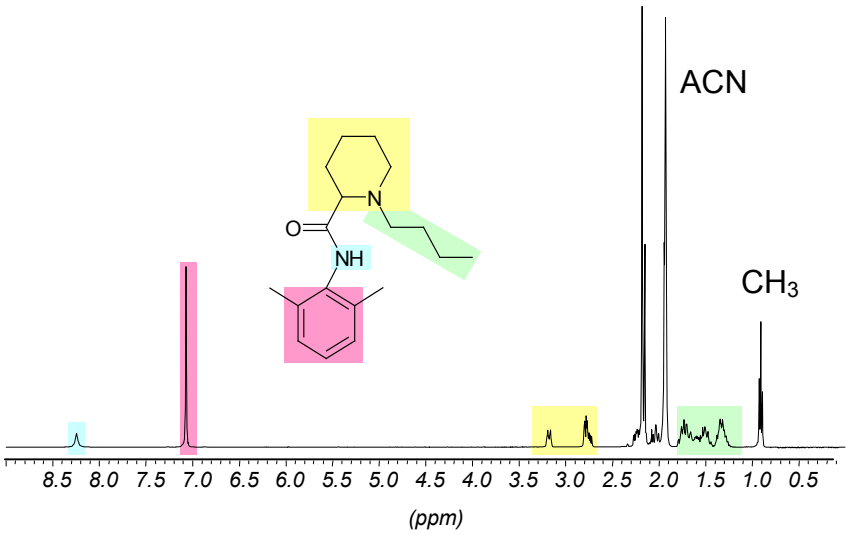

Figure 83: ^{1}H HR-MAS NMR spectrum of a bupivacaine solution in ACN-d_3.

Since grinding of the MIP monolith would probably lead to a partial destruction of the imprinted sites, the rotor was directly filled with a complete piece of monolith, and the analyte solution was added afterwards.

The ^{1}H STD HR-MAS NMR spectra of bupivacaine in presence of MIP and NIP respectively still showed all analyte peaks at a similar chemical shift (see figure 84). However, upon comparison of the integrals of both spectra, referenced on signal a, which was set to an integral of one, considerable differences could be observed. The extracted data (see table 2) reveal larger intensities for the bupivacaine protons located at the aromatic ring and the NH in presence of MIP compared to NIP which indicates a stronger binding of the aromatic side of bupivacaine to the MIP. On the contrary, larger integrals are observed for the alkyl chain protons in presence of the NIP. To express this more clearly, the aromatic part of bupivacaine seems to interact stronger with the MIP whereas its alkyl chain interacts stronger with the NIP. This is a suprising observation, which leads to a considerable difference of the recognition behaviour between the imprinted and non-imprinted polymers yielding the assumption that, in the MIP, the selective binding is exceeding the non-selective interactions. Hence, the polar groups of the MAA form a specific binding site for the bupivacaine [Courtois 06 b]. The bupivacaine is most likely to interact hydrophobically with the NIP, thus the alkyl chain shows the highest saturation in the STD NMR spectrum.

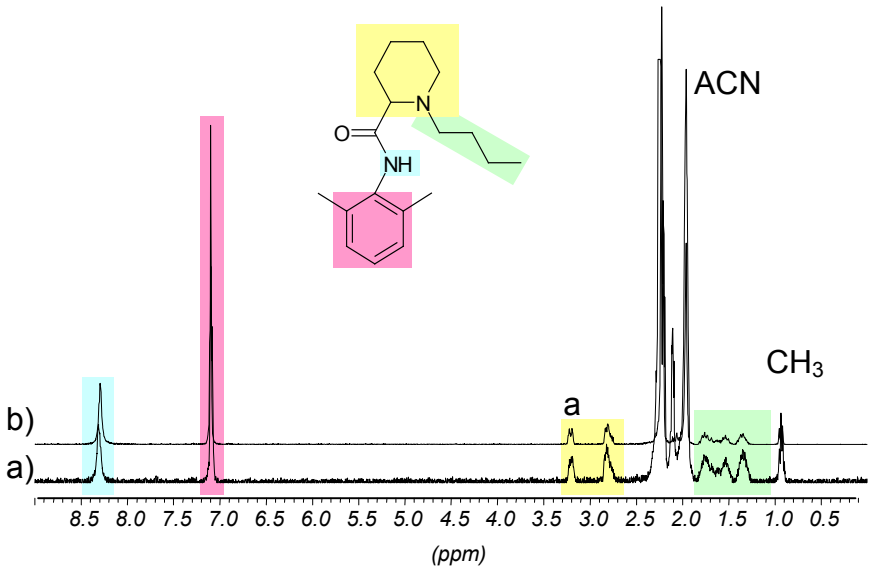

Figure 84: ^{1}H suspended-state STD HR-MAS NMR spectra of bupivacaine in ACN-d_3 in presence of a) NIP and b) MIP.

NIP	2,5	5	1	2	6	2
MIP	5	8,5	1	2	4	1

Table 2: Relative integrals of proton peaks derived from the ^{1}H suspended-state STD HR-MAS NMR spectra of bupivacaine in presence of NIP and MIP.

4.4 Conclusion

It was shown that ^{1}H suspended-state HR-MAS NMR spectroscopy is a suitable technique to study the dynamic behaviour of interphase systems. Sensitive systems of mobile and stationary phase with analytes were investigated in order to gain information about mutual influences leading to valuable insight in interaction and retention mechanisms.

The influence of mobile phase composition and concentration on the analyte was shown on methylphenyl succinimide. Two possible dynamic schemes were suggested.

Suspended-state STD HR-MAS NMR spectroscopy was also applied on different systems and showed its suitability to locate the active sites of analyte molecules interacting with macromolecules.

In particular, the shape selectivity of C_{30} and PEAA phases could be monitored. The rebinding and molecular recognition quality of molecularly imprinted polymers could also be tested using this technique. However, further experiments on the MIP monolith revealed problems arising from the STD NMR experiment showing that the obtained results are not always reproducible. The technique is not suitable for all polymer/analyte systems due to the possibility of accidental direct saturation of the analyte. A mere irradiation on the polymer, distant from the analyte resonances, has to be achieved.

To increase the experience on interpreting the obtained results, suspended-state HR-MAS NMR spectroscopy of additional chromatographic systems should be performed.

5 Summary

New materials, suitable for the application in reversed phase liquid chromatography and fuel cell membranes, were characterized regarding their structure and dynamic properties using solid-state and suspended-state NMR spectroscopy. Both methods were found to be suitable to study the dynamic behaviour, the first to observe intrinsic mobilities of phosphonic acids, the second to monitor interaction processes taking place in a chromatography-like system.

Several *phosphonic acids*, which are promising materials for high temperature fuel cell membranes, were investigated with respect to proton mobility and transport applying various solid-state NMR methods. In addition, water uptake and its effects on anhydride formation were studied on samples that were equilibrated with saturated salt solutions. For PVPA substantial, reversible anhydride formation was found, while MePA did not show condensation. Variable temperature ^{1}H MAS NMR spectroscopy of PVPA ionomer, MePA, and PVBzPA revealed single proton sites. Their chemical shifts indicate stronger hydrogen bonds in PVPA ionomer and rather weak bonds in PVBzPA. Since ^{2}H NMR spectroscopy allows for the observation of quadrupolar tensor reorientation, static as well as MAS ^{2}H NMR spectra were recorded, revealing information about deuteron mobilities, especially for PVPA ionomer, MePA, and PVBzPA. It was found, that PVPA ionomer shows high proton mobility, despite rather strong hydrogen bonds. Low proton mobilities were observed for both MePA and PVBzPA, though the hydrogen bond strength in MePA is similar to that of PVPA ionomer, while PVBzPA possesses weaker hydrogen bridges.
These results show that the relation between hydrogen bond strength and proton mobility is complex. In particular, this work demonstrates that the application of simple 1D ^{1}H and ^{2}H NMR experiments provides easy access to information about proton/deuteron mobility on short time scales, needed for an identification of materials with high intrinsic proton conductivities.

Stationary phases for reversed phase liquid chomatography were characterized by solid-state NMR spectroscopy, and their influence on different analytes was studied using suspended-state HR-MAS NMR spectroscopy. Suspended-state HR-MAS NMR spectroscopy showed to be suitable to model the separation process of analytes on chromatographic sorbents. For this, the stationary phase was suspended in a solution of analyte dissolved in mobile phase.

MePhSucc showed a peak doubling of the CH_2 group in presence of monomeric C_{18} phase, leading to the coexistence of a narrow and a broadened peak. Thus, the dynamic interactions of MePhSucc towards the stationary phase, and under the influence of the mobile phase, could be directly observed using ^{1}H HR-MAS NMR spectroscopy. Changing the mobile phase concentration and composition caused a shift of the broadened peak towards the narrow CH_2 signal, resulting in the fusion of both. These effects were explained by two different theories, one of which substantiates with polarity differences, the other with the winding up of the C_{18} alkyl chains.

Separating interactions were also investigated using the suspended-state STD HR-MAS NMR technique that unveiled the part of analyte molecule interacting with the chromatographic sorbent. The shape selectivity of C_{30} and PEAA phases, known from HPLC, could be confirmed by ^{1}H STD HR-MAS NMR spectroscopy on the example of β- and γ-tocopherol. The spectra of the tocopherol homologues in presence of the C_{30} phase revealed the largest interaction differences, thus showing similarity to the retention order observed in HPLC.

Furthermore, the molecular recognition of a particulate and a monolithic MIP towards their respective template molecules was investigated using ^{1}H STD HR-MAS NMR spectroscopy. The obtained data proved superiority of the respective MIP over the NIP, and definite knowledge of the interaction site at the analyte molecules could be gained. Differences between specific and non-specific binding could be observed.

However, continued investigations of chromatographic and molecular recognition systems may aid further interpretation of the obtained results and thus the understanding of such separation and rebinding mechanisms.

6 Experimental Details

Phosphonic acids

Samples and chemicals:

Most samples were provided by cooperation partners participating in the DryD project. PVPA ionomer was donated by PEMEAS GmbH, Frankfurt. Methylphosphonic acid was commercially obtained from Acros Organics. Deuteriumoxide and methanol-d_4 were obtained from Merck, Darmstadt.

NMR spectroscopy:

All MAS NMR experiments were carried out in 2.5 mm double bearing rotors made from ZrO_2 at spinning speeds ranging from 10 to 25 kHz. Most of the ^{1}H, ^{13}C, and ^{31}P NMR experiments were performed on a Bruker ASX 500 MHz spectrometer with respective frequencies of 500.13 MHz for ^{1}H, 125.758 MHz for ^{13}C and 202.456 MHz for ^{31}P. The pulse length was 2.5 µs for all nuclei. Some of the ^{1}H and all ^{2}H MAS NMR experiments were carried out on a Bruker DRX 700 MHz spectrometer with respective frequencies of 700.13 MHz for ^{1}H and 107.474 MHz for ^{2}H. The pulse length again was 2.5 µs for all nuclei.

Static ^{2}H NMR experiments were performed on a Bruker DSX 300 MHz spectrometer in a static probehead equipped with a 7 mm coil. The ^{2}H frequency is 46.072 MHz, and the pulse length was 4.2 µs.

The data used for Arrhenius plots to extract activation energies was temperature calibrated with respect to the MAS frequency using $Sm_2Sn_2O_7$ [Langer 99].

Deuteration:

All samples, except PVBzPA, were deuterated by dissolving them in D_2O at room temperature and freeze-drying them afterwards. PVBzPA underwent the same procedure but with deuterated methanol as solvent instead.

Proton conductivity measurements:

Pellets were formed for all samples using a standard press for KBr pellets. To ensure the contact of the brass electrodes to the rough surface of the pellets, E-TEK carbon cloth electrodes loaded with platinum particles were used. Proton conductivity measurements were

performed by dielectric spectroscopy in a two-electrode geometry using a SI 1260 impedance/gain-phase analyzer.
The conductivities were measured in a temperature range of –30 °C to +70 °C in steps of 10 °C at different frequencies. For each temperature the saturation point was determined to yield the actual conductivity at the certain temperature.

Water uptake studies:
The experimental setup is explained in chapter 3.2.

Chromatographic Stationary Phases

Samples and chemicals:
The two MIP samples were provided by the cooperation partners of the AquaMIP project. The monomeric C_{18} and polymeric C_{30} phases were donated by Bischoff Chromatography GmbH, Leonberg. PEAA was provided by Meyer [Meyer 04, 05], and the tocopherols were ordered from CalBiochem, USA. Methylphenyl succinimide, TSPSA, and all deuterated organic solvents were commercially obtained from Acros Organics. Deuteriumoxide was obtained from Merck, Darmstadt. 2,4-D was commercially available from Aldrich. Bupivacaine was donated by AstraZeneca, Sweden. The deuterated TRIS buffer was obtained from Cambridge Isotope Labs, GB.

NMR spectroscopy:
All solid-state NMR experiments were carried out in 4 mm or 7 mm (^{29}Si) double bearing rotors made from ZrO_2 on Bruker DSX 200 MHz and ASX 300 MHz spectrometers with resonance frequencies at 50.312 MHz and 75.468 MHz for ^{13}C and at 39.75 MHz and 59.63 MHz for ^{29}Si respectively. The pulse length for ^{13}C was 3.5 µs, and the contact time of ^{1}H-^{13}C CP was 2-5 ms. The pulse length for ^{29}Si was 7 µs, and the contact time for {^{1}H}-^{29}Si CP was 5 ms.
The ^{1}H HR-MAS NMR experiments were all performed in 4 mm HR-MAS rotors on a Bruker ARX 400 MHz spectrometer. The ^{1}H pulse length was 9.5 µs. Stock solutions were made from all analytes in the particular mobile phase respectivley. The rotors were then carefully filled with each, ~5 mg of stationary phase and ~68 µl of analyte solution, and spun up to 4 kHz. In case of the MIP monoliths the samples were measured in complete pieces of ~5 mg.

Chemical shift referencing was performed externally on the applied solvent compositions for each experiment respectively using 3-(trimethylsilyl) propane sulfonic acid Na salt (TSPSA) as an internal standard. For this, TSPSA was dissolved in the given solvent composition, and the chemical shift of the methyl protons was determined.

HPLC:

The tocopherols were separated on a C_{30} column with an isocratic mobile phase mixture of 96% methanol and 4% water with a flow rate of 1 ml/min [Krucker 04 a, b]. The tocopherol homologues were separated on a PEAA column, using an isocratic mixture of 90% methanol and 10% water with a flow rate of 5 µl/min [Grynbaum 06 a, b].

Analytical HPLC was performed on an Agilent HPLC system, equipped with binary pump, degasser, and UV detector (Agilent Technologies, Waldbronn). HyStar NT 2.0 (Bruker Daltonik GmbH, Bremen) and Agilent ChemStation were used as control software.

Capillary HPLC was performed on a ternary modular capillary HPLC pump (Waters, USA) with a Bischoff Lambda 1010 UV detector (Bischoff Analysentechnik und –geräte GmbH, Leonberg). HyStar NT 2.3.b74 was used as control software.

7 Literature

[Albert 96] K Albert, H Händel, M Pursch, S Strohschein "Structure elucidation of β-carotene isomers by HPLC-NMR coupling using a C_{30} bonded phase" Chem Mod Sur, RCS **6** *30-45* (1996)

[Allcock 02] HR Allcock, MA Hofmann, CM Ambler, SN Lvov, XY Zhou, E Chalkova, J Weston "Phenyl phosphonic acid functionalized poly[aryloxyphosphazenes] as proton-conducting membranes for direct methanol fuel cells" J Membr Sci **201** *47-54* (2002)

HR Allcock, MA Hoffmann, CM Ambler, RV Morford "Phenylphosphonic acid functionalized poly[aryloxyphosphazenes]" Macromol **35** *3484-3489* (2002)

[Bachmann 00] S Bachmann, J Wegmann, K Albert "Sphärische Kieselgel-Partikel mit unterschiedlichen Durchmessern" GIT Spez Sep **20** *24-26* (2000)

[Barsoukov 05] E Barsoukov, JR MacDonald "Impedance spectroscopy. Theory, experiment, and applications" John Wiley and Sons **2** (2005)

[Bayer 83] E Bayer, K Albert, J Reiners, M Nieder, D Müller "Characterization of chemically modified silica gels by ^{29}Si and ^{13}C cross-polarization and magic angle spinning nuclear magnetic resonance" J Chrom **264** *197-213* (1983)

[Biesalski 97] HK Biesalski, J Schrezenmeier, P Weber, HE Weiß "Vitamin: Physiologie, Pathophysiologie, Therapie" Georg Thieme, Stuttgart (1997)

[Bingöl 06] B Bingöl, WH Meyer, M Wagner, G Wegner "Synthesis, microstructure, and acidity of poly(vinylphosphonic acid)" Macromol Rap Commun **27** *1719-1724* (2006)

[Bruker a] WINNMR software

[Bruker b] Bruker Almanach, NMR tables *32-34* (2006)

[Courtois 06 a] J Courtois, G Fischer, B Sellergren, K Irgum "Molecularly imprinted polymers grafted to flow through poly(trimethylolpropane trimethacrylate) monoliths for capillary-based solid-phase extraction" J Chrom A **1109** *92-99* (2006)

[Courtois 06 b] J Courtois, G Fischer, S Schauff, K Albert, K Irgum "Interactions of bupivacaine with a molecularly imprinted polymer in a monolithic format studied by NMR" Anal Chem **78** *580-584* (2006)

[Cutajar 06] M Cutajar, SE Ashbrook, S Wimperis "^{2}H double-quantum NMR as a probe of dynamics on the microsecond timescale in solids" Chem Phys Lett **423** *276-281* (2006)

[Dirion 03] B Dirion, Z Cobb, E Schillinger, LI Andersson, B Sellergren "Water-compatible molecularly imprinted polymers obtained via high-throughput synthesis and experimental design" JACS **125** *15101-15109* (2003)

[Dotelli 04] G Dotelli, MC Gallazzi, CM Mari, F Greppi, E Montoneri, A Manuelli "Polyalkylphosphazenes as solid proton conducting electrolytes" J Mat Sci **39** *6937-6943* (2004)

[Engelhardt 87] G Engelhardt, D Michel "High-resolution solid state NMR of silicates and zeolithes" John Wiley and Sons, Chichester (1987)

[Fischer 35] K Fischer "Neues Verfahren zur maßanalytischen Bestimmung des Wassergehaltes von Flüssigkeiten und festen Körpern" Angew Chem **26** *394-396* (1935)

[Fischer 03] G Fischer, U Skogsberg, S Bachmann, H Yüksel, S Steinbrecher, E Plies, K Albert "Synthesis, characterization, and evaluation of divinylbenzene-coated spherical nonporous silica" Chem Mater **15** *4394-4400* (2003)

[Fischer 04] G Fischer "Entwicklung, Charakterisierung und Anwendung neuer, funktionalisierter Hybridmaterialien für die HPLC" PhD thesis, Universität Tübingen (2004)

[Göpel 94] W Göpel, C Ziegler "Struktur und Materie: Grundlagen, Mikroskopie und Spektroskopie" Teubner (1994)

[Goward 02] GR Goward, MFH Schuster, D Sebastiani, I Schnell, HW Spiess "High-resolution solid-state NMR studies of imidazole-based proton conductors: Structure motifs and chemical exchange from ^{1}H NMR" J Phys Chem B **106** *9322-9334* (2002)

[Grant 96] DM Grant, RK Harris "Encyclopedia of Nuclear Magnetic Resonance" (1996)

[Greenspan 77] Greenspan J Res Nat Bur of Stand A **81A** *89-96* (1977)

[Gritti 05] F Gritti, G Guiochon "Adsorption mechanism in RPLC. Effect of the nature of the organic modifier" Anal Chem **77** *4257-4272* (2005)

[Gritti 06] F Gritti, G Guiochon "Adsorption mechanisms and effect of temperature in reversed-phase liquid chromatography. Meaning of the classical van`t Hoff plot in chromatography" Anal Chem **78** *4642-4653* (2006)

[Grynbaum 06 a] M Grynbaum "Analytik und Wirkungsweise pharmakologisch aktiver Substanzen" PhD thesis, Tübingen (2006)

[Grynbaum 06 b] M Grynbaum, C Meyer, K Putzbach, J Rehbein, K Albert "Application of polymer based stationary phases in high performance liquid chromatography and capillary high performance liquid chromatography hyphenated to microcoil 1H nuclear magnetic resonance spectroscopy" J Chrom A *article in press* (2006), doi: 10.1016/j.chroma.2006.11.032

[Händel 03] H Händel, E Gesele, K Gottschall, K Albert "Anwendung der HR-MAS-^{1}H-NMR-Spektroskopie zur Untersuchung der Wechselwirkung zwischen Liganden und synthetischen Rezeptoren" Angew Chem **115** *454-458* (2003);
Angew Chem Int Ed **42** *438-442* (2003)

[Hellriegel 04] C Hellriegel, U Skogsberg, K Albert, M Lämmerhofer, NM Maier, W Lindner "Characterization of a chiral stationary phase by HR/MAS NMR spectroscopy and investigation of enantioselective interaction with chiral ligates by transferred NOE" JACS **126** *3809-3816* (2004)

[Hahn 50] EL Hahn "Spin Echoes" Phys Rev **80** *580-594* (1950)

[Hickner 04] MA Hickner, H Ghassemi, YS Kim, BR Einsla, JE McGrath "Alternative polymer systems for proton exchange membranes (PEMs)" Chem Rev **104** *4587-4612* (2004)

[h-tec 03] h-tec Wasserstoff-Energie-Systeme GmbH, Lübeck, *www.h-tec.com* (2003)

[Kaltbeitzel] A Kaltbeitzel, S Schauff, H Steininger, B Bingöl, G Brunklaus, WH Meyer, HW Spiess "Water sorption of poly(vinylphosphonic) acid and its influence on proton conductivity" SSI, *manuscript submitted*

[Kreuer 96] KD Kreuer "Proton conductivity: Materials and application" Chem Mater **8** *610-641* (1996)

[Kreuer 00] KD Kreuer "On the complexity of proton conduction phenomena" SSI **136-137** *149-160* (2000)

[Kreuer 04] KD Kreuer, SJ Paddison, E Spohr, M Schuster "Transport in proton conductors for fuel-cell applications: Simulations, elementary reactions, and phenomenology" Chem Rev **104** *4637-4678* (2004)

[Krucker 04 a] M Krucker "Direktgekoppelte miniaturisierte Analysensysteme zum Nachweis pharmakologisch aktiver Substanzen aus biologischen Proben" PhD thesis, Tübingen (2004)

[Krucker 04 b] M Krucker, A Lienau, K Putzbach, MD Grynbaum, P Schuler, K Albert "Hyphenation of capillary HPLC to microcoil ^{1}H NMR spectroscopy for the determination of tocopherol homologues" Anal Chem **76** *2623-2628* (2004)

[Langer 99] B Langer, I Schnell, HW Spiess, A-R Grimmer "Temperature calibration under ultrafast MAS conditions" JMR **138** *182-186* (1999)

[Lee] YJ Lee, B Bingöl, T Murakhtina, D Sebastiani, JH Ok, WH Meyer, G Wegner, HW Spiess "High resolution solid state NMR studies of poly(vinyl phosphonic acid), a new proton conducting polymer for fuel cell application" *manuscript submitted*

[Lowe 59] IJ Lowe "Free induction decays of rotating solids" Phys Rev Lett **2** *285-287* (1959)

[Macho 01] V Macho, L Brombacher, HW Spiess "The NMR-WEBLAB: An internet approach to NMR lineshape analysis" Appl Magn Res **20** *405-432* (2001)

[Maciel 80] GE Maciel, DW Sindorf "Silicon-29 NMR study of the surface of silica gel by cross polarization and magic-angle spinning" JACS **102** *7606-7607* (1980)

[Markova] D Markova, M Klapper, K Müllen, manuscript in preparation

[Massiot 02] dmfit program: D Massiot, F Fayon, M Capron, I King, S Le Calvé, B Alonso, J-O Durand, B Bujoli, Z Gan, G Hoatson "Modelling one- and two-dimensional solid-state NMR spectra" Magn Res Chem **40** *70-76* (2002)

[Mayer 99] M Mayer, B Meyer "Charakterisierung von Ligandenbindung durch Sättigungs-Transfer-Differenz-NMR-Spektroskopie" Angew Chem **111** *1902-1906* (1999);

Angew Chem Int Ed **119** *1727-1736* (1999)

[Meng 03] YZ Meng, SC Tjong, AS Hay, SJ Wang "Proton-exchange membrane electrolytes derived from phosphonic acid containing poly(arylene ether)s" Eur Pol J **39** *627-631* (2003)

[Meyer 99] V Meyer "Praxis der Hochleistungs-Flüssigchromatographie" 8. Auflage, Salle+Sauerländer, 1999

[Meyer 03] B Meyer, T Peters "NMR-Techniken zum Screening und zur Identifizierung der Bindung von Liganden an Proteinrezeptoren" Angew Chem **115** *890-918* (2003);
Angew Chem Int Ed **42** *864-890* (2003)

[Meyer 05] C Meyer "Polymer-based chromatographic sorbents: Synthesis, characterization, and application" PhD thesis, Tübingen (2005)

[Meyer 06] C Meyer, U Skogsberg, N Welsch, K Albert "Nuclear magnetic resonance and high-performance liquid chromatography evaluation of polymer-based stationary phases immobilized on silica" Analyt Bioanalyt Chem **382** *679-690* (2005)

[Miyabe 04] K Miyabe, G Guiochon "Characterization of monolithic columns for HPLC" J Sep Sci **27** *853-873* (2004)

[Miyatake 01] K Miyatake, AS Hay "New poly(arylene ether)s with pendant phosphonic acid groups" J Polym Sci A (Polym Chem) **39** *3770-3779* (2001)

[Moka 97] D Moka, R Vorreuther, H Schicha, M Spraul, E Humpfer, M Lipinski, PJD Foxall, JK Nicholson, JC Lindon "Magic angle spinning proton Nuclear Magnetic Resonance spectroscopic analysis of intact kidney tissue samples" Anal Commun **24** *107-109* (1997)

[Pages 06] G Pages, C Delaurent, S Caldarelli "Simplified analysis of mixtures of small molecules by chromatographic NMR spectroscopy" Angew Chem Int Ed **45** *5950-5953* (2006)

[Partch 98] R Partch, S Brown "Aerosol and solution modification of particle-polymer interfaces" J Adhes **67** *259-267* (1998)

[Pereira 06] RP Pereira, MI Felisberti, AM Rocco "Intermolecular interactions and formation of the hydration sphere in phosphonic acid model systems as an approach to the description of vinyl phosphonic acid based polymers" Polym **47** *1414-1422* (2006)

[Pines72] A Pines, W-K Rhim, JS Waugh "Homogeneous and inhomogeneous nuclear spin echos in solids" J Magn Reson **6** *457–465* (1972)

[Pines 73] A Pines, MG Gibby, JS Waugh "Proton-enhanced NMR of dilute spins in solids" J Chem Phys **59** *569–590* (1973)

[Rapp 04] E Rapp "Miniaturisierte Trennverfahren und ihre On-line-Kopplung mit der NMR-Spektroskopie: Entwicklung und Anwendungen" PhD thesis, Tübingen (2004)

[Raitza 98] M Raitza "Untersuchungen zum molekularen Erkennungsprozeß von Interphasen-Systemen über Festkörper- und Suspensions-NMR-Spektroskopie sowie Molecular Modelling" PhD thesis, Tübingen (1998)

[Raitza 00] M Raitza, J Wegmann, S Bachmann, K Albert "Bestimmung der Oberflächenmorphologie von Triacontyl-Trennphasen über Spindiffusions-Festkörper-NMR-Untersuchungen" Angew Chem **112** *3629-3632* (2000)

[Roper 95] DK Roper, EN Lightfoot "Separation of biomolecules using adsorptive membranes" J Chrom A **702** *3-26* (1995)

[Rössler 90] E Rössler, M Taupitz, K Börner, M Schulz, H-M Vieth "A simple method analyzing ^{2}H nuclear magnetic resonance line shapes to determine the activation energy distribution of mobile guest molecules in disordered systems" J Chem Phys **92** *5847-5855* (1990)

[Sander 94] LC Sander, KE Sharpless, NE Craft, SA Wise "Development of engineered stationary phases for the separation of carotenoid isomers" Anal Chem **66** *1676-1674* (1994)

[Schauff 03] S Schauff "Synthese, Coating und Charakterisierung von mono-dispersen Kieselgelpartikeln" diploma thesis, Tübingen (2003)

[Schauff 04] S Schauff, U Skogsberg, K Albert "^{1}H suspended-state HR/MAS NMR spectroscopy as a model system for the chromatographic separation process" poster, National NMR meeting, Aachen (2004); *manuscript in preparation*

[Schauff 06] S Schauff, G Brunklaus, HW Spiess "Solid-state NMR spectroscopy on phosphonic acids" poster, National NMR meeting, Tübingen (2006); *manuscript in preparation*

[Schetter 03] B Schetter "Synthese und Charakterisierung von Kieselgel-Nanopartikeln mit Ferrocenmodifikation und einiger neuer N, N`-disubstituierter Ferrocenoylharnstoffderivate" diploma thesis, Tübingen (2003)

[Schmidt-Rohr 94] K Schmidt-Rohr, HW Spiess "Multidimensional solid-state NMR and polymers" Academic Press, London (1994)

[Schuster 05] M Schuster, T Rager, A Noda, KD Kreuer, J Maier "About the choice of the protogenic group in PEM separator materials for intermediate temperature, low humidity operation: A critical comparison of sulfonic acid, phosphonic acid and imidazole functionalized model compounds" Fuel Cells **5** *355-365* (2005)

[Skogsberg 04] U Skogsberg, H Händel, D Sanchez, K Albert "Comparisons of the interactions between two analytes and two structurally similar chiral stationary phases using high-performance liquid chromatography, suspended-state high-resolution magic angle spinning nuclear magnetic resonance and solid-state nuclear magnetic resonance spectroscopy" J Chrom A **1023** *215-223* (2004)

[Skogsberg 06] U Skogsberg, C Meyer, J Rehbein, G Fischer, S Schauff, N Welsch, K Albert, AJ Hall, B Sellergren "A solid-state and suspended-state magic angle spinning nuclear magnetic resonance spectroscopic investigation of a 9-ethyladenine molecularly imprinted polymer" Polym *article in press* (2006), doi:10.1016/j.polymer.2006.10.036

[Skoog 92] DA Skoog, JJ Leary "Principles of instrumental analysis" Saunders College Publ **4** (1992)

[Spiess 85] HW Spiess "Deuteron NMR - A new tool for studying chain mobility and orientation in polymers" Adv Pol Sci **66** *24-56* (1985)

[Srinivasan 04] G Srinivasan, M Pursch, L Sander, K Müller "FTIR studies of C_{30} self-assembled monolayers on silica, titania, and zirconia" Langmuir **20** *1746-1752* (2004)

[Steininger] unpublished results, kindly provided

[Steininger 06] H Steininger, M Schuster, KD Kreuer, J Maier "Intermediate temperature proton conductors based on phosphonic acid as protogenic group" SSI **177** *2457-2462* (2006)

[Stejskal 94] EO Stejskal, JD Memory, "High Resolution NMR in the Solid State" (1994)

[Strohschein 98] S Strohschein, M Pursch, D Lubda, K Albert "Shape selectivity of C_{30} phases for RP-HPLC separation of tocopherol isomers and correlation with MAS NMR data from suspended stationary phases" Anal Chem **70** *13-18* (1998)

[Tomlins 98] AM Tomlins, RJD Foxall, JC Lindon, MJ Lynch, M Spraul, JR Everett, JK Nicholson "High resolution magic angle spinning ^{1}H nuclear magnetic resonance analysis of intact prostatic hyperplastic and tomour tissues" Anal Commun **35**, *113-115* (1998)

[Tseng 00] LH Tseng "Application of high-resolution-magic-angle-spinning (HR-MAS) NMR spectroscopy to cosmetic emulsions" Zeitschr Naturforsch B **55** *651-656* (2000)

[Viklund 00] C Viklund, K Irgum "Synthesis of porous zwitterionic sulfobetaine monoliths and characterization of their interaction with proteins" Macromol **33** *2539-2544* (2000)

[Villanueva 06] J Villanueva-Garibay, K Müller "NMR studies of disordered solids" Lect Notes Phys **684** *65-86* (2006)

[Wehrle 87] M Wehrle, GP Hellmann, HW Spiess "Phenylene motion in polycarbonate and polycarbonate/additive mixtures" Coll & Polym Sci **265** *815-822* (1987)

[Welsch 05] N Welsch "Beiträge zum Verständnis des chromatographischen Trennprozesses der RP-HPLC mit den Mitteln der Computer-Visualisierung" PhD thesis, Tübingen (2005)

[Ye 06] G Ye, N Janzen, GR Goward "Solid-state NMR study of two classic proton conducting polymers: Nafion and sulfonated poly(ether ether ketone)s" Macromol **39** *3283-3290* (2006)

[Zurutuza] A Zurutuza, unpublished results

Meine akademischen Lehrer waren:

K. Albert, H. Bertagnolli, F. Brandstetter, D. Christen, H. Eckstein, H.J. Egelhaaf, G. Gauglitz, J. Gierschner, G. Häfelinger, M. Hanack, D. Hoffmann, V. Hoffmann, W. Jäger, D. Krug, N. Kuhn, E. Lindner, M.E. Maier, H. Mayer, H.-J. Meyer, U. Nagel, H. Oberhammer, C. Ochsenfeld, D. Oelkrug, G. Pausewang, H. Pommer, W. Rosenstiel, V. Schurig, E. Schweda, F.F. Seelig, B. Speiser, H.W. Spiess, J. Strähle, U. Weimar, L. Wesemann, K.H. Wiesmüller, K.-P. Zeller, C. Ziegler, T. Ziegler